

## ABSTRACT

Title of Dissertation: INVESTIGATION OF *ARABIDOPSIS TSO1*,  
A REGULATOR OF CELL  
PROLIFERATION AND  
DIFFERENTIATION

Wanpeng Wang, Doctor of Philosophy, 2017

Dissertation directed by: Professor Zhongchi Liu,  
Department of Cell Biology and Molecular  
Genetics

Multicellular eukaryotic organisms build complex body structures from a single cell. Through coordinated cell proliferation and differentiation, the collective behavior of cells forms organs that achieve physiological functions. Underlying the developmental processes are the molecular machineries that integrate cell cycle regulation with cell fate acquisition. While animal organogenesis occurs early during embryogenesis, plants maintain pluripotent stem cells at the growing tips (meristems) and generate organs iteratively throughout lifespan. The amazing ability to balance stem cell self-renewal and differentiation underlies the extreme longevity of some plants species. Despite the differences, common mechanisms exist across plant and animal developmental regulation. Understanding both unique and common mechanisms of plant development has broad implications on basic science as well as agriculture and medicine.

The *Arabidopsis TSO1* gene is a regulator of cell proliferation and differentiation at the shoot and root meristems. *TSO1* encodes a CXC domain protein and its animal homologs encode core components of a cell cycle regulatory complex, the DREAM complex. To investigate *TSO1* function and identify factors that act together with *TSO1*, I carried out two genetic screens for suppressors and enhancers of *tso1* mutants. I discovered that loss-of-function mutations in *MYB3R1*, which encodes the *Arabidopsis* ortholog of human *B-Myb*, can suppress *tso1* mutant defects at both the shoot and root meristems. In *tso1-1* mutant, *MYB3R1* is over and ectopically expressed at the shoot and root meristems. Furthermore, MYB3R1 phospho mimic enhanced the *tso1-3* phenotype, indicating that hyper-active MYB3R1 may mediate the *tso1-1* phenotype. *TSO1* physically interacts with *MYB3R1* and likely forms a plant DREAM-like complex that operates in the plant meristems to balance cell proliferation with differentiation.

A gain-of-function mutation of a *HD-ZIP III* transcription factor, *REVOLUTA (REV)*, was identified as an enhancer of *tso1* mutants. *TSO1* directly represses *REV* transcription to balance adaxial and abaxial polarity of lateral organs and maintains the shoot apical meristem. This genetic and molecular interaction between *TSO1* and the adaxial factor *REV* presents an integration point of cell cycle, lateral organ polarity, and meristem regulation.

Together, our findings demonstrate a cell cycle regulatory module conserved across plants and animals and describe its integration into plant specific developmental context.

INVESTIGATION OF *ARABIDOPSIS TSO1*, A REGULATOR OF  
CELL PROLIFERATION AND DIFFERENTIATION

by

Wanpeng Wang

Dissertation submitted to the Faculty of the Graduate School of the  
University of Maryland, College Park, in partial fulfillment  
of the requirements for the degree of  
Doctor of Philosophy  
2017

Advisory Committee:  
Professor Zhongchi Liu, Chair  
Associate Professor Stephen Mount  
Professor Eric Haag  
Associate Professor Kan Cao  
Associate Professor Antony M Jose

© Copyright by  
Wanpeng Wang  
2017

## Acknowledgements

I would like to thank my advisor Dr. Zhongchi Liu for giving me such an interesting project. The mystery of *TSOI* occupied my mind over the years and kept my passion for science burning ever so strongly. I thank her for challenging me to think critically and guiding me through experiments and writing. I thank her for her patience and tolerance for the folly of an overly ambitious young man.

I thank my advisory committee members for their critique and guidance. I enjoyed teaching for Dr. Mount (twice). Special thanks go to Dr. Kan Cao for kindly sharing her lab equipments with me.

The people of Liu lab made every day in the lab a blast. Former members of the Liu lab including Dr. Paja Sijacic, laid the foundation of my project. I feel lucky to have taken on this project at a good time and carried on their good work. Dr. Paja Sijacic and Dr. Courtney Hollender trained me at the beginning of my Ph.D research.

Courtney also introduced me to podcasts and took me shopping in my early days in the US. She's been a great friend. Dr. Charles Hawkins introduced me to awk and regular expressions and kindly helped with coding. I thank Dr. Julie Caruana and Rachel Shahan for their great company as they sit next to me in the lab. I could not list everyone here, but they gave me a family when I'm far away from home.

My project would not be possible without my amazing undergrads. Michael Wellen and Rao Fu helped with seed collection at the early stage of the genetic screen. Dae Ik Yi and Xixi Zhou made constructs and carried out yeast work. Song Yun made crosses and constructed the vectors for MYB3R1 phospho mimics. Nicole Szeluga

made significant contributions to the work in Chapter III. Just talking with them made me speak the language better.

Our collaborators, Dr. Hongli Lian and her student Pengbo Xu solved our long-standing Co-IP obstacle. With their expertise, they made my DREAM come true. The great people of Cao lab provided advice and assistance on my western work. I thank Dr. Zhengmei Xiong and Di Wu for their help and for their friendship.

I would like to thank Dr. Caren Chang and Dr. Heven Sze for lending me chamber space for my genetic screen. Without this valuable space, I would not have healthy plants (so many plants).

I'm grateful for support from the Chinese Scholarship Council. The 4-year fellowship gave me great freedom to explore and to be productive.

I thank my fiancée, my best friend, Qiong, for her love and the joy she brings to my life. Her encouragement has gotten me through the difficult times.

Finally, I thank my family for their unconditional love and tireless support. My parents went through a lot at home during my stay here in US. I could never repay the sacrifice that they made. They made me who I am.

# Table of Contents

Acknowledgements.....	ii
Table of Contents.....	iv
List of Figures.....	vi
Chapter 1: Introduction.....	1
1.1 Plant meristems on the main axis.....	2
1.1.1 Shoot Apical Meristem (SAM): cellular organization and genetic regulation.....	2
1.1.2 Root Apical Meristem (RAM): cellular organization and genetic regulation.....	5
1.2 Adaxial/Abaxial polarity in plant development.....	10
1.2.1 Adaxial/Abaxial polarity defining factors.....	12
1.2.2 The adaxial environment promotes shoot meristem activity.....	13
1.2.3 <i>REVOLUTA</i> function during shoot meristem patterning.....	15
1.3 <i>TSO1</i> encodes a meristem regulator in <i>Arabidopsis thaliana</i> .....	17
1.3.1 <i>TSO1</i> encodes a CHC domain chromatin factor.....	17
1.3.2 <i>TSO1</i> gene expression.....	22
1.3.3 Class I <i>tso1</i> alleles.....	22
1.3.4 Class II <i>tso1</i> alleles.....	25
1.3.5 Class I <i>tso1</i> alleles are recessive antimorphic alleles.....	25
1.4 MYB proteins in animals and plants.....	28
1.4.1 Myb proteins in animals.....	28
1.4.2 DREAM complex and B-Myb.....	31
1.4.3 MYB3R proteins in plants.....	33
1.5 Concluding remarks.....	36
Chapter 2: <i>TSO1-MYB3R1</i> regulatory module at the shoot and root meristems.....	38
2.1 Introduction.....	38
2.2 Material and methods.....	42
2.3 Results.....	49
2.3.1 Identification of <i>tso1-1</i> suppressor mutations.....	49
2.3.2 <i>tso1-1</i> intragenic suppressors support the antimorphic nature of <i>tso1-1</i> ..	53
2.3.3 Identification of <i>MYB3R1</i> as an extragenic suppressor of <i>tso1-1</i> ..	54
2.3.4 CRISPR-induced <i>myb3r1</i> mutations also suppresses <i>tso1-1</i> ..	58
2.3.5 Mutations in <i>MYB3R1</i> suppress <i>tso1-1</i> root phenotype.....	61
2.3.6 Mis-expression of <i>MYB3R1</i> was found in <i>tso1-1</i> mutant SAM.....	64
2.3.7 Mis-expression of <i>MYB3R1</i> mediates <i>tso1-1</i> mutant RAM phenotype.....	67
2.3.8 Overexpression of <i>MYB3R1</i> is not sufficient to cause <i>tso1-1</i> mutant phenotype.....	71
2.3.9 MYB3R1 phospho mimic enhanced <i>tso1-3</i> phenotype.....	71
2.3.10 MYB3R1 physically interact with <i>TSO1</i> .....	74
2.3.11 <i>myb3r4</i> loss-of-function mutation cannot suppress <i>tso1-1</i> phenotype ..	75
2.4 Discussion.....	78
2.4.1 <i>TSO1</i> and <i>MYB3R1</i> form a regulatory module functioning in multiple developmental processes.....	78

2.4.2 TSO1-MYB3R1 likely function as a plant DREAM complex .....	79
2.4.3 Insights of <i>MYB3R1</i> function and regulation.....	83
2.4.4 MYB3R1 may play a unique role among R1R2R3 MYB proteins in Arabidopsis .....	84
Chapter 3: Identification of <i>REVOLUTA</i> , a <i>HD-ZIP III</i> transcription factor, as a downstream target of TSO1 .....	86
3.1 Introduction.....	86
3.2 Material and methods.....	89
3.3 Results.....	93
3.3.1 Isolation of genetic modifiers of <i>tso1-1</i> ; <i>myb3r1-5</i> ( <i>B12</i> ).....	93
3.3.2 <i>REVOLUTA</i> gain-of-function mutation enhances <i>B12</i> phenotype .....	94
3.3.3 Synergistic interaction between <i>rev-11d/+</i> and <i>B12</i> at the shoot apical meristem.....	97
3.3.4 Genome wide identification and analysis of TSO1 downstream targets by DNA microarray .....	100
3.3.5 TSO1 and TSO1 homologs directly bind to the promoters of <i>HD-ZIP III</i> genes .....	103
3.3.6 Genome-wide comparisons between <i>tso1-1</i> differentially expressed (DE) genes and SAM expressed genes. ....	105
3.3.7 <i>REV</i> may mediate the pleiotropic meristem defects of <i>tso1-1</i> .....	107
3.4 Discussion.....	111
3.4.1 <i>B12</i> as a sensitized background for identifying enhancers of <i>tso1</i> mutation .....	111
3.4.2 TSO1 maintains meristem size partly by repressing <i>REV</i> gene expression. ....	112
3.4.3 Model .....	114
Chapter 4: A144, a novel suppressor of <i>tso1-1</i> .....	117
4.1 Introduction.....	117
4.2 Material and method .....	117
4.3 Results.....	119
4.3.1 Isolation and phenotypic characterization of suppressor A144 .....	119
4.3.2 A144 is defective in <i>AT1G49170</i> coding for a small protein with unknown function. ....	124
4.4 Discussion.....	130
Chapter 5: Conclusions and future directions.....	134
Appendix I: Analysis of male meiosis and germline defects of <i>tso1-3</i> .....	139
Reference .....	149

## List of Figures

Figure 1.1 Tissue organization and genetic regulation at the shoot apical meristem ...	3
Figure 1.2 Tissue organization and genetic regulation at the root apical meristem .....	7
Figure 1.3 Adaxial/abxial polarity in plant development .....	11
Figure 1.4 TSO1 encodes a CHC domain protein .....	18
Figure 1.5 <i>tso1-1</i> mutant shoot apical meristem and floral meristem phenotype .....	23
Figure 1.6 Two classes of <i>TSO1</i> mutant alleles .....	24
Figure 1.7 BiFC analyses showing <i>TSO1</i> to <i>TSO1</i> as well as <i>tso1-1</i> to <i>SOL2</i> interactions .....	27
Figure 1.8 MYB proteins in eukaryotes .....	30
Figure 1.9 DREAM complex coordinates cell cycle gene expression .....	32
Figure 2.1 Scheme of the suppressor screen and generation of mapping populations	51
Figure 2.2 Phenotype of an inducible <i>TSO1</i> line and suppressors isolated .....	52
Figure 2.3 Identification of two <i>tso1-1</i> intragenic suppressors .....	54
Figure 2.4 Summary of <i>myb3r1</i> mutations isolated from the <i>tso1-1</i> suppressor screen .....	57
Figure 2.5 <i>myb3r1</i> knockout mutations by CRISPR suppress both <i>tso1-1</i> and <i>tso1-360</i>	
Figure 2.6 The <i>tso1-1</i> root phenotype can be suppressed by <i>myb3r1</i> mutations .....	63
Figure 2.7 Comparisons of <i>TSO1</i> and <i>MYB3R1</i> expression at the SAM .....	66
Figure 2.8 <i>TSO1</i> and <i>MYB3R1</i> expression at the RAM .....	69
Figure 2.9 <i>MYB3R1</i> phospho mimic S656D enhanced <i>tso1-3</i> mutant .....	73
Figure 2.10 <i>TSO1</i> physically interact with <i>MYB3R1</i> .....	74
Figure 2.11 <i>MYB3R4</i> is not part of the <i>TSO1</i> - <i>MYB3R1</i> module .....	77
Figure 2.12 Working model .....	81
Figure 3.1 Diagram summarizing the EMS mutagenesis screen .....	94
Figure 3.2 A gain-of-function allele in the <i>REVOLUTA</i> gene enhances <i>B12</i> phenotype .....	95
Figure 3.3 Demonstration of synergistic interaction between <i>B12</i> and <i>rev-11d/+</i> .....	99
Figure 3.4 Summary of <i>TSO1</i> microarray and yeast-one-hybrid data .....	102
Figure 3.5 <i>REV</i> overexpression underlies <i>tso1-1</i> AM phenotype .....	109
Figure 3.6 A Model illustrating the <i>TSO1</i> - <i>REV</i> pathway in regulating meristems ..	115
Figure 4.1 Isolation of A144, a novel suppressor of <i>tso1-1</i> .....	121
Figure 4.2 A144 suppresses the meristem fasciation but not short root defect of the <i>tso1-1</i> allele .....	122
Figure 4.3 A144 suppresses the fertility defect of the <i>tso1-3</i> allele .....	123
Figure 4.4 Phylogeny of <i>AT1G49170</i> , a conserved DUF167 gene from prokaryotes to eukaryotes .....	126
Figure 4.5 Modeled <i>AT1G49170</i> protein structure .....	128
Figure 4.6 <i>AT1G49170</i> is expressed at the shoot and the root apical meristem .....	130
Figure A1. Both male and female contribute to <i>tso1-3</i> fertility defects .....	142
Figure A2. <i>TSO1</i> is expressed in reproductive organs .....	143
Figure A3. Anther development of wild type and <i>tso1-3</i> flower .....	143
Figure A4: <i>tso1-3</i> male meiosis progression defects .....	145
Figure A5. Normal germline development can occur in <i>tso1-3</i> pollen .....	146
Figure A6. Decondensed chromosomes observed in <i>tso1-3</i> pollen .....	147

## Chapter 1: Introduction

My thesis focuses on the *Arabidopsis TSO1* gene to understand plant development.

*TSO1* is involved in patterning meristems at the shoot and root growing tips which are responsible for growth on the longitudinal axis and lateral organ generation. I will first discuss the distinct tissue organization and the underlying molecular genetic regulation of the meristems on the main axis.

The balance of meristem activity and proper patterning of lateral organs are interdependent. The adaxial/abaxial (or dorsal/ventral) polarity of the lateral organs is established during embryogenesis and has profound influence on plant development. During my thesis study, I discovered that *TSO1* plays a role in repressing the adaxial polarity at the shoot tip to balance meristem activity. I have included, in the section 1.2, an overview of the major factors that define adaxial/abaxial polarity and their roles in meristem regulations.

To understand *TSO1*'s molecular function, our lab has previously carried out extensive characterization of *TSO1* gene and its mutant phenotypes. *TSO1* homologs in animals are components of the master cell cycle regulator, the DREAM complex. Different alleles of *tso1* mutants revealed *TSO1* function in different developmental contexts. In section 1.3, I will summarize features of *TSO1* protein and its two classes of mutant alleles.

To unveil the *TSO1* genetic pathway, I carried out a genetic screen and discovered that mutations in the *MYB3R1* gene can suppress all aspects of *tso1* mutant phenotype, indicating that *TSO1* function is mediated by *MYB3R1*. *MYB3R1* encodes a transcription factor that plays the conserved role of cell cycle regulation across plants and animals. In section 1.4, I will introduce the MYB proteins in animals and plants, and discuss their roles in cell cycle regulation.

## **1.1 Plant meristems on the main axis**

### **1.1.1 Shoot Apical Meristem (SAM): cellular organization and genetic regulation**

The lifelong growth and iterative organogenesis of plants depend on mechanisms that properly maintain and pattern the stem cell population at growing tips. Pluripotent stem cells are maintained in specialized microenvironments, called meristems. The shoot apical meristem (SAM) is responsible for above ground growth and the root apical meristem (RAM) for the underground growth. In *Arabidopsis*, SAM can be divided into zones based on distinct cell division activities and functions (Figure 1.1A). Cells in the **Central Zone (CZ)** divide slowly, and are capable of self-renewal to maintain their pluripotency. The CZ consists of clonal cell layers L1 and L2 where cells divide anticlinally (plane of cell division is at the right angle to the SAM surface). The stem cell identity in CZ is promoted by signals from the **Organizing Center (OC)** beneath the CZ (Figure 1.1A). Cells in the OC belong to the L3 layer and divide in randomly oriented planes. The progeny cells of CZ then enter the **Peripheral Zone (PZ)** and start proliferating rapidly, acquiring identities according to the positional context. Cells within the PZ further accelerate their growth rate

leading to the primordium outgrowth. The PZ and the growing primordium are delimited by the organ boundary domain with reduced cell growth and proliferation.

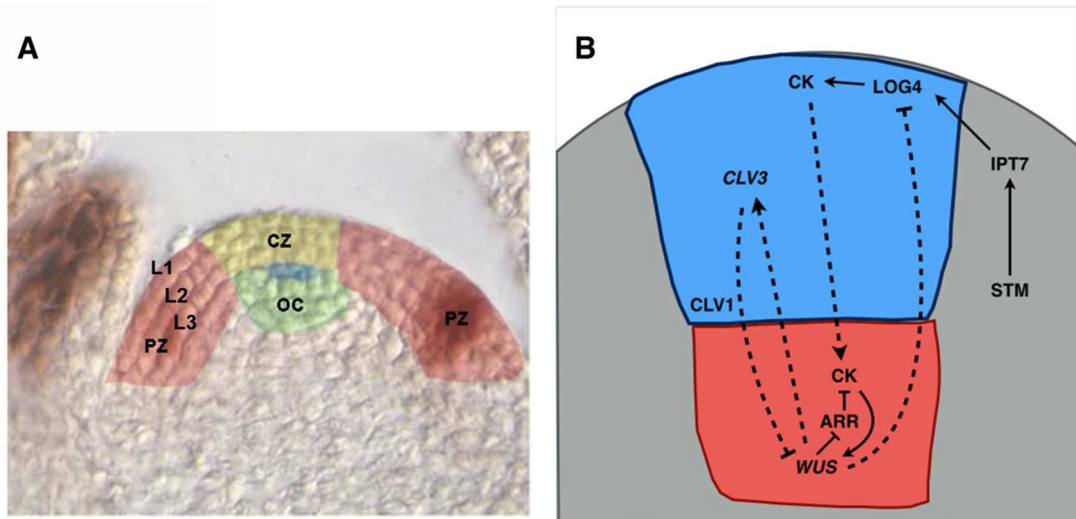


**Figure 1.1 Tissue organization and genetic regulation at the shoot apical meristem**

(A) Tissue organization of the shoot apical meristem. The stem cell pool (blue) is situated under layers of cells in central zone (CZ) (yellow). The stem cell pool is promoted by a group of cell in the organizing center (OC) (green). Cells in the peripheral zone (PZ) (pink) then differentiate to form floral or organ primordium. (Adapted from (Bowman and Eshed 2000) Figure 1). (B) Genetic regulation of the shoot apical meristem. *WUS* is expressed at the OC (red) and promotes stem cells above OC. *WUS-CLV3* negative feedback loop controls the size of the stem cell pool. *STM* promotes the biosynthesis of plant hormone cytokinins (CKs). *WUS-CKs* negative feedback loop controls the relative positioning of the stem cell population. *CLV3* expressing CZ is labeled in blue and *WUS* expressing OC is labeled in red. (Adapted from (Aichinger et al. 2012) Figure 1C).

Throughout the plant adult life, the relative tissue organization of SAM is maintained by interacting molecular modules (Figure 1.1B). The stem cells in the CZ are promoted by the plant-specific homeodomain transcription factor WUSCHEL (*WUS*). *WUS* is expressed in the OC (Organizing Center) and produces a non-cell autonomous proliferative signal to the stem cells above (T. Laux et al. 1996; Mayer et

al. 1998). The *WUS* expressing domain (OC) and the few stem cells above constitute the stem cell niche in SAM. Overexpression of *WUS* leads to increased pool of stem cells (Brand et al. 2002; Lenhard, Jürgens, and Laux 2002; Schoof et al. 2000; Yadav, Tavakkoli, and Reddy 2010). *WUS* promotes the expression of the *CLAVATA3* (*CLV3*) gene at CZ (Schoof et al. 2000) which encodes a mobile peptide signal (CLV3p). CLV3p moves downward from CZ to the OC (Figure 1.1B), where CLV3p binds and activates the receptors, CLV1/CRN-CLV2/RPK2. The receptor kinase complexes act to repress *WUS* expression, thus establishing a feedback loop that restricts the size of *WUS* expressing domain and the stem cell pool (Fletcher et al. 1999; Kinoshita et al. 2010; Müller, Bleckmann, and Simon 2008).

A feedback loop also exists between *WUS* and plant hormone **cytokinins (CKs)** at SAM (Gordon et al. 2009). *SHOOTMERISTEMLESS* (*STM*), another homeodomain transcription factor, promotes the transcription of cytokinin biosynthetic enzyme gene *IPT7* throughout SAM except organ primordia. *LONELY GUY4* (*LOG4*) encodes the enzyme catalyzing the final step of cytokinin biosynthesis and is specifically expressed in the L1 layer in CZ. Thus, cytokinin derived from the L1 layer forms a gradient along the apical/basal axis of SAM (Chickarmane et al. 2012). The cytokinin signal is perceived by the cytokinin receptors including *ARABIDOPSIS HISTIDINE KINASE4* (*AHK4*). The *AHK4* expression domain overlaps with OC and establishes a CK sensitive region that promotes *WUS* expression (Chickarmane et al. 2012). *WUS* also represses *ARABIDOPSIS RESPONSE REGULATOR* (*ARR*) genes, which are negative regulators of cytokinin signaling, to reinforce CK signaling (Leibfried et

al. 2005). In turn, *WUS* also negatively regulates cytokinin biosynthesis at L1 layer of SAM, thus establishing another feedback loop (Chickarmane et al. 2012). This positional cue provided by cytokinin antagonizing *CLV3* function, leads to a feedback control mechanism that maintains the relative position of *WUS* expressing cells and hence the stem cell niche in the SAM over space and time (Chickarmane et al. 2012).

Antagonizing CK's function of promoting stem cell identity, the plant hormone auxin plays roles in promoting differentiation at the SAM. High concentration of auxin accompanies and potentially dictates tissue outgrowth. The polar auxin efflux carrier PIN1 directs auxin flow to form auxin maximum that potentiates primordia formation (Heisler et al. 2005). Once a primordium is established, auxin is depleted from the primordium by reversing auxin transport direction by PIN1 (Heisler et al. 2005). This auxin depletion results in an auxin minimum at the boundary region between the meristem and the growing primordium (Heisler et al. 2005). Mutations in the *PIN1* gene lead to pin-shaped meristem without functional organ formation, suggesting the spatial-temporal control of auxin concentration at the SAM is crucial for primordium outgrowth and lateral organ formation.

### **1.1.2 Root Apical Meristem (RAM): cellular organization and genetic regulation**

The plant root apical meristem (RAM) is derived from the opposite pole from SAM during embryogenesis. Although the tissue organization differs between SAM and RAM, molecular mechanisms and principles of tissue patterning are shared. In *Arabidopsis*, the quiescent center (QC) in the center of the RAM consists of

mitotically relatively inactive cells and function as the organizer of RAM (Figure 1.2). QC cells and the stem cells immediately surrounding the QC constitute the stem cell niche at the RAM. The stem cells divide asymmetrically to produce one stem cell and one differentiating daughter cell. Based on their relative position to the QC, the daughter cells acquire the cell fates of stele, ground tissue (cortex/endodermis), epidermis, lateral root cap and columella. As a result, each longitudinal cell file is made of one cell type and the cell files form concentric cylinders enclosing the vasculature tissue in the middle. Cells divide rapidly and symmetrically along the longitudinal axis in the meristematic zone (MZ), exit mitotic cell cycle and initiate differentiation in transition zone (TZ), increase the length-to-width ratio in elongation zone (EZ), and finally acquire distinct identity and function in the differentiation zone (DZ) (Figure 1.2). This unique structure presents all cell types across the radial axis and all stages of the development along the longitudinal axis of the primary root.

Interestingly, in contrast to *Arabidopsis* SAM where stem cells function in a population mode upon positional cue, the RAM stem cells appears to operate on a lineage-based mode in which each stem cell only generates one type of daughter cells (Thomas Laux 2003). However, laser ablation experiments demonstrated that cues from differentiated cells guide the cell fate acquisition, suggesting that positional information surrounding environment seems to be the ultimate determinant of cell identity (van den Berg et al. 1995).

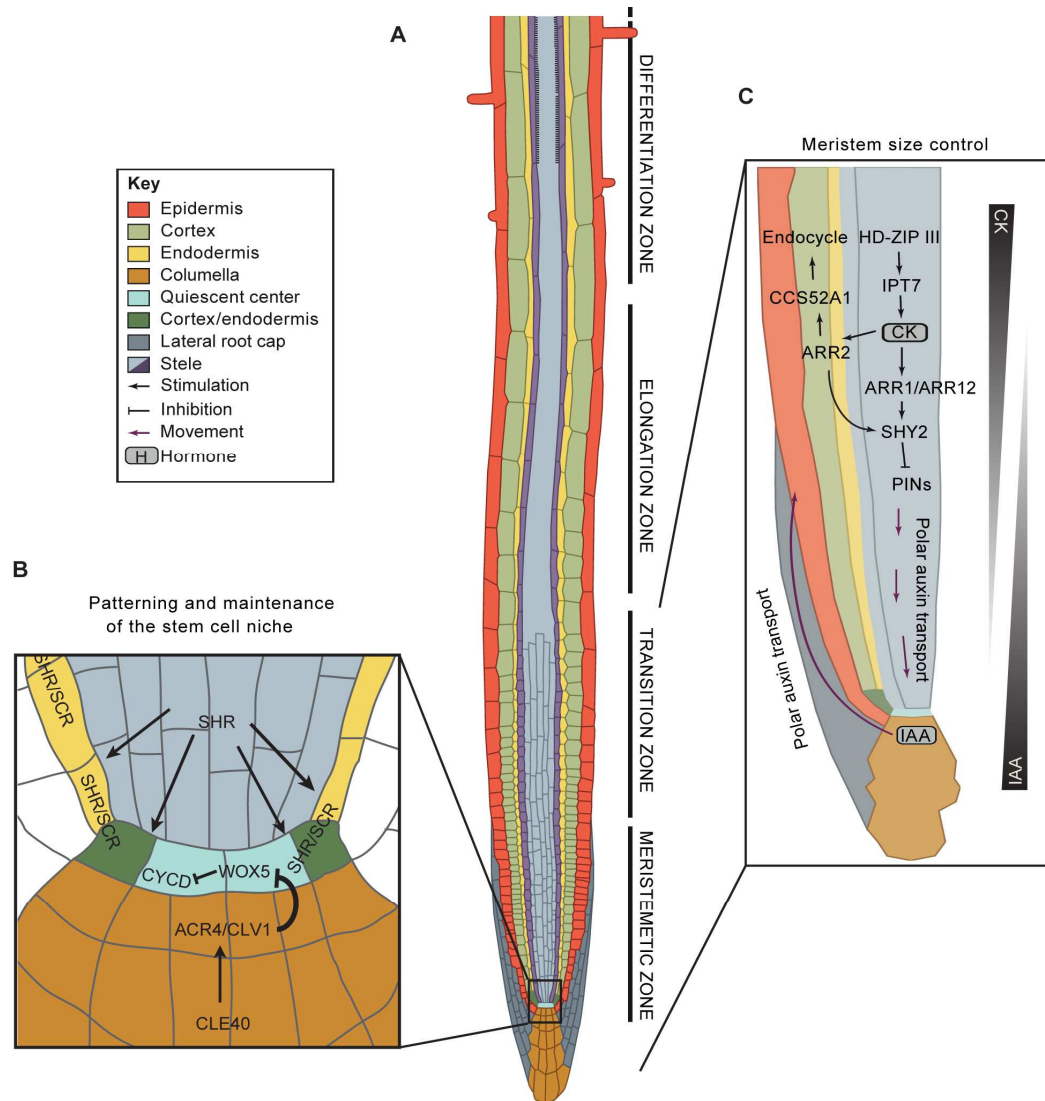


**Figure 1.2 Tissue organization and genetic regulation at the root apical meristem**

**(A)** Schematic representation of whole root longitudinal section. Stem cells are maintained around the quiescent center and generate all cell types of the root. Cells undergo rapid division in the meristematic zone and exit mitotic cycles in the transition zone. The cells then elongate and differentiate. **(B)** Patterning and maintenance of the root apical meristem stem cell niche. *WOX5* is expressed at quiescent center and promotes stem cell identity. The *WOX5-CLE40* feedback loop controls the number of stem cell. *SHR* moves from stele tissue to quiescent center to promote *WOX5* function. **(C)** Root apical meristem size control. Plant hormone auxin (IAA) maximum marks the root stem cell niche. Plant hormone cytokinins (CKs) antagonize auxin and promote cell differentiation at the transition zone. (Adapted from (Wilson et al. 2013))

Similar to the SAM, the positional information that patterns RAM also consists of interacting circuits of mobile peptides and plant hormone signaling modules. The QC promotes stem cell identity of its neighboring cells through a yet unknown mechanism. The *WUS* homolog, *WUSCHEL-RELATED HOMEBOX 5 (WOX5)* is specifically expressed in QC and is required for QC function. *WOX5* suppresses QC mitotic division by repressing CYCLIN D activity (Forzani et al. 2014). Laser ablation of QC, as well as a loss of *WOX5* function lead to differentiation of columella stem cells (Haecker et al. 2004; Sarkar et al. 2007). Conversely, over-expression of *WOX5* generates supernumerary stem cell-like cells (Sarkar et al. 2007). The *CLV3* homolog *CLE40*, is expressed in the columella and encodes a mobile peptide that restricts *WOX5* expression at the QC (Stahl et al. 2009). CLE40 peptide signal is perceived by the ARABIDOPSIS CRINKLY4 (ACR4)/CLV1 receptor like kinases which then promote stem cells differentiation (Stahl et al. 2009). The CLE40-*WOX5* module is similar to CLV3-WUS, in restricting meristem organizer cell population, but different in that CLE40 is expressed in differentiating cells while CLV3 is derived from stem cells. (Figure 1.1B, Figure 1.2B)

While the plant hormone auxin promotes growth and differentiation of organ primordia at the SAM, auxin promotes stem cell identity at the RAM (Sabatini et al. 1999; Petersson et al. 2009). Localization of the polar auxin transporter PIN1 in the root suggests a root-ward-directed auxin flow in the vasculature and a shoot-ward flow of auxin in the lateral root cap and epidermis (Figure 1.2C). Such auxin flow creates the auxin maximum at the QC (Grieneisen et al. 2007; Wisniewska et al.

2006). Auxin signaling mediated by the auxin response regulators including MONOPTEROS then activates *WOX5* expression and specifies QC identity (Sarkar et al. 2007). The QC and stem cells are also promoted by the GRAS family transcription factor SHORTROOT(SHR) and SCARECROW (SCR) (Figure 1.2B). *SHR* is expressed in the stele and moves one layer outside into the endodermis, endodermis/cortex initials and QC to activate the expression of *SCR*. SHR and SCR proteins then form a complex that maintains QC identity (Helariutta et al. 2000; Cui et al. 2007).

In contrast to the SAM, where complex lateral organs are generated immediately off the apex, the RAM is spatially and functionally separated from lateral root initiation. Thus, the size of the RAM is determined by the timing of cell proliferation to differentiation transition, and therefore the relative position of the transition zone (TZ) along the longitudinal axis. Plant hormone cytokinins play an essential role in promoting differentiation and positioning the transition zone through two major pathways (Figure 1.2C). In the first pathway, the cytokinin responsive transcription factor *ARABIDOPSIS RESPONSE REGULATOR (ARR1)* and *ARR12* are specifically expressed at the transition zone and activate the *SHY2/IAA3 (SHY2)* gene, a repressor of the auxin signaling (Dello Ioio et al. 2008). *SHY2* encodes an AUX/IAA protein which mediates the degradation of the polar auxin transporter PIN1. Activation of *SHY2* at the RAM stops the auxin flow, thus repressing cell division and promoting differentiation (Dello Ioio et al. 2008). Alternatively, *ARR2* directly promotes the endocycle onset by activating the expression of *CCS52A1*, an activator of the E3

ubiquitin ligase, anaphase-promoting complex/cyclosome (APC/C) (N. Takahashi et al. 2013). Once entered endocycle, the root cells are committed to differentiation. Cytokinin synthesis is promoted by the *HD-ZIP III* family genes that directly activate the cytokinin synthesis enzyme gene *IPT7* in the root (Ioio et al. 2012). Cytokinin signaling in turn represses the expression of *HD-ZIP III* genes thus forming a feedback loop that balances cell proliferation and differentiation at the RAM (Ioio et al. 2012) (Figure 1.2C). *HD-ZIP III* genes involved in the adaxial/abaxial tissue polarity specification will be introduced in the following section.

## **1.2 Adaxial/Abaxial polarity in plant development**

In plants, the adaxial/abaxial polarity defines an axis of the plant lateral organs relative to the main shoot (longitudinal axis): the side facing the main shoot or closer to SAM is defined as adaxial (ad), while the tissue facing away from the main shoot or SAM is defined as abaxial (ab) (Figure 1.3) (Bowman, Eshed, and Baum 2002; Chandler, Nardmann, and Werr 2008). The ad/ab polarity is exemplified by the leaf upward facing side (adaxial) and downward facing side (abaxial). The first ad identity mutant *phantastica* isolated in *Antirrhinum* produced radial symmetric rod-like structures instead of flat leaves, demonstrating the balance of ad/ab polarity is required for laminar outgrowth and the cell fate determination along the ad/ab axis (Waites and Hudson 1995). Since plant lateral organs are either leaves or modified leaves, proper ad/ab patterning is essential for proper lateral organ formation. Established during embryogenesis, elements of ad/ab tissue polarity are incorporated in the patterning of all major meristems in plant, thus have profound influence on

plant development (reviewed by Aichinger et al. 2012). Here we focus on the ad/ab polarity at the shoot apical meristem and axillary meristem.

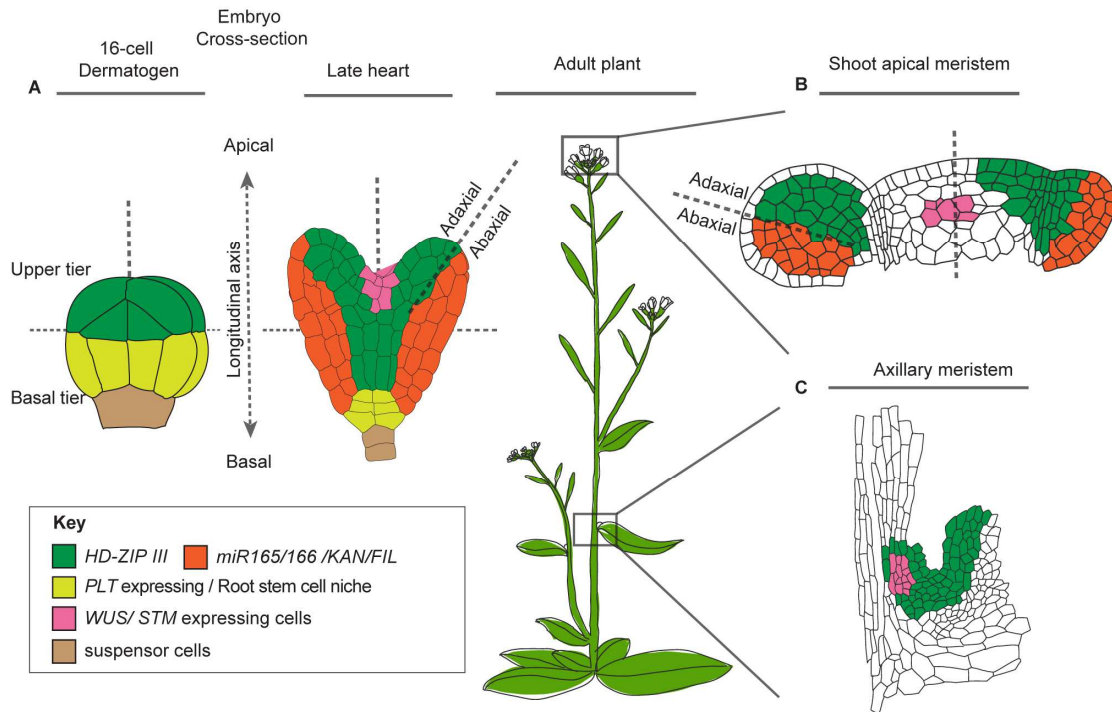


### Figure 1.3 Adaxial/abaxial polarity in plant development

**(A)** Adaxial/abaxial polarity in embryo development. At 16 cell stage, *HD-ZIP III* genes define the apical fate of the upper tier cells while *PLTs* define the basal cell fate. The apical cells later generate all aerial tissue with the shoot apical meristem forming in the center of *HD-ZIP III* expressing domain. The adaxial polarity established by *HD-ZIP III* is antagonized by abaxial factors including *miR165/166*, *KAN* and *FIL*. (Adapted from (ten Hove, Lu, and Weijers 2015) Figure 1). **(B)** Adaxial/abaxial polarity in shoot meristem development in adult plant. Lateral organs adapt adaxial/abaxial polarity as they emerge from the SAM peripheral zone. **(C)** The axillary meristem forms at the leaf axil on the adaxial side. The adaxial environment provided by *HD-ZIP III* function promote the expression of meristem identity gene *STM*.

### 1.2.1 Adaxial/Abaxial polarity defining factors

In *Arabidopsis*, the adaxial identity is promoted by the homeodomain-leucine zipper HD-ZIP III family of transcription factors, PHABULOSA, PHAVOLUTA, REVOLUTA, INCURVATA4 (CORONA/ATHB15) and ATHB8 (Emery et al. 2003; Ruiqin Zhong and Ye 2004; McConnell et al. 2001; McConnell and Barton 1998; Ochando et al. 2008). These transcription factors share a conserved homeobox domain at the N-terminus. The homeodomain is followed by a leucine zipper domain for dimerization and then a putative sterol binding START domain (Prigge and Clark 2006). All five *HD-ZIP III* family genes are targeted by miR165/166, which are specifically expressed at the abaxial (ab) domain, hence restricting the HD-ZIP III function to the ad side of the lateral organ. In addition to miR165/166, other abaxial defining factors that antagonize *HD-ZIP III* gene function include the GRAP family transcription factor KANADI (KAN) and the Zinc-finger transcription factor FILAMENTOUS FLOWER (FIL)/YABBY. ChIP-seq experiments have shown that REV and KAN regulate a cohort of target genes with opposite effect (REV as activator and KAN1 as repressor) (Brandt et al. 2012; Merelo et al. 2013). Ectopic expression of the *HD-ZIP III* genes in the ab domain results in radially symmetric leaves as ab side of the leaf has adopted the ad identity (Emery et al. 2003). Similar adaxialized leaf phenotype were also observed in *KANADI* loss of function mutants or plants with reduced level of miR165/166 (Kerstetter et al. 2001; Yan et al. 2012). Because floral organs evolved from modified leaves, the floral organs of these mutants also display polarity defects, resulting in reduced fertility (Kerstetter et al. 2001; Ruiqin Zhong and Ye 2004). In summary, the major ad/ab polarity defining

factors form antagonistic regulatory modules that regulate lateral organ formation throughout plant development.

### **1.2.2 The adaxial environment promotes shoot meristem activity**

Early during embryogenesis, before adaxial environment is formed, the *HD-ZIP III* genes function as morphogens to specify apical cell fate of the embryo. In 16-cell globular stage embryo, the upper tier cells expressing *HD-ZIP III* genes will generate all aerial shoot tissue (Yoshida et al. 2014). *HD-ZIP III* functions are antagonized by the AP2-domain *PLETHORA(PLT)* family genes expressed in the basal tier of cells (Smith and Long 2010). Expressing one of the *HD-ZIP III* factor *REVOLUTA (REV)* using the *PLT* promoter transformed the RAM into another SAM, producing a “two-headed” embryo (Smith and Long 2010). Thus, adaxial factors dictate shoot fate during embryogenesis and potentiate cells to form shoot meristem.

As the embryo reaches heart stage, the SAM forms in the center of the expanded *HD-ZIP III* genes expression domain and the adaxial/abaxial polarity becomes visible in the two emerging embryonic leaves (Figure 1.3A). The ad/ab polarity is maintained by the antagonizing module between miR165/166, *KANADI(KAN)* family genes and *HD-ZIP III* genes. Having these modules allows defined adaxial domain, which then provides the environment that promotes and maintains the stem cell pool. Over and ectopic accumulation of miR165/166 in the mutant of *ZWILLE/ARGONAUTE10* gene leads to early termination of shoot meristem due to loss of *HD-ZIP III* gene expression (B. Moussian et al. 1998; Bernard Moussian, Haecker, and Laux 2003).

The shoot meristem termination defect of *ago10* mutant can be rescued by expressing a mutant form of *REV* or *PHB* that is resistant to miR165/166 or by knocking down miR165/166 using RNA mimicry (Q. Liu et al. 2009). Similarly, ectopic expression of *KANI* leads to early shoot meristem termination due to its down regulation of *HD-ZIP III* (Kerstetter et al. 2001; Izhaki and Bowman 2007).

Adaxial environment also promotes axillary meristem (AM) formation. Axillary meristems (AMs) are initiated in the leaf axils (between leaves and the main stem) on the adaxial side (Figure 1.3B). AMs differ from the SAMs as they emerge between developed tissues and are responsible for generating side branches. Low auxin at the leaf axils allows the expression of *STM*, which is further activated by the adaxial factor *REV* (Wang et al. 2014; Shi et al. 2016). Loss of function *rev* mutants showed reduced AM formation (Talbert et al. 1995; Otsuga et al. 2001). Furthermore, a dominant gain-of-function allele of *PHB* not only led to adaxialized lateral organs and bigger SAM, but also AM formation on the abaxial side of the leaves (McConnell and Barton 1998).

All together, these data demonstrate that the adaxial environment promotes shoot meristem identity. *HD-ZIP III* factors act to promote adaxial fate and hence may regulate the competence of cells to form meristems in the shoot.

### 1.2.3 *REVOLUTA* function during shoot meristem patterning

*REV* encodes one of the most well studied HD-ZIP III proteins due to its more prominent function among its family members. *rev* loss of function alleles showed early termination of shoot apical meristem and reduced axillary meristems formation due to its mutant effect on reducing ad identify (Talbert et al. 1995); (Prigge et al. 2005b; Otsuga et al. 2001). Although *rev* loss of function mutants can still produce some flowers, most of their flowers are missing floral organs and sterile. Despite the downward curling leaves, the adaxial/abaxial polarity in these mutant leaves are normal due to redundancies among *HD-ZIP III* genes (Talbert et al. 1995).

*PHB* and *PHV* function redundantly with *REV* in promoting meristem formation. Triple mutant of *phb-6 phv-5 rev-9* failed to initiate SAM (Emery et al. 2003). This phenotype is rescued by loss-of-function mutations in the *CNA* and *ATHB8* genes, suggesting *CNA* and *ATHB8* play antagonizing roles with *REV*, *PHB* and *PHV* in meristem formation (Prigge et al. 2005a). Despite the complex redundant and antagonistic relationship among the *HD-ZIP III* family genes, *REV* seems to play a prominent role in meristem regulation as it is the only member whose single loss-of-function alleles showed meristem phenotypes (Prigge et al. 2005a).

*REV* is expressed in the upper layers of the central zone of the SAM and extends to the boundary region before primordium inception (Heisler et al. 2005). Once the primordium is established, *REV* expression is maintained at the adaxial side of the growing organ (Heisler et al. 2005). This dynamic expression pattern suggests *REV*

may be involved in the spatial-temporal regulation of tissue patterning especially at organ boundaries and differentiating organ primordia.

Ectopic expression of *REV* leads to tissue adaxilization and meristem fasciation.

Gain-of-function dominant allele, *rev-10d* (*Ler* ecotype), due to its mutated miR165/166 target sequence, was first discovered for its adaxilized leaves and adaxilized vascular tissue (Emery et al. 2003). The meristem and floral organs are otherwise normal in *rev-10d*. The same mutation was later identified in a different ecotype as *avb1* (*Col-0* ecotype), where the tissue adaxialization extended to floral organs accompanied by over proliferation of shoot meristem cells (Ruiqin Zhong and Ye 2004; R. Zhong and Ye 1999), suggesting that genetic modifiers exist in different backgrounds.

Emerging evidences suggest that *REV* may play a direct role in promoting shoot meristem identity. It has been shown that *REV* binds *STM* promoter and activates *STM* expression both in inflorescence shoot apices and leaf axils (Shi et al. 2016). *REV* directly promotes *WUS* expression during de novo shoot meristem generation in tissue culture (Zhang et al. 2017). Since *STM* and *WUS* are stem cell markers, these data suggest *REV* may promote shoot meristem by directly activating meristem identity genes.

### **1.3 *TSO1* encodes a meristem regulator in *Arabidopsis thaliana***

*TSO1* plays an important role in regulating meristem patterning. The strong allele *tso1-1* was first discovered by Dr. Zhongchi Liu in an EMS mutagenesis for its extremely fasciated SAM and infertility (Z. Liu, Running, and Meyerowitz 1997). The *TSO1* gene was subsequently cloned by the Liu lab (Song et al., 2000). My thesis focuses on elucidating the genetic pathway and molecular mechanism of *TSO1*.

#### **1.3.1 *TSO1* encodes a CHC domain chromatin factor**

*Arabidopsis TSO1* encodes a nuclear protein with two cysteine rich (CXC) domains connected by a conserved hinge region (termed CXC-hinge-CXC (CHC) domain) (Song et al. 2000a). Each CXC domain has 9 invariant cysteines (Cys) with conserved spacing pattern. The CXC domain has been shown to bind zinc in vitro and is essential for *TSO1* function (Andersen et al. 2007; Song et al. 2000a). Mutations altering the conserved cysteine residues resulted in the most severe mutant alleles. The CHC domain defines a small family of proteins that are conserved across plants and animals (but not in fungi and prokaryotes), and play important roles in developmental processes (Z. Liu, Running, and Meyerowitz 1997; Andersen et al. 2007). Eight CHC domain genes exist in *Arabidopsis* and are divided into two clades (Figure 1.4 C) based on sequences alignment of the CHC domain (Figure 1.4 B). Clade I includes *TSO1*, *TSO1-like 1 (SOL1)/At3g22760*, *TSO1-like 2 (SOL2)/At4g14700* and *At3g04850*. Clade II includes the remaining four genes. *TSO1* and *SOL2* are the only genes that have been characterized to have function in meristem patterning and floral organ differentiation (Sijacic et al., 2011).



*sativa*, *M. musculus*, *H. sapiens*, *D. melanogaster*, *C. elegans*, and *D. discoideum* based on an alignment of their CHC domains in **(B)**. Numbers at nodes are bootstrap confidence values, 100 indicating maximum confidence. The bar placed under the tree shows the evolutionary distance corresponding to 0.1 amino acid substitutions per site. (Adapted from (Andersen et al. 2007) Figure 2A)

Other plant CHC domain proteins characterized to date include the soybean CPP1 protein and the maize CBBP protein. The soybean CHC protein CPP1 directly represses the leghemoglobin gene *Gmlbc3* that is involved in symbiotic root nodule formation (Cvitanich et al. 2000). The maize CBBP (CXC domain b1-repeat binding protein) contains two CXC domains. Expressing CBBP by a transgene can silence the *b1* locus and trigger the paramutation phenomenon, where a silenced epiallele is inheritable in transgene free progenies and can induce silencing of an active allele (Brzeska et al. 2010). These studies indicate that CHC domain proteins can bind DNA and mediate transcription or epigenetic regulations.

CHC domain proteins in animals form a distant clade from the plant CHC proteins with limited conservation outside the CHC domain (Figure 1.4C). Functional significance of CHC genes was first revealed by the genetic work from the Robert Horvitz lab regarding *C. elegans* vulva development. Increased activation of the epidermal growth factor (EGF) - RAS pathway resulted in worms with multiple egg-laying organ (vulva), coined the multi-vulva phenotype (Aroian et al. 1990; Beitel, Clark, and Horvitz 1990; Han and Sternberg 1990). The multi-vulva (Muv) phenotype can be caused by combining mutants of two classes of genes: synthetic multivulva (*synMuv*) A and *synMuv*B (Ferguson and Horvitz 1989). While *synMuv*

A class of genes are EGF regulators, the synMuv B class genes encode Retinoblastoma (RB), E2F, E2F dimerization partner (DP) and several other genes, including the *TSO1* homolog, *lin-54* (Ceol and Horvitz 2001; Fay, Han, and Others 2000). Later studies revealed that the homologs of *C.elegans* synMuv B genes encode components of multi-subunit protein complexes that regulate cell cycle gene expression in *Drosophila* and human (Eileen L. Beall et al. 2002; Lewis et al. 2004; Korenjak et al. 2004; Litovchick et al. 2007). Since different variation of the complex was discovered in different developmental context and species, we refer to them in general as DREAM (Sadasivam and DeCaprio 2013). The human DREAM complex has been shown to recruit RB/E2F to repress G1/S genes to remain quiescence and recruit B-Myb to activate G2/M phase genes during G2/M transition (Litovchick et al. 2007). Also, the DREAM complex recruits tissue specific components to integrate cell cycle regulation into specific developmental context (E. L. Beall et al. 2007; Sim et al. 2012). Further, DREAM complex has also been shown to regulate gene expression by mediating histone methylation or recruit repressive histone variants to its target gene body (Sim et al. 2012; Latorre et al. 2015). Thus, the DREAM complex is deemed the master coordinator of cell cycle gene expression with synMuvB proteins forming the invariable core (Sadasivam and DeCaprio 2013). Mutations in DREAM complex components lead to mis-regulation of cell cycle genes and are associated with poor prognosis in various types of cancer (Sadasivam and DeCaprio 2013). Homologs of synMuvB genes exist in *Arabidopsis* and a plant DREAM-like complex have been proposed by Kobayashi et, al (Table 1.1). *Arabidopsis* homologs of RB, E2F and MYB have been shown to function in cell

cycle regulation during developmental (ref). Thus, we hypothesize that TSO1 may function in a plant DREAM-like complex that coordinates cell cycle regulation with developmental processes at the *Arabidopsis* meristems.

Intriguingly, the CXC domain is also found in the SET domain proteins (named after the three genes discovered in *Drosophila*, *Su(var)3-9*, *enhancer of zeste E(z)* and *Trithorax*) (Jenuwein et al. 1998). SET domain proteins consist of major histone lysine methyltransferases (HKMTs) that put methylation marks on the histone tail for epigenetic gene regulation. The E(z) class HKMTs in *Arabidopsis* feature a cysteine rich domain in front of the catalytic SET domain, termed the pre-SET domain. The E(z) pre-SET domain has 8 cysteines that shared nearly identical spacing configuration with the second CXC domain of TSO1. These HKMTs, CURLY LEAF (CLF), Polycomb-Group and MEDEA (MEA), are epigenetic regulators during major developmental transitions, including flowering phase transition and fertilization (Thorstensen, Grini, and Aalen 2011). The E(z) pre-SET domain is conserved between plants and animals and is required for HKMT function of *Drosophila* E(z) and *C.elegans* E(z) orthologs (Ketel et al. 2005). The *Su(var)* class of HKMTs also feature a cysteine rich pre-SET domain. Although the cysteine spacing configuration in the amino acid sequence is markedly different from the TSO1 CXC domains, the *Su(var)* pre-SET domain also forms a zinc-chelating structure (Zhang et al. 2002). The pre-SET domain is indispensable for the function of SUV39 family proteins which mediate both histone and DNA methylation in animals and plants (O'Carroll et al. 2000; Rea et al. 2000; Tachibana et al. 2001; Tamaru and Selker 2001; Jackson et

al. 2002). Structurally similar to the Su(var) pre-SET domain is the CXC-like domain of the *Drosophila* male-specific lethal 2 (MSL2) protein (Zheng et al. 2012). The MSL2 targets the dosage compensation complex to the X chromosome by the CXC-like domain in a sequence-independent manner (Fauth et al. 2010). These structurally similar CXC-like domains are functionally significant in epigenetic chromatin regulation, suggesting that TSO1 may function as a chromatin factor.

### **1.3.2 *TSO1* gene expression**

*TSO1* is expressed at the shoot apical meristem and floral primordia at low level shown by in situ hybridization (Song et al. 2000a; B. A. Hauser et al. 2000). As the floral primordia develop, *TSO1* expression persists in the floral meristem and young floral organ tissues with fast dividing cells. When differentiation is complete and floral organs are fully formed, *TSO1* expression is restricted to the male and female reproductive tissue (Song et al. 2000a; B. A. Hauser et al. 2000). *TSO1* has two putative transcription start sites and the transcripts length appear to be under tissue specific regulation (Song et al. 2000). The *TSO1* homolog, *SOLI*, is also expressed in the reproductive tissues in mature flowers (B. A. Hauser et al. 2000). These expression patterns support TSO1's function in patterning shoot meristem and reproductive organs.

### **1.3.3 Class I *tsol* alleles**

To date, six *tsol* mutant alleles have been identified and they are all recessive mutations (Figure 1.4B). Missense mutations in *tsol-1* and *tsol-2* change the conserved Cys residues in the CXC domains to tyrosine, leading to severe

developmental defects and sterility (Song et al. 2000b; Z. Liu, Running, and Meyerowitz 1997; B. a. Hauser, Villanueva, and Gasser 1998). These two missense mutations that altered the conserved cysteines show strong phenotypes and are grouped together as class I alleles. The remaining 4 alleles can be grouped into class II alleles due to their significantly milder phenotypes. Interestingly, these 4 alleles are caused by T-DNA insertions or nonsense mutations.

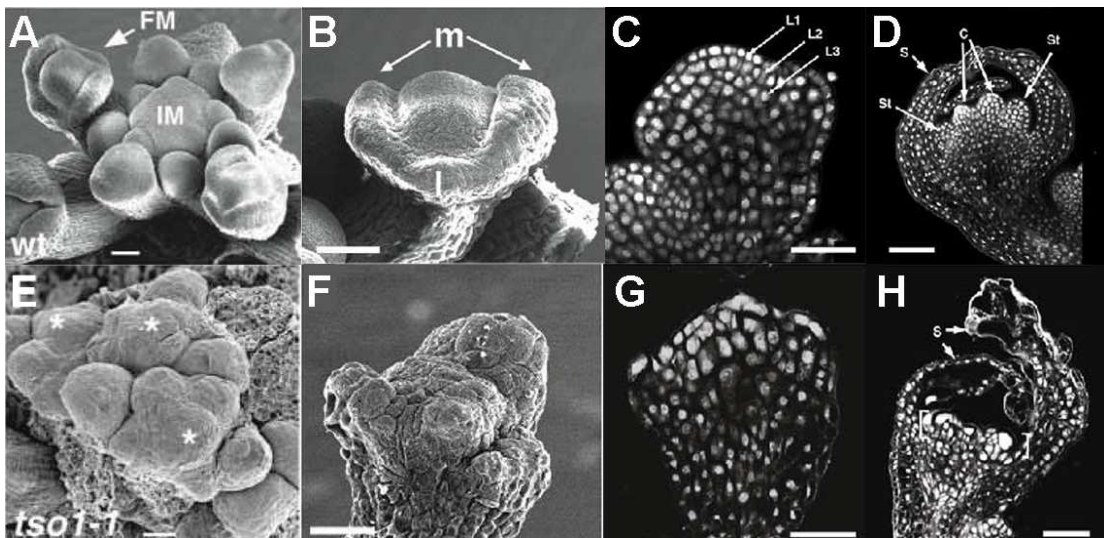


**Figure 1.5 *tso1-1* mutant shoot apical meristem and floral meristem phenotype** (A) A wild type inflorescence meristem. (B) A wild type floral meristem. (C) A wild type stage 3 floral meristem. (D) A wild type stage 6-7 floral meristem with floral organs. (E) A *tso1-1* mutant shoot apex. Three inflorescence meristems are formed on the same shoot apex; each indicated by an asterisk. (F) A *tso1-1* mutant floral meristem with flat SAM dome. (G) A *tso1-1* mutant stage 3 floral meristem. (H) A *tso1-1* stage 6 or 7 floral meristem. Shown are two abnormal sepals, interior to which no floral organ develops. A, B, E, F: SEM pictures. C, D, G, H: Confocal microscopy. Tissues stained with propidium iodide (PI). Bar 20 um in A, B, D, F; 25 um in C, G; 50um in D,H. (Adapted from Song et al. 2000b; Z. Liu, Running, and Meyerowitz 1997)

The shoot apical meristems (SAMs) of the class I mutants are enlarged and frequently split into two or more meristems (Figure 1.5, 1.6). Stem-cell marker genes *WUS* and *CLV3* expression revealed by  $\beta$ -glucuronidase (GUS) transcriptional reporter showed multiple meristem centers (Paja Sijacic unpublished data). Electron microscopy of meristem sections showed aberrant nuclear shape, incompletely formed cell wall and increased DNA ploidy, indicating severe defects in cell division (Z. Liu, Running, and Meyerowitz 1997). *tso1-1* flowers fail to form discernible inner whorl floral organs, resulting in sterile flowers with only distorted sepals (Figure 1.5, 1.6B) (Z. Liu, Running, and Meyerowitz 1997). Thus, the phenotypes of *tso1-1* mutant at shoot meristems could be categorized into two aspects: over proliferation of meristems and lack of differentiation of floral organs, suggesting a role of *TSO1* in repressing cell proliferation and promoting cell differentiation at SAM.

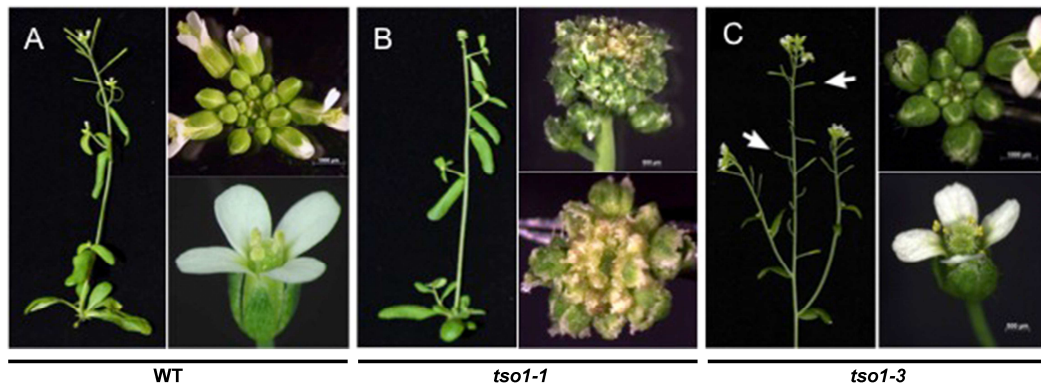


**Figure 1.6 Two classes of *TSO1* mutant alleles**

(A) A wild type (WT) plant with limited secondary branches and normal seed pods (siliques). A normal inflorescence and a flower are also shown. (B) A young *tso1-1* plant, which represents an example of class I *tso1* mutant. Severe meristem fasciation and failure of proper floral organ formation are shown. (C) A *tso1-3* plant, which represents Class II alleles. Reduced fertility is evident, indicated by smaller seed pods (arrows). Normal inflorescence and flower are shown.

#### **1.3.4 Class II *tso1* alleles**

The *tso1-3* (same mutation as *tso1-4*) allele is caused by a nonsense mutation that resulted in a truncated TSO1 missing the hinge domain, the second CXC domain, and the putative coiled-coil domain (B. a. Hauser, Villanueva, and Gasser 1998). *tso1-5* and *tso1-6* are caused by T-DNA insertions that led to unstable transcripts. Both *tso1-3* and *tso1-5* are grouped as class II alleles and show weaker and different phenotypes when compared to class I alleles (*tso1-1* and *tso1-2*) (Liu et al. 1997; Hauser et al. 1998; Song et al. 2000).

Since class I mutants failed to develop floral organs, their effects on gamete development is not known. However, class II alleles, which develop normal floral organs and do not show any meristem fasciation, exhibited severely reduced fertility (Figure 1.6C). The *tso1-3* allele often produces aberrant ovules without embryo sack (B. a. Hauser, Villanueva, and Gasser 1998). Although the cells in the ovule structure are sometimes misshapen, the partially formed cell wall phenotype of the Class I alleles was not observed (B. a. Hauser, Villanueva, and Gasser 1998). Similar ovule phenotype was observed in *tso1-5* and *tso1-6* (Andersen et al. 2007). In addition, the *tso1-5* and *tso1-6* produced enlarged and collapsed pollen grains (Andersen et al. 2007). Thus, the Class II alleles of *TSO1* are defective in male and female reproductive tissues and gametogenesis.

#### **1.3.5 Class I *tso1* alleles are recessive antimorphic alleles**

Work reported by our lab revealed that the class I alleles not only lost *TSO1* function but also disrupted the function of *TSO1* homolog *SOL2*, which led to a severe

phenotype (Sijacic, Wang, and Liu 2011). This was shown by artificial microRNA knockdown of *tso1-1* transcripts in *tso1-1* plants, which converted the class I allele to resemble class II alleles in phenotype. Further, when we combined class II alleles (*tso1-3* or *tso1-5*) with a loss-of-function allele of *SOL2* (*sol2-1* or *sol2-2*), the resulting *tso1-3; sol2-1* mutant plants showed class I allele phenotype including fasciated SAM and deformed floral organs. Thus, we concluded that Class II alleles (*tso1-3*, and *tso1-5*) are null or close to null alleles while class I alleles are recessive antimorphic alleles that possess the ability to disrupt the function of *SOL2*, a *TSO1* homolog. To further support this notion, I showed that the mutant *TSO1-1* protein could directly interacted with *SOL2* protein in BiFC assay in tobacco leaf cells. The wild type *TSO1* protein could interact with itself but not with *SOL2* (Figure 1.7). These results provided a potential mechanism for why *tso1-1* interferes with *SOL2* function (Sijacic et al.,2011).

Based on our analysis of *tso1* mutant alleles and surveys of *Arabidopsis* literature, we found that recessive point mutations that overcome gene family redundancy and show more severe phenotypes than null alleles are commonly found in *Arabidopsis*. We proposed that antimorphism is not limited to mutant allele interfering with its own locus (dominant), but also includes interference with related loci (recessive). The renewed concept of antimorphism reflects the complexity of genome architecture and has broad implications for understanding mutant alleles in both agriculture and medicine.

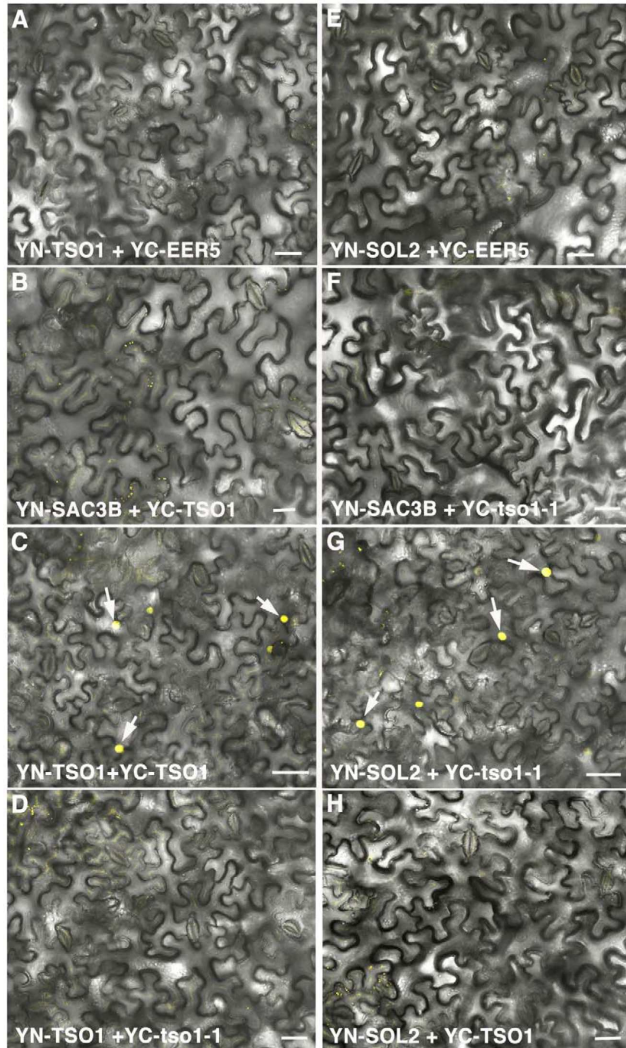


**Figure 1.7 BiFC analyses showing TSO1 to TSO1 as well as tso1-1 to SOL2 interactions**

Protein-protein Interactions were detected by YFP reconstitution between the YN and YC fusion proteins, leading to yellow fluorescence shown by single confocal section images overlaid with Nomarsky differential interference contrast (DIC) images. YC-EER5 and YN-SAC3B nuclear proteins serve as negative controls as they function in unrelated processes from TSO1 or SOL2. Arrows point to nuclei expressing YFP fluorescence. Scale bars represent 50 mm. **(A-B)** Negative control combination of YN-TSO1 with YC-EER5 (**A**), or YN-SAC3B with YC-TSO1 (**B**). **(C)** Positive interaction between YN-TSO1 and YC-TSO1 indicated by fluorescent nuclei (arrows). **(D)** An absence of interaction between YN-TSO1 and YC-tso1-1 indicated by an absence of fluorescent signals. **(E-F)** Negative control combination of YNSOL2 with YC-EER5 (**E**), or YN-SAC3B with YC-tso1-1 (**F**). **(G)** in vivo interaction between YN-SOL2 and YC-tso1-1 shown by fluorescent nuclei (arrows). **(H)** An absence of interaction between YN-SOL2 and YC-TSO1. Image taken from doi:10.1371/journal.pgen.1002352.g006

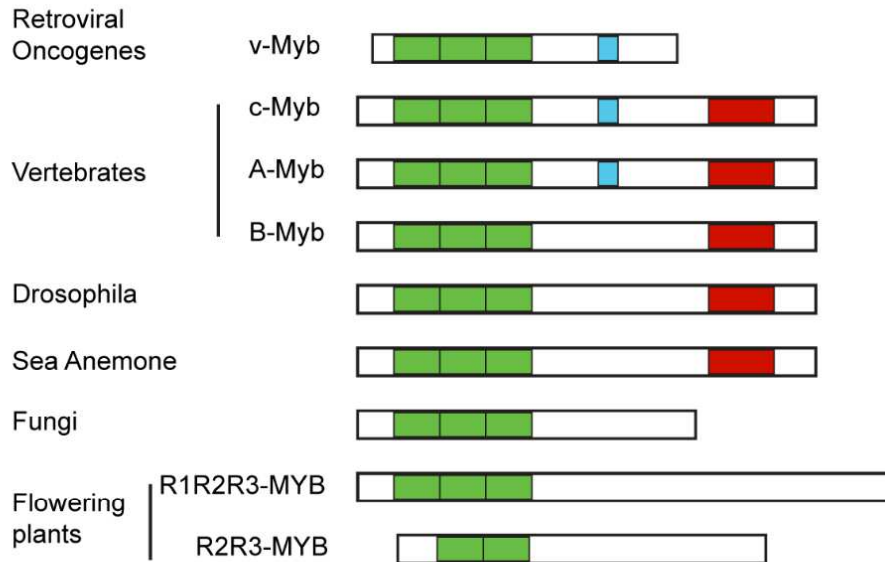
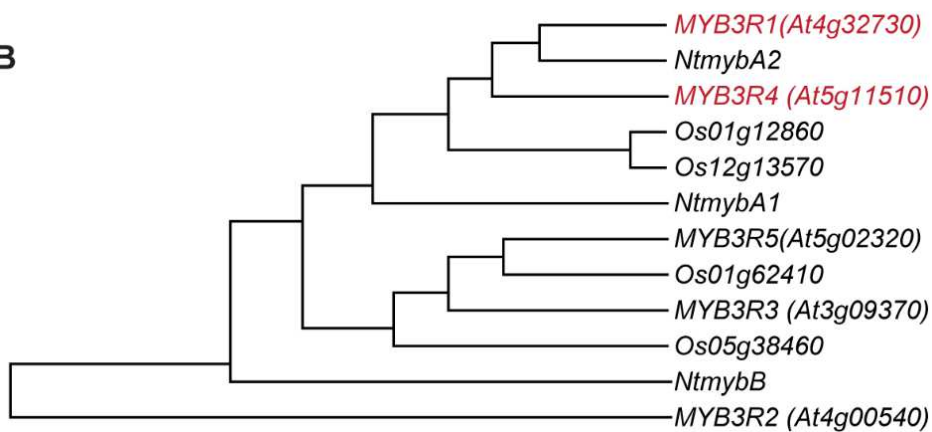
## 1.4 MYB proteins in animals and plants

### 1.4.1 Myb proteins in animals

The *Myb* gene was first discovered as the oncoprotein in myeloblastosis produced by avian retroviruses AMV and E26 (Klempnauer and Bishop 1984; Gerondakis and Bishop 1986; Beug et al. 1979). Through reverse transcription, the retroviruses produced viral Myb (v-Myb) that drove the leukaemia phenotype in animals (Klempnauer and Bishop 1984; Beug et al. 1979). The human Myb transcription factor family consists of three genes, *c-Myb*, *A-Myb* (*MYBL1*) and *B-Myb* (*MBL2*) (Figure 1.8). All studied vertebrates to date have orthologs of these three *Myb* genes. Animal Myb proteins share three conserved DNA binding repeats (R1, R2, and R3) and bind DNA through the t/cAACT/gG motif (Biedenkapp et al. 1988).

Both *c-Myb* and *A-Myb* encode transcription activators that are expressed in specific tissues. *c-Myb* is expressed at the bone marrow, colonic crypt and neurogenic stem cell niches and is required for the self-renewal of these stem cell populations. These same tissues are subject to oncogenesis when *c-Myb* is over or ectopically expressed (Ramsay and Gonda 2008). *A-Myb* functions in a similar manner as *c-Myb* at the spermatogenic tissue, the mammary gland, the central nervous system and lymphocytes (Trauth et al. 1994). In contrast, *B-Myb* is more ubiquitously expressed in all dividing cells and loss of function leads to early embryo lethality (Tanaka et al. 1999). Although B-Myb lacks the transcription activation domain that's conserved between c-Myb and A-Myb, B-Myb also function as transcription activators of G2/M phase cell cycle genes (Simon, Stone, and Sidow 2002; Zhu, Giangrande, and Nevins

2004). *Drosophila* has a single *Myb* gene that encodes a protein lacking the central activation domain conserved in vertebrate c-Myb and A-Myb (Katzen, Kornberg, and Bishop 1985). The *Drosophila Myb* knockout mutant exhibits hemocyte and lymph gland developmental defects and could only be complemented by the vertebrate B-Myb, but not c-Myb and A-Myb (Davidson et al. 2005). Thus, vertebrate *B-Myb* is the ortholog to *Drosophila Myb* gene and likely resembles a more ancient form. Hence, *c-Myb* and *A-Myb* likely evolved from gene duplication events and are integrated into specific stem cell niches (Lipsick 2004). *Myb* gene seems to have been lost during evolution of the *C.elegans*.

**A****B****Figure 1.8 MYB proteins in eukaryotes**

(A) Schematic representation of MYB proteins encoded by representative eukaryotic organisms. The DNA binding repeats are labeled in green, the transcriptional activation domain is labeled in blue, and the negative regulatory domain is labeled in red. (Adapted from (Davidson et al. 2005) Figure 6 and

[https://www.stanford.edu/group/lipsick/cgi-bin/wordpress/?page\\_id=369](https://www.stanford.edu/group/lipsick/cgi-bin/wordpress/?page_id=369))

(B) Phylogenetic relationship of MYB3R proteins in plants. The phylogenetic tree was constructed based on the amino acid sequence similarities in the Myb domains of MYB3R proteins from tobacco (*NtmybA1*, *NtmybA2* and *NtmybB*), *Arabidopsis* (*MYB3R1*-*MYB3R5*) and rice (*Os01g12860*, *Os12g13570*, *Os01g62410* and *Os05g38460*). (Adapted from (Haga et al. 2007) Figure 1A) *MYB3R1* and *MYB3R4* related to this study is labeled in red.

#### 1.4.2 DREAM complex and B-Myb

The human DREAM complex exists in two distinct states during the progression of the cell cycle (Figure 1.9). In G<sub>0</sub> phase or quiescence, the MuvB core binds to RB and the repressive E2Fs to repress cell cycle genes, including *B-Myb* (Litovchick et al. 2007). Once the G<sub>1</sub>/S checkpoint is satisfied, RB is phosphorylated by the D-cyclin-dependent kinase and dissociate from the repressive E2Fs and the MuvB core (Litovchick et al. 2007). The activator E2Fs subsequently bind the promoters of the early cell cycle genes to facilitate the G<sub>1</sub>/S transition (Y. Takahashi, Rayman, and Dynlacht 2000). At G<sub>2</sub>/M transition, B-Myb and MuvB core bind to the promoter of G<sub>2</sub>/M genes in a co-dependent manner and activate G<sub>2</sub>/M genes expression (Sadasivam, Duan, and DeCaprio 2012; Litovchick et al. 2007). B-Myb function requires phosphorylation by the Cyclin A-CDK2 and is attenuated by the degradation of anaphase promoting complex/cyclosome (APC/C) (Figure 1.9). Thus, the MuvB core of DREAM complex orchestrates the timed expression of hundreds of cell cycle genes.

Importantly, B-Myb is both a target (during G<sub>0</sub>) and a component (during S-G<sub>2</sub>-M) of the DREAM complex. *B-Myb* is repressed by the dREAM complex at G<sub>0</sub> and the B-Myb protein is a component of DREAM and activates G<sub>2</sub>/M genes to facilitate cell cycle completion and exit. Overexpression of *B-Myb* and its target genes are found in tumors and is associated with poor prognosis in breast cancer patients (Perou et al. 2000; Thorner et al. 2009). On the other hand, loss of function *B-Myb* mutants often exhibit mitotic defects associated with reduced late cell cycle genes expression (Sadasivam, Duan, and DeCaprio 2012; Zhan et al. 2012). Because of the cooperative

relationship between B-Myb and MuvB core, disruptions of the MuvB core also lead to G2/M defects. Knocking down *Lin9* leads to mitotic arrest in cultured cells and in mice (Knight, Notaridou, and Watson 2009; Reichert et al. 2010). Knocking down *LIN54* by RNAi or expressing a mutated *LIN54* with a substitution of the conserved cysteine in the CXC domain lead to down regulation of late cell cycle genes and cytokinesis defects (Schmit, Cremer, and Gaubatz 2009; Kittler et al. 2007; Matsuo et al. 2012). These G2/M defects are reminiscent of *tso1-1* cytokinesis defects at the SAM.

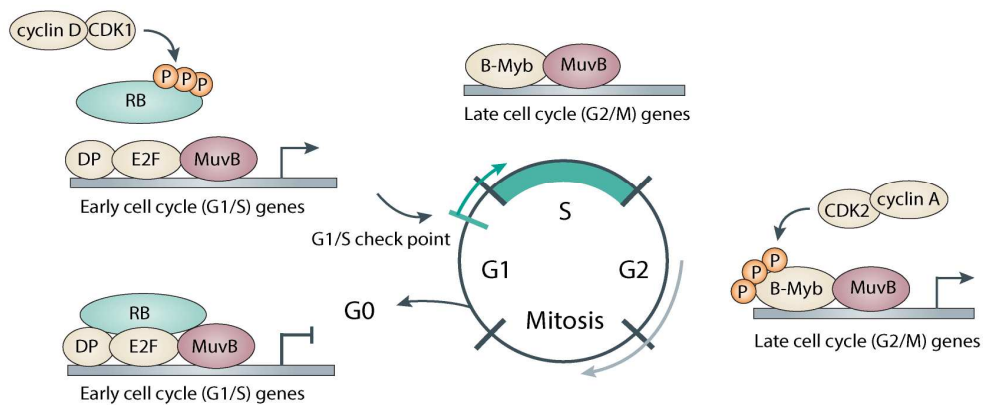


### Figure 1.9 DREAM complex coordinates cell cycle gene expression

In G0, the DREAM complex MuvB core is bound by the RB/DP/E2F transcription repressors to repress early cell cycle genes expression and to maintain quiescence. Once proliferation signal is perceived, RB is phosphorylated by the cyclin D-CDK1 and dissociates from the MuvB core. Release of RB suppression allows for the expression of early cell cycle genes and cell cycle entry. During S phase, the MuvB core and B-Myb bind to the late cell cycle genes promoter in a co-dependent manner. B-Myb is subsequently phosphorylated by cyclin A-CDK2 and activates late cell cycle genes expression to allow for G2/M transition. (Adapted from (Sadasivam and DeCaprio 2013))

### 1.4.3 MYB3R proteins in plants

In plants, the *MYB* gene family expanded significantly especially with large numbers of the R2R3 type *MYB* genes. (Stracke, Werber, and Weisshaar 2001). The *Arabidopsis* genome encodes 5 MYB proteins with all 3 conserved DNA binding repeats (R1R2R3-MYB) and 125 MYB proteins with only the second and third DNA binding repeats (R2R3-MYB) (Table 1.1) (Figure 1.8). Although R2R3-MYB genes were long thought to evolve from R1R2R3-MYB proteins, a recent analysis proposed that the R2R3-MYBs represent the more ancient form of MYB proteins that existed in the plant and animal common ancestor (Du et al. 2015). In plants, the large number of R2R3-MYB proteins regulate diverse biological processes from development, metabolism to response to environmental challenges (Dubos et al. 2010). In contrast, the R1R2R3-MYB proteins seem to carry out the conserved function of cell cycle regulation just as the animal Myb proteins do (Ito 2005; Haga et al. 2007). Among the five R1R2R3-Myb genes in *Arabidopsis* (*MYB3R1* to *MYB3R5*), the closely related *MYB3R1* and *MYB3R4* have been shown to promote the expression of G2/M-specific genes in leaf stomatal cells; these G2/M target genes include the B1 type cyclin *CYCB1* and the plant specific syntaxin *KNOLLE(KN)* involved in plant cell cytokinesis (Haga et al. 2007). Double mutant of *myb3r1;myb3r4* showed cytokinesis defects in embryos and leaf stomatal development (Haga et al. 2007, 2011). *MYB3R4* has been shown to form a complex with the activator type E2F protein, consistent with its role as an activator of G2/M phase genes (Kobayashi et al. 2015). On the other hand, *MYB3R3* was shown to form a repressor complex with repressor E2F and RB and repress G2/M specific genes (Kobayashi et al. 2015). Single mutants of

*myb3r* do not show changes in G2/M gene expression nor mitotic defects. Only *myb3r1;myb3r4* double mutant and *myb3r1;myb3r3;myb3r5* triple mutants exhibited G2/M gene expression changes and cell cycle related phenotypes, suggesting that the *Arabidopsis* MYB3R1 function redundantly with both activator and repressor MYB3R genes and plays a unique role among the 5 MYB3R proteins in *Arabidopsis* (Kobayashi et al. 2015). Based on these data, MYB3R proteins are grouped into activator MYB3Rs (MYB3R1 and MYB3R4) and repressor MYB3Rs (MYB3R1, MYB3R3 and MYB3R5).

DREAM complex components

Human	<i>Drosophila</i>	<i>C.elegans</i>	<i>Arabidopsis</i>		Representative references/Remarks		
			AGI code	Protein name			
MYBL2	Myb		At4g32730	MYB3R1	Haga et al., 2007; Ito 2005		
			At5g00540	MYB3R2	Ito, 2005		
			At3g09370	MYB3R3	Ito, 2005; this study		
			At5g11510	MYB3R4	Haga et al., 2007; Ito 2005		
			At5g02320	MYB3R5	Ito, 2005; this study		
E2F	E2f2	EFL-1	At2g36010	E2FA	Mariconti et al., 2002; De Veylder et al., 2002		
			At5g22220	E2FB	Mariconti et al., 2002; Magyar et al., 2005		
			At1g47870	E2FC	Mariconti et al., 2002; del Pozo et al., 2006		
			At5g14960	E2FD/DEL2	Mariconti et al., 2002; Sozzani et al., 2010		
			At3g48160	E2FE/DEL1	Mariconti et al., 2002; Vlieghe et al., 2005		
			At3g01330	E2FF/DEL3	Mariconti et al., 2002; Vlieghe et al., 2005		
DP	Dp	DPL-1	At5g02470	DPa	Magyar et al., 2000; De Veylder et al., 2002		
			At5g03415	DPb	Magyar et al., 2000; del Pozo et al., 2006		
RBL	Rbf	LIN-35	At3g12280	RBR	Ebel et al., 2004; Mariconti et al., 2005		
LIN-9	Mip130	LIN-9	At5g27610	ALY1	Bhatt et al., 2004; Bowen et al., 2010 Plant homologs specifically contain Myb domain		
			At3g05380	ALY2			
			At3g21430	ALY3			
LIN-54	Mip120	LIN-54	At5g25790	SOL1	Song et al., 2000; Hauser et al., 2000; Andersen et al., 2007; Sijacic et al., 2011  Plant homologs constitute a family of Tesmin/ TSO-like CXC domain-containing proteins		
			At4g29000				
			At2g20110				
			At3g22760				
			At4g14770			SOL2	
			At3g15160				
	At3g22780	TSO1					
LIN-37	Mip40	LIN-37			no homolog in <i>Arabidopsis</i>		
LIN-52	dLin52	LIN-52			no homolog in <i>Arabidopsis</i>		
RBBP4	Caf1	LIN-53	At5g58230	MSI1	Guillon and Berger, 2005; Bouveret et al., 2006		
				At2g16780		MSI2	
				At4g35050		MSI3	
				At2g19520		MSI4	Pazhouhandeh et al., 2011
				At4g29730		MSI5	Xu et al., 2013
L3MBTL	L(3)mbt	LIN-61			no homolog in <i>Arabidopsis</i>		
HDAC1/2	Ppd3	HDA-1	AT4G38130	HDA1	for review, see Hollender and Liu, 2008		
			AT5G26040	HDA2			
			AT5G61060	HDA5			
			AT5G63110	HDA6			
			AT5G35600	HDA7			
			AT1G08460	HDA8			
			AT3G44680	HDA9			
			AT3G44660	HDA10			
			AT4G33470	HDA14			
			AT3G18520	HDA15			
			AT3G44490	HDA17			
			AT5G61070	HDA18			

**Table 1.1** List of *Arabidopsis* homologs of DREAM complex components from human, fly and worm. (Adapted from (Kobayashi et al. 2015) supplemental table S6). The MuvB core components were shaded in green.

## 1.5 Concluding remarks

The *Arabidopsis TSO1* gene with its fascinating collection of mutant alleles provides a unique opportunity to investigate mechanisms of stem cell maintenance, lateral organ growth and differentiation. Through my Ph.D study, I utilized the plethora of tools available for the model organism *Arabidopsis thaliana* to uncover the *TSO1* genetic pathway. I screened, identified, and characterized several genetic modifiers of *tso1-1* mutant, taking advantage of genome sequencing technology and CRISPR-CAS9 genome editing tools. My work demonstrates that *TSO1* forms a regulatory module with *MYB3R1* to balance cell proliferation with differentiation (Chapter II). The *TSO1-MYB3R1* module likely functions as a protein complex that resembles the animal DREAM complex, which regulates cell cycle progression. My work on another genetic modifier of *tso1* led to the identification of an *HD-ZIP III* class gene *REV*. By repressing *REV*, the *TSO1-MYB3R1* module attenuates the meristem promoting effect of *REV* and the adaxial polarity of lateral organs (Chapter III). Chapter IV analyzed yet another modifier, whose function is not yet established.

These discoveries establish *TSO1* and *TSO1-MYB3R1* module as the key coordinator between cell proliferation and differentiation at plant meristems and provide explanations and insights into various defects exhibited by *tso1* mutants (Chapter II). Further, the thesis work revealed a cell-cycle regulating machinery shared between plants and animals. The involvement of this common module in plant organ polarity regulation shed light on how such as a common cell cycle regulatory module is incorporated into plant-specific transcriptional network for polarity establishment

(Chapter III). A novel gene identified in the *TSO1* pathway (Chapter IV), as well as other as yet uncharacterized enhancers and suppressors, provided a rich resource to uncover previously unknown genes, gene networks, and functional interactions during higher plant meristem development.

## Chapter 2: *TSO1-MYB3R1* regulatory module at the shoot and root meristems

### 2.1 Introduction

Fundamental to the proper development of a multicellular organism is the progressive differentiation of stem cells with a more restricted cell fate. Both genetic and epigenetic regulators gradually stabilize the specialized gene expression programs and hence specialized cell fate. A simultaneous change in a cell that accompanies cell fate specialization is the underlying cell cycle regulation. Undifferentiated cells retain the ability to rapidly proliferate upon inductive cues while differentiated cells appear to “permanently” exit the cell cycle and express highly specialized morphology and function.

Disruption of cell cycle control lead to development disorder such as cancer, as cancerous cells often proliferate and fail to commit to a normal cell type. And many proto-oncogenes or cancer suppressor genes encode cell cycle regulators such as B-Myb and Retinoblastoma (RB), respectively. RB binds to E2F transcription factors during G1 phase and inhibit the cells from passing the G1/S checkpoint (Cam et al. 2004; Litovchick et al. 2007). However, CDK-Cyclin-mediated phosphorylation of RB resulted in release of E2F, allowing E2F to activate genes involved in DNA synthesis and cells entering the S phase of the cell cycle (Weinberg 1995). Loss-of-function mutations in the *Rb* gene or reduced expression of *Rb* due to alteration in *Rb* regulators are common themes in cancer (Sherr and McCormick 2002). The *B-Myb* genes on the other hand encode activators of G2/M genes involved in mitosis. While

loss of B-Myb leads to G2/M defects (Sadasivam et al. 2012; Zhan et al. 2012), overexpression of *B-Myb* is correlated with poor prognosis in breast cancer (Amatschek et al. 2004). Therefore, understanding the mechanism of how genes coordinate cell cycle with cell fate commitment is critical to the understanding of cancer initiation and development.

In the past 10-15 years, a multiprotein complex, the DREAM complex, has gained increasing recognition as a critical cell cycle regulatory complex that not only coordinates G1/S with G2/M phases but also maintains cells at the G0 quiescent phase. Initially found and biochemically characterized in *Drosophila*, *C. elegans*, and mammals, the core complex consists of five conserved members: LIN9, LIN37, LIN52, LIN53, LIN54 (Sadasivam and DeCaprio 2013). Depending on the organism, these components are also called MIP (MYB-Interacting Protein) or MuvB (Multivulva class B proteins) (Beall et al. 2007; Ceol and Horvitz 2001). The core complex (termed MuvB core) associates with different co-factors at different cell cycle phases. In G0 phase, the core complex binds to RB-like pocket proteins (p130 or p107) and repressor E2F/DP to control the G1 to S checkpoint (Litovchick et al. 2007). Once a cell enters the S phase, the DREAM core complex recruits B-Myb and then recruits FOXM1 to the promoters of G2/M phase-expressed genes to promote their expression (Sadasivam et al. 2012). Hence the core complex, depending on which co-factors it binds or associates with, supports either repression or activation of gene expression and plays a critical role in regulating cell-cycle phase-specific gene expression. Interestingly, in *Drosophila*, *myb* mutant adult lethality can be suppressed

by mutations in the core component (LIN9/mip130/ALY) (Beall et al. 2004), suggesting that B-Myb and MuvB core component are interdependent for their normal function. Although tremendous knowledge about cell cycle were gained from animal cell lines, less is known about how cell cycle control is integrated into specific developmental context.

In contrast to animals where cell lineage commitment occurs during embryogenesis, plants maintain stem cells at the growing tips (meristems) and generate new organs de novo throughout life span. The progenies of the stem cells go through rapid proliferation and quickly differentiate. Plant cells have high developmental plasticity and acquire cell fate mainly from positional cues rather than lineage information. Thus, the interplay between cell cycle and developmental context is at the center of the stage.

Plants and animals shared conserved cell cycle regulation machinery. In addition to the conserved cyclin-CDKs system, recently the DREAM complexes have also been isolated (Kobayashi et al., 2015; Fischer and DeCaprio, 2015). While human DREAM has one activator B-Myb, *Drosophila* Myb is both an activator and repressor, *Arabidopsis* genome has 5 MYB3R genes that are divided into activator and repressor MYB3Rs (Kobayashi et al. 2015); both activator and repressor MYB3Rs appear to bind to the DREAM core complex (TCX5, ALY2, ALY3, RBR1) and regulate G2/M cell cycle genes (Kobayashi et al. 2015). While the core complex associates with activator MYB3R (MYB3R4) and the activator E2Fs (E2FB) to activate G2/M phase-specific gene expression, the core complex also associates with

the repressor MYB3R (MYB3R3) and E2FC to repress G2/M genes to maintain quiescence or enter endocycle (Kobayashi et al. 2015; Fischer and DeCaprio 2015). Therefore, one obvious complication for the plant DREAM core complex when compared with the animal DREAM core complex is that each of the core complex component can have either activator or repressor MYBs as well as activator or repressor E2Fs.

The discovery of the DREAM complex in *Arabidopsis* offers an exciting opportunity to investigate the conserved cell cycle regulating machinery in the plant developmental scheme. What are the phenotypes of the core complex components? How do the mutant members of the DREAM core complex genetically interact? What is the mechanism of coordination between cell cycle regulation and plant organ development and differentiation? Could the unique features of a plant DREAM complex underlie the plasticity of higher plant development? The excellent genetic system and molecular tools in *Arabidopsis* offers an unprecedented opportunity to address these questions.

To address the question of how TSO1, homolog of the DREAM complex core component LIN54, affect stem cells at SAM and RAM as well as floral organ development and differentiation, I have taken a genetic approach to identify genetic interactors. The hypothesis is that if TSO1 acts in a plant DREAM-like complex, mutations in components of this complex could be identified as suppressors or enhancers of the *tsol* mutation. These genetic interactors will provide mechanistic

insights to how TSO1 regulates plant stem cells.

## **2.2 Material and methods**

### **Plant materials and growth conditions**

*Arabidopsis thaliana* ecotype Landsberg *erecta* (*Ler*) was used as the wild type. All mutants are in the *Ler*-0 background and were described previously: *tso1-1* (Liu, Running, and Meyerowitz 1997), *tso1-1*<sup>+/+</sup>*sup-5* (Sijacic, Wang, and Liu 2011) and *tso1-3* (Hauser, Villanueva, and Gasser 1998). *tso1-3*<sup>+/+</sup>*sup-5* heterozygous line was created by crossing *tso1-3* stigma with *sup-5* (Gaiser, Robinson-Beers, and Gasser 1995) pollen. dCAPs markers used to genotype these mutant alleles were also described previously (Sijacic, Wang, and Liu 2011).

Plants were grown on Metromix soil (Griffin) under a 16 hour light-8 hour dark cycle at 25°C. Sterilized seeds were germinated on half-strength Murashige and Skoog (1/2 MS) medium containing 1% (w/v) sucrose and 0.6% (w/v) phyto agar.

### **Vector construction and plant transformation**

To construct 35S::TSO1-GR, full length TSO1 cDNA was amplified from floral RNA with primer TSO1-GR.F and TSO1-GR.R (Table 2.1) containing BamHI sites and the PCR fragment was inserted into pBI121(Clontech)-based pBI-ΔGRBX vector (Lloyd et al. 1994) at the BamHI site. The construct was transformed into *tso1-1*<sup>+/+</sup>*sup-5* heterozygous plants via *Agrobacterium* (GV3101). Plants that are homozygous for both *tso1-1* and 35S::TSO1-GR transgene were identified through PCR genotyping. One line was chosen due to good rescue of the *tso1-1* phenotype by dexamethasone

(DEX) treatment. DEX was sprayed daily to plant shoots for 10 days at 50  $\mu$ M concentration. DEX was dissolved in water containing 0.015% Silwet L-77.

To generate *pTSO1::TSO1-GFP* and *pTSO1::TSO1-cMyc* translational fusion lines, 4.1kb TSO1 genomic sequence containing 1kb promoter and full length coding region (without the stop codon) was PCR amplified using Phusion® (NEB) with primers TSO1.geno.F and TSO1.geno.R (Table 2.1) and cloned into pCR8/GW/TOPO®. After sequence confirmation, the genomic fragment was recombined into pMDC107 (Curtis and Grossniklaus 2003) and pEarlyGate303 (Earley et al. 2006) to create *pTSO1::TSO1-GFP* and *pTSO1::TSO1-cMyc*, respectively. These constructs were introduced into *tsol-1+/+sup-5*. T2 plants homozygous for *tsol-1* and the transgene were subsequently identified through PCR genotyping.

*pMYB3R1::GUS* and *pMYB3R4::GUS* reporter constructs were generously provided by Masaki Ito (Haga et al. 2007). Because of antibiotic selection incompatibility, the promoters from above vectors were cloned into pMDC162 (Curtis and Grossniklaus 2003). Specifically, the above *pMYB3R1::GUS* and *pMYB3R4::GUS* served as templates, and respective promoters were PCR amplified using Q5® (NEB) and cloned into pCR8/GW/TOPO®, which were then recombined into the pMDC162 vector via LR reaction. The resulting pMDC162-based vectors of *pMYB3R1::GUS* and *pMYB3R4::GUS* were introduced into *tsol-1+/+sup-5* and *35S::TSO1-GR; tsol-1* plants, respectively, via *Agrobacterium* (GV3101). At least 5 T1 transgenic lines for each construct were characterized, and 10 T2 plants derived from three T1 lines (4-5, 4-6 and 4-8) were analyzed. To generate fluorescent transcriptional reporter,

*pMYB3R1* and *pMYB3R4* fragments described above in pCR8/GW/TOPO entry vector? were recombined into pGreenII-*NLS-3xEGFP* (Takada and Jürgens 2007). The constructs were then introduced into *tso1-1/sup-5* plants.

To generate translational reporters for *MYB3R1*, a 6.4kb genomic fragment was PCR amplified using Q5® (NEB) with primers *pMYB3R1.F*, *MYB3R1.non.stop.R* (Table 2.1) from *Ler* wild type DNA and cloned into pCR8/GW/TOPO. After sequencing confirmation, the genomic fragment of *MYB3R1* were recombined into pMDC107 (Curtis and Grossniklaus 2003) and pEarlyGate303 (Earley et al. 2006) to create *pMYB3R1::MYB3R1-GFP* and *pMYB3R1::MYB3R1-cMyc*, respectively. To generate a fluorescent translational reporter line with enhanced GFP signal, the 6.4kb genomic fragment of *MYB3R1* was PCR amplified with primers *pMYB3R1.F* and *MYB3R1.3xGFP.n.R* (Table 2.1) to correct the reading frame and was recombined into pGreenII-*NLS-3xEGFP* (Takada and Jürgens 2007). These constructs were introduced into *tso1-1/sup-5* plants.

To generate phospho-mimicking *pMYB3R1::MYB3R1-GFP* constructs, the pCR8/GW/TOPO vector harboring the 6.4 kb *MYB3R1* genomic fragment was modified using the Q5® Site-Directed Mutagenesis Kit (NEB) following the manufacturer's instruction. Briefly, primers S656D.F/S656D.R were used to amplify the *MYB3R1* gDNA TOPO construct. The changes in the coding sequence result in the change of 656 serine to aspartic acid (S656D) in the protein sequence. Similarly, primers S709D.F/S709D.R were used to generate the S709D change. The modified *MYB3R1* gDNA pCR8/GW/TOPO constructs were recombined into pMDC107

(Curtis and Grossniklaus 2003) to generate *gMYB3R1-S656D* and *gMYB3R1-S709D* respectively.

To generate construct for Co-IP assay, the *TSO1* cDNA was cloned into PHB-FLAG-X vector to generate *35S::Flag-TSO1*. The *35S::MYB3R1*(cDNA) construct were generously provided by Masaki Ito (Haga et al. 2007). The cDNA was subcloned into pEarleyGate104 (Earley et al. 2006) to generate *35S::YFP-MYB3R1*. Both constructs were transformed into *Agrobacterium* strain GV3101.

### **Suppressor screen and complementation tests**

The genetic screen scheme is shown in Figure 2.1A. *35S::TSO1-GR; tso1-1* homozygous seeds were treated with 0.2% EMS solution for 12 hours. After repeatedly washing off the mutagen with water, the seeds were germinated in soil. Dexamethasone (DEX) was supplied to M1 plants at the stage of bolting. For the first 2000 M1 plants, seeds were collected from individual M1; for the next 1000 M1 plants, seeds were pooled into one pool. These seeds were grown into M2 plants and screened for the ability to set seeds, forming elongating siliques. 45 suppressors were identified from screening the progeny of ~3000 M1 plants. These M2 suppressor plants were backcrossed to the parental line, *35S::TSO1-GR; tso1-1*. For each suppressor, the F1 progeny at bolting was supplied with DEX to allow for seed production. The resulting F2 progeny showed suppressed (~25%) and unsuppressed (~75%) phenotype; these two populations served as the mapping populations (Figure 2.1B).

For complementation test, M2 suppressor lines were crossed with one another. Since the suppressors are recessive, F1 progeny should show un-suppressed phenotype unless the suppressor mutations are allelic to each other, which would show suppressed phenotype in F1.

### **Mapping by sequencing**

For each suppressor F2 mapping population, leaf tissues were collected and pooled from 35 to 50 plants, and genomic DNA was extracted from the pooled leaf tissue using the NucleoSpin Plant II Midi kit (MACHEREY-NAGEL). Each DNA pool was sequenced at 15-20x coverage with 51bp single end reads (Table 2.2). Reads were aligned to TAIR10 *Arabidopsis* genome with Bowtie2 (Langmead and Salzberg 2012) and variants were called with SAMtools (Li et al. 2009). Six independent suppressors (A144, A156, A176, A317, B636, B763) were mapped and sequenced as described above. A *35S::TSO1-GR; tso1-1* parental line was also sequenced at about 8X coverage (Table 2.2). Variants shared among all 6 samples (556864 total variants) are likely carried over from prior EMS mutagenesis that generated *tso1-1* in the *Ler* background; they were removed from further analysis. SNPs unique to each suppressor pool were identified using the genotype calling feature of SAMtools. G-to-A or C-to-T changes were further selected as candidate SNPs as they are most likely caused by EMS. Enrichment of candidate SNPs in 0.1Mbp window was plotted using R and circos (Krzywinski et al. 2009). Annotation of variants was done using the VariantAnnotation package (Obenchain et al. 2014) from Bioconductor to identify nonsynonymous SNPs within exons as well as SNPs affecting splicing.

### **CRISPR/Cas9 gene editing and genotyping of resulted mutants**

Single guide RNA (gRNA) was designed to target the 4th exon of the *MYB3R1* gene.

The gRNA sequence (ACGGTCCTTTCACAAGCTCT) was inserted between the *AtU6* promoter and scaffold followed by the *AtU6* terminator using overlapping PCR (Table 2.1) with pCAMBIA-CAS9+gRNA (Jiang, Yang, and Weeks 2014) as the template. The above PCR fragment was cloned into pCR8/GW/TOPO, excised by Sall and KpnI, and ligated into Sall and KpnI sites in pCAMBIA-CAS9+sgRNA, which was provided by Dr. Donald Week (Jiang, Yang, and Weeks 2014).

*Agrobacterium tumefaciens* (GV3101) harboring the CRISPR/Cas9 vectors were then used to transform the *tso1-1*+/+*sup-5* and *tso1-3* plant by floral dip. T1 seeds were selected on 1/2 MS plates containing hygromycin. No phenotypic change was observed in T1 plants. For *tso1-1*, seeds from 5 individual T1 WT plants were collected and 2 of the 5 T1 plants (line 19 and 9) gave rise T2 plants showing genetic chimeric with part of the branches showing wild type phenotype in *tso1-1* homozygous plants . Specifically, for line 19, seventeen of 236 *tso1-1* plants developed chimeric branches; for line 9, eighteen of the 39 *tso1-1* plants developed chimeric branches, DNA was extracted from individual suppressed branches of the *tso1-1* T2 chimera, and PCR primers (MYB3R1.CRISPR.con.F/R; Table 2.1) were used to amplify DNA fragment spanning the gRNA target site within *MYB3R1*, which were then sequenced.

For *tso1-3* transformed with the CRISPR constructs, seeds from 7 individual T1

plants were collected and 1 of the 7 T1 plants (line 16) gave rise to 6 T2 plants (out of 750) with partially rescued seed set. DNA was extracted from the 6 T2 plants and sequenced to reveal heterozygous mutation in *MYB3R1*. T3 progeny of these 6 T2 plants segregated 25% completely rescued plants.

To construct CRISPR vector for *MYB3R4* gene editing, gRNA was designed to target the 2nd exon. Primers MYB3R4.CRIPSR.F/R (Table 2.1) were annealed and ligated into the BsaI cutting site of pHEE401E vector (Z.-P. Wang et al. 2015). The construct was introduced into *tsol-1/sup-5* plants via *Agrobacterium* by floral dipping. CRISPR generated mutations likely destroy a BbvCI restriction site at the gRNA target, which allows for screening of CRISPR generated mutants. PCR primers MYB3R4.seq.pro.F and MYB3R4.4th.exon.R (Table 2.1) were used to amplify DNA fragment spanning the gRNA target site within *MYB3R4*, which were then sequenced.

### **Propidium iodide (PI) staining and microscopy**

Seven days old seedlings were immersed in 10ug/ml PI in water for 2 minutes. Roots were then mounted on slides in water and observed using the 63X (1.2 HCXPLAPO CS) water objective of Leica SPX5 confocal microscope. Fluorescent signal, excited by a white light laser at 536nm, was detected with detection channel set at 550nm-660nm. Tile scans were taken and processed using Leica Application Suite 2.0.0 software.

### **Beta-Glucuronidase (GUS) staining**

GUS staining was carried out as previously described (Takahashi et al. 2013). Briefly, samples were washed with phosphate buffer (pH 7.4), and then incubated in the staining buffer (100 mM sodium phosphate buffer, 1 mg/ml 5-bromo-4-chloro-3-indolyl  $\beta$ -D-glucuronide, 0.5 mM ferricyanide and 0.5 mM ferrocyanide (pH 7.4)) in the dark at 37 °C for 12 hours. The root tips were then incubated with clearing solution (8 g chloral hydrate: 1ml 100% glycerol: 1 ml water) for 1 hour and mounted on slides in clearing solution.

### **Co-immunoprecipitation assays**

The *Agrobacterium* harboring *35S::Flag-TSO1* and *35S::YFP-MYB3R1* were used to co-transfect tobacco leaves. Samples were collected after 48h and were ground in liquid nitrogen and homogenized in lysis buffer (50 mM Tris-HCl pH7.5, 150 mM NaCl, 1 mM EDTA, 10% glycerol, 0.2% Trition-X-100, 1 mM Pefabloc, cocktail, 50 uM MG132) were used. After centrifugation, supernatant was incubated with 1 uL anti-Flag (Sigma) antibody bound to 10 uL protein G (Invitrogen) beads for 2 h at 4 °C. Then the beads were washed three times with 1 mL lysis buffer and eluted by boiling with 20 uL 2X SDS sample buffer for 5 min and then separated in 10%SDS-PAGE gel. Anti-Flag (Sigma,1:5000) and anti-GFP (Abmart,1:2000) antibodies were used to detect Flag-TSO1 and YFP-MYB3R1, respectively.

## **2.3 Results**

### **2.3.1 Identification of *tso1-1* suppressor mutations**

To investigate the molecular mechanism of *TSO1* function, we have taken a genetic

approach to identify suppressors of *tso1* mutants. Suppressor mutations may identify critical co-regulators or downstream targets of TSO1; they may help place *TSO1* into existing or novel regulatory pathways. We chose to mutagenize *tso1-1* as it is 100% sterile and the strongest allele, making suppressed phenotype easily detectable.

Since *tso1-1* produces no seed, we first developed an inducible system to conditionally rescue *tso1-1*. TSO1 full length cDNA was fused with the rat glucocorticoid receptor (GR) hormone binding domain driven by the constitutive 35S promoter. The transgenic *tso1-1* plant harboring this construct (*tso1-1; 35S::TSO1-GR*) produces seeds upon treatment with dexamethasone (DEX) (Figure 2.2 B, C). These seeds were then subject to EMS mutagenesis (Figure 2.1A).

By screening the M2 progeny of about 3000 M1 *tso1-1; 35S::TSO1-GR* plants, 45 suppressors were isolated based on their ability to develop seeds, which result in elongated seed pods (siliques). The degree of suppression varied from weak to strong based on the size of the seed pod (Figure 2.2 D, E) or number of seeds produced per silique. To quantify these varied degree of suppression in different suppressor lines, the number seeds produced per silique was measured for each line and shown (Figure 2.2 F). (*tso1-1* mutant is 100% sterile and do not set any seeds).

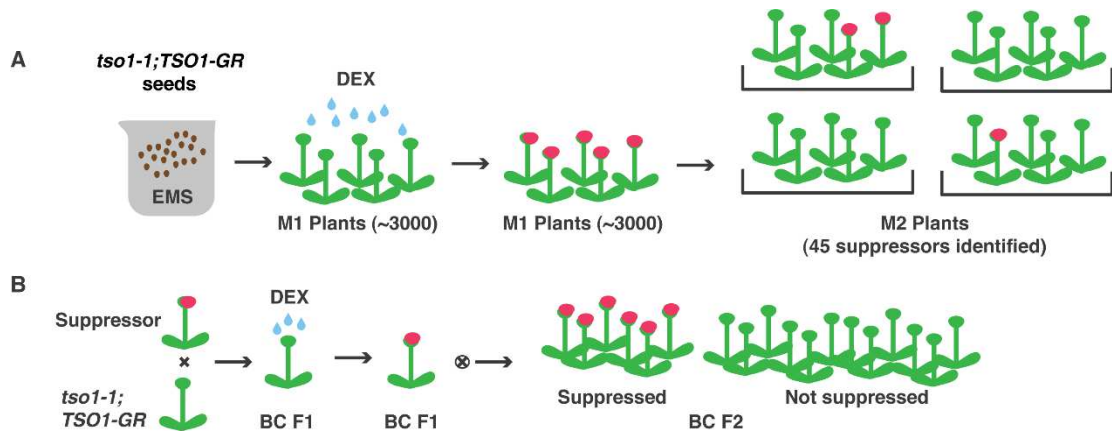


**Figure 2.1 Scheme of the suppressor screen and generation of mapping populations**

(A) *35S::TSO1-GR; tso1-1* seeds were treated with EMS. Then seeds were germinated on soil. Since these M1 *35S::TSO1-GR; tso1-1* plants were completely sterile, they were sprayed with DEX at bolting to give rise to seeds for M2 generation. Multiple M2 plants from individual M1 family were grown and screened for their ability to set seeds and form siliques. (B) Individual suppressor was back crossed with its unmutagenized parent *35S::TSO1-GR; tso1-1*. F1 cross progeny was supplied with DEX to set F2 seeds. F2 plants are grouped into suppressed and unsuppressed mapping populations. BC: Backcross. Red shoot apex denotes fertile flowers.

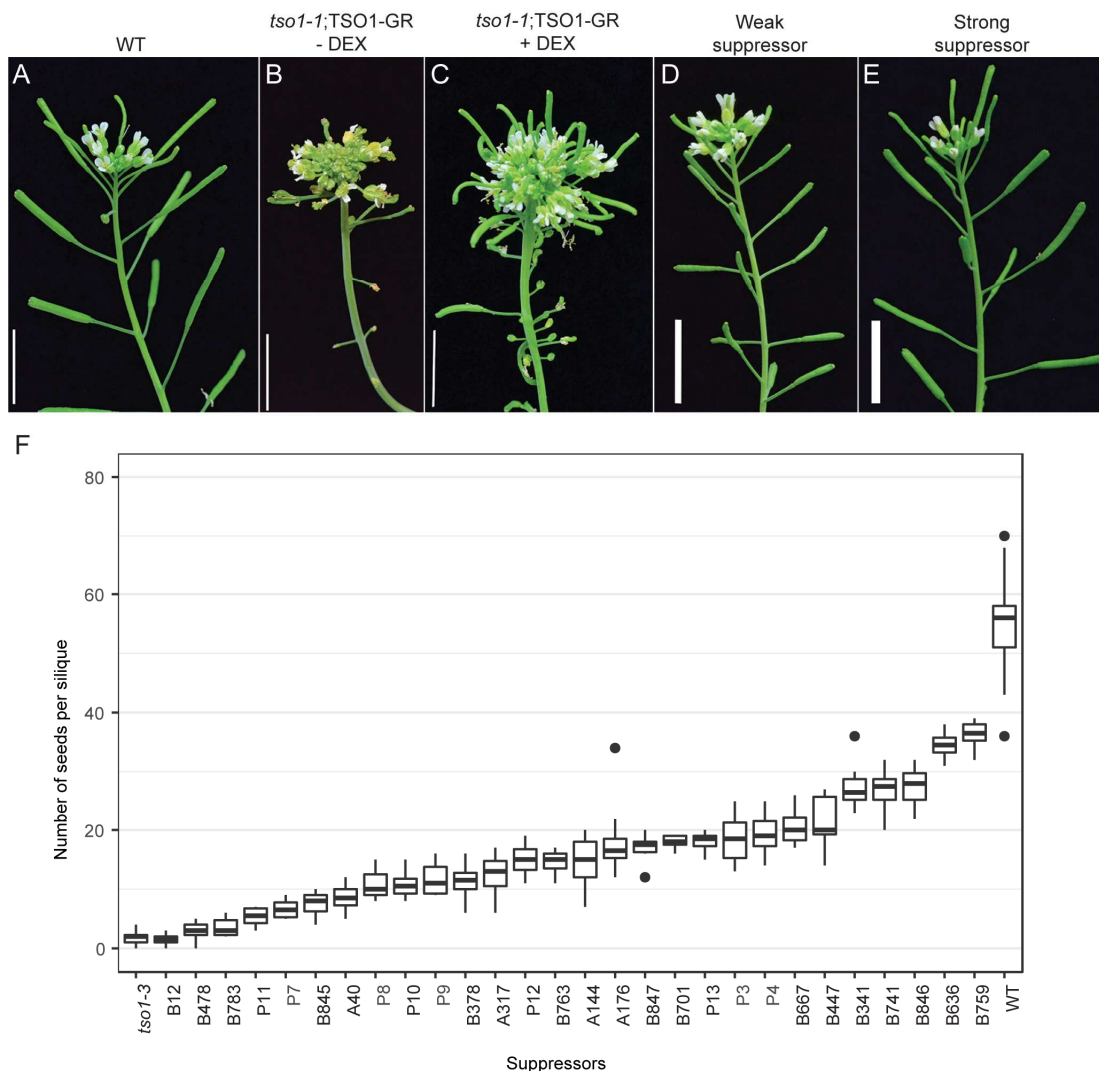


**Figure 2.2 Phenotype of an inducible *TSO1* line and suppressors isolated**  
**(A)** The flowering shoot of a wild type (WT) *Arabidopsis* of the *Ler* accession. **(B)** The inflorescence shoot of a *tso1-1* mutant containing the *35S::TSO1-GR* construct. No dexamethasone (DEX) was applied. **(C)** An *tso1-1* mutant inflorescence containing the *35S::TSO1-GR* construct. DEX treatment (+DEX) resulted in the rescue of the fertility defect. Note the long siliques. **(D)** A weak suppressor in the *tso1-1*; *TSO1-GR* background. No DEX was applied. Siliques are formed although shorter than WT. **(E)** A strong suppressor identified in the *tso1-1*; *TSO1-GR* background. No DEX was applied. Siliques are long similarly to those of wild type. **(F)** Box plot of seeds set per silique from wild type plant (*Ler*), *tso1-3* mutant and 28 suppressors isolated. Data ranked and ordered by median. (around 10 siliques were sampled from representative M3 suppressor plants).

### 2.3.2 *tsol-1* intragenic suppressors support the antimorphic nature of *tsol-1*

To determine the molecular identity of these suppressors, we used the bulk-segregant mapping-by-sequencing approach. To generate mapping populations, five suppressors were back crossed with the *tsol-1; 35S::TSO1-GR* parent line to yield F2 mapping populations (Figure 2.1 B). Genomic DNA from about 35 to 50 F2 plants showing suppressed phenotype were sequenced. Analysis of the DNA sequence for linked SNPs mapped five suppressors to specific regions (Figure 2.1; Figure 2.3, Figure 2.4 Table 2.2). Two suppressors (A156 and A176) were mapped to *TSO1* and thus are intragenic suppressors (Figure 2.3). Suppressor A176 contains a G-A mutation at the splicing acceptor sites in the first intron of *TSO1*. Suppressor A156 contains a G-A change at the splicing donor site in the 8th intron. Both mutations likely alter splicing and shift the translational reading frame, which may lead to truncated protein and nonsense-mediated decay (NMD). The identification of intragenic suppressors is not surprising given that the *tsol-1* allele is antimorphic in nature (Sijacic, Wang, and Liu 2011) and mutations that abolish *tsol-1* proteins could suppress the *tsol-1* phenotype. In fact, the identification of intragenic suppressors further supported our previous finding of *tsol-1* being antimorphic. However, the two suppressors are more fertile than the *tsol-3* allele, which causes a stop codon and a truncated protein with only a single CXC domain. Notably, the A156 mutation disrupted the DGSL motif at the end of the second CXC domain, suggesting the importance of this motif, which is conserved between *TSO1* and *Arabidopsis* Enhancer of zeste (E(z)) homologs (Song et al. 2000).

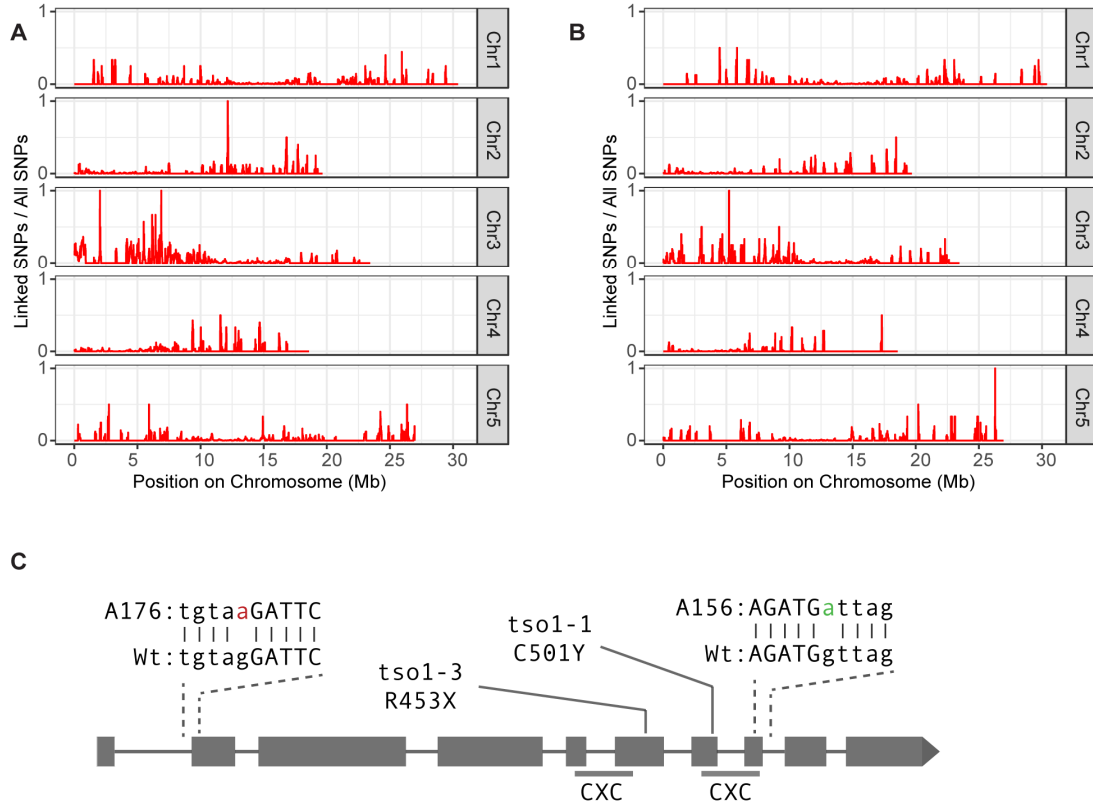


### Figure 2.3 Identification of two *tso1-1* intragenic suppressors

(A-B) Genome wide SNP mapping of F2 mapping populations, showing the linked SNP distribution for suppressor A156 (A) and suppressor A176 (B). Peaks of linked SNP for both A156 and A176 are located at the upper arm of *Arabidopsis* chromosome 3. Y-axis indicates the ratio of linked SNPs to all SNPs in a 100,000bp sliding window. X-axis denotes position on the chromosomes. (C) A diagram of TSO1 gene structure with mutations relevant to this study indicated. The corresponding two CXC domains are underlined. The *tso1-1* and *tso1-3* mutations are denoted above the CXC domains. The A156 suppressor mutation (green) altered the splicing donor site of the 8<sup>th</sup> intron. The A176 suppressor mutation (red) altered the splicing acceptor site of the 1<sup>st</sup> intron. Capital letters indicate exon sequence, lower case letter indicate intron sequence.

#### 2.3.3 Identification of *MYB3R1* as an extragenic suppressor of *tso1-1*

Three suppressors (A317, B636, B763) however were all mapped to the same locus coding for the *MYB3R1* gene (Figure 2.4 A, B, C). A317 causes a non-sense mutation at the C-terminus region while B636 and B763 cause mis-sense mutation in the DNA

binding repeats of MYB3R1. Therefore, loss-of-function mutations in MYB3R1 suppress *tsol-1*.

For the remaining 39 suppressors, we performed complementation tests by performing strategic pairwise crosses among some of the suppressors. Surprisingly, most of the 39 suppressors failed to complement alleles of *myb3r1* and hence define additional *myb3r1* alleles (Figure 2.4 F; Table 2.3). DNA sequencing of a portion of these alleles identified specific mutations in the *MYB3R1* gene (Figure 2.4 D; Table 2.3). In total, 14 independent *myb3r1* suppressor mutations were confirmed and were named as *myb3r1-2* to *myb3r1-13*. Interestingly, 12 of the 13 alleles cause changes in the DNA-binding domain (R1, R2, or R3); only *myb3r1-13* causes a missense mutation outside the DNA-binding domain, indicating the critical role the R1R2R3 domains play (Figure 2.4E). Alleles *myb3r1-3*, *myb3r1-4* and *myb3r1-14* were isolated independently multiple times (Figure 2.4; Table 2.3), suggesting that our screen has reached saturation under the current screening scheme.

Missense mutations (B341, B636, B667) in the DNA binding repeats are strong suppressors (Figure 2.4 D, F and Figure 2.2F). B667 (C125Y) altered a conserved Cys residue, which was thought as a redox sensor for the MYB protein (Heine, Hernandez, and Grotewold 2004); mutations of the equivalent amino acid (Cys130 in human MYB) significantly impair the activity of c-Myb and v-Myb (Grässer et al. 1992; Guehmann et al. 1992). Our work reveals that the critical amino acid in maintaining structure and function of MYB is conserved from animal to plants. B12

(G88R) is a weak suppressor (Figure 2.4 D, F and Figure 2.2F); it changes a glycine to a bulkier arginine in the loop region connecting the R1 and R2 DNA-binding domains and hence likely only moderately reduces the MYB3R1 activity. A317 (R652X) is a nonsense mutation, leading to a truncated MYB3R1 missing the two c-terminal uncharacterized domains. The seed set is partially rescued by A317, suggesting A317 caused a hypomorphic mutation and the c-terminal domains play a minor role for MYB3R1 function (Figure 2.4 D and Figure 2.2F). These data not only confirm the critical residues and domains of MYB3R1 but also provide novel insights on MYB protein structure and function applicable to other systems including human. The correlation between the extent of loss of MYB3R1 activity and the ability to suppress *tsol-1* indicates that the level of MYB3R1 activity maybe the underlying factor mediating the *tsol-1* mutant phenotypes.

We showed that in the *tsol-1* background, *myb3r1* single mutations exhibit significant phenotype in suppressing *tsol-1* mutant phenotype including short root, shoot meristem fasciation, sterility, and lack of floral organ differentiation. The degree of suppression conferred by these newly isolated *myb3r1* mutations (*myb3r1-2* to *myb3r1-14*) positively correlates with the severity of the *myb3r1* loss-of-function mutations (Figure 2.2 F, Figure 2.4D and Figure 2.6 F).

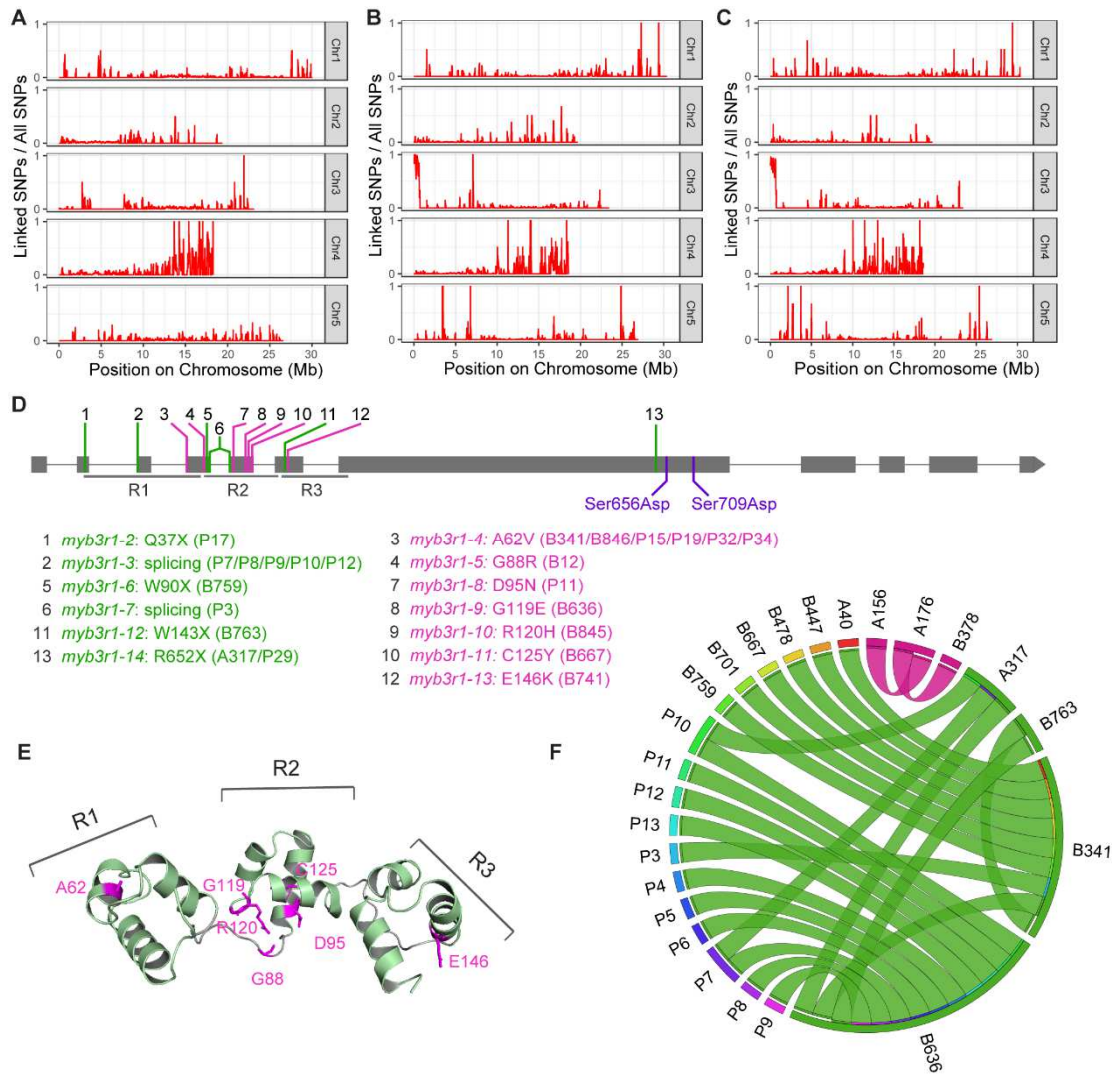


**Figure 2.4 Summary of *myb3r1* mutations isolated from the *tsol-1* suppressor screen**

(A-C) Genome wide SNP mapping of F2 mapping populations for suppressor A317 (A), B636 (B), and B763 (C). Linked SNP peaks in each case resides at the lower arm of *Arabidopsis* chromosome 4. Y-axis indicates the ratio of linked SNPs to all SNPs detected in a 100,000bp sliding window. X-axis denotes position on the chromosome. (D) Diagram of *MYB3R1* gene structures and mutations relevant to this study. The R1, R2, R3 DNA binding domains are underlined. Mutant alleles identified in this study 1-13 (Refer to Table 2.3) are shown. Nonsense mutations are labeled in green and missense mutations are labeled in pink. Serine 656 and serine 709 are changed into aspartic acid in the phosphomimic constructs. (E). 3D structure of the R1R2R3 DNA binding domains modeled using Phyre2 (Kelley et al. 2015) with the structure of human c-Myb DNA binding domain (PDB:1H88) as template. Residues mutated in the suppressors isolated are highlighted in pink. (F) Summary of results of complementation tests displayed in a Circos graph. Each suppressor pair that failed to

complement each other is connected by a ribbon, indicating allelic relationship. Two loci were identified by the complementation tests indicated by green and pink colored ribbons. A156, A176 and B378 are allelic with each other and represent intragenic suppressors of *tsol-1*. The rest of suppressors are allelic to each other and reside in the *MYB3R1* gene.

#### **2.3.4 CRISPR-induced *myb3r1* mutations also suppresses *tsol-1***

The EMS mutagen generally induces several hundred to even thousands of mutations in the genome, and it is difficult to separate the effect of *myb3r1* mutation from possibly background mutations in the absence of extensive backcrosses. Further, there exists the possibility that the suppressors acted indirectly by facilitating TSO1-GR's entry into the nucleus in the absence of DEX treatment. To eliminate these possibilities, we applied CRISPR/CAS9 to knockout *MYB3R1* in the *tsol-1* background without the TSO1-GR transgene or EMS induced background mutations. An gRNA targeting the 4<sup>th</sup> exon of *MYB3R1* was designed (Figure 2.5H). The CAS9-gRNA construct was transformed into *tsol-1*<sup>+/+</sup>*sup-5* heterozygous plants. In T2 generation, we identified *tsol-1* mutant plants harboring wild type (suppressed) branches (Figure 2.5 A,B). These plants are chimeric in that they harbor wild type clones/branches in the *tsol-1* genetic background. Sequence analysis of the *MYB3R1* gene from the wild type clones/branches revealed homozygous or bi-allelic mutations in the *MYB3R1* gene (Figure 2.5 H). Seeds collected from the suppressed branches germinated to form plants indistinguishable from wild type (Figure 2.5 C). Therefore, germline-transmitted *myb3r1* alleles completely suppressed the *tsol-1*. This experiment indicates that it is the *myb3r1* mutations that completely suppress *tsol-1*. Neither the *TSO1-GR* transgene nor EMS-background mutations contributed to the suppression of *tsol-1*.

To determine if *myb3r1* mutations are suppressing specific *tso1* allele, ie. *tso1-1* or suppress any *tso1* alleles (including class I and class II alleles), we transformed the same CAS9-sgRNA into *tso1-3*, a nonsense mutation occurring between the two CXC domain in TSO1 (Sijacic, Wang, and Liu 2011). Unlike *tso1-1*, *tso1-3* is a class II mutation. Mutants of *tso1-3* exhibit severely reduced fertility (Figure 2.5 D) but show normal inflorescence meristem and normal floral organs. Suppressed *tso1-3* could be identified in the T2 generation of *tso1-3* plants transformed with the CRISPR-sgRNA vector. Plants heterozygous for a CRISPR-induced mutation in *MYB3R1* showed slightly elongated siliques (Figure 2.5 E, G), while those *tso1-3* plants homozygous for the CRISPR-induced *myb3r1* mutation are wild-type like (Figure 2.5 F, G). Therefore, *myb3r1* mutations are not allele-specific suppressors; they are general suppressors of *tso1* mutations.

Together, our data indicate that the suppression effect of *myb3r1* mutations are *tso1* gene-specific not allele-specific, suggesting that *MYB3R1* and *TSO1* may interact in a biological process that depends on each other's function. Further, the *myb3r1* mutations appear to suppress all defects of *tso1-1* including sterility, meristem fasciation, and floral organ differentiation (Liu, Running, and Meyerowitz 1997; Sijacic, Wang, and Liu 2011). This indicates that proper interaction between *TSO1* and *MYB3R1* is required in regulating all three aspects of development regulated by TSO1.

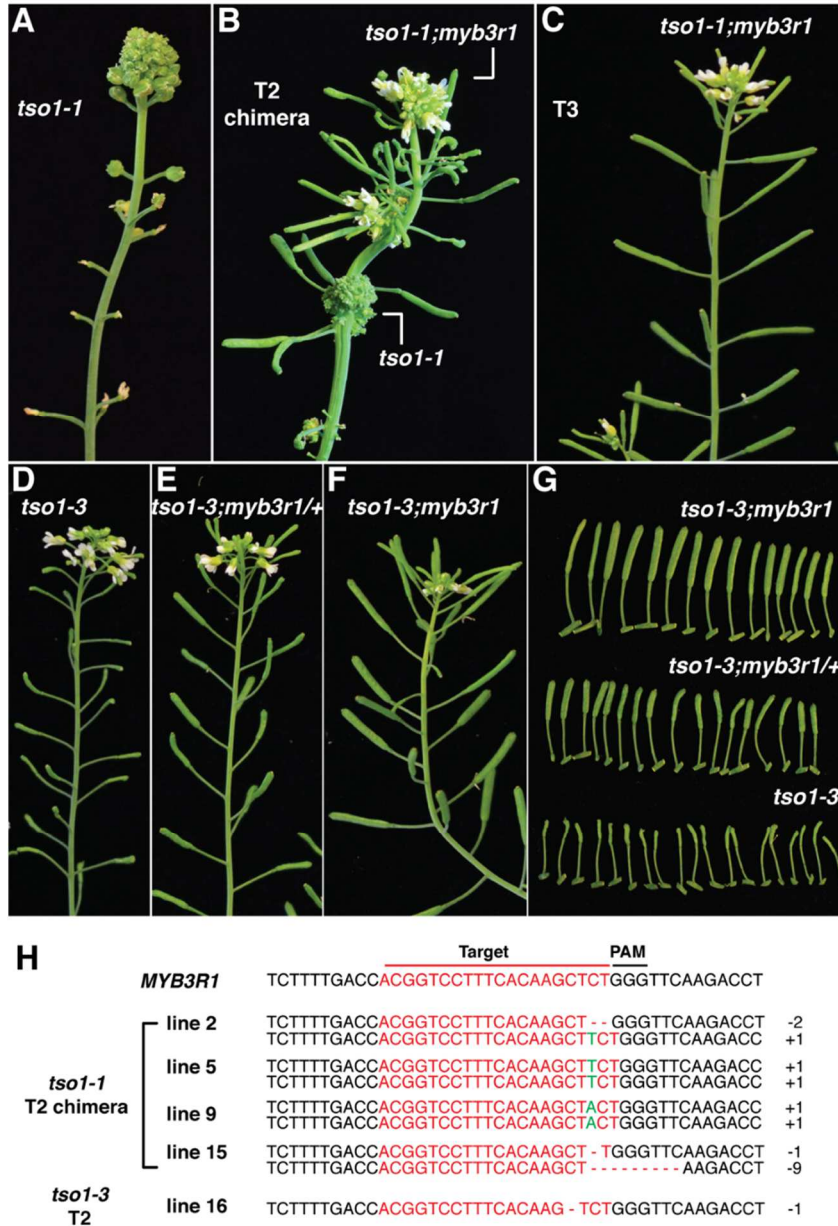


**Figure 2.5** *myb3r1* knockout mutations by CRISPR suppress both *tso1-1* and *tso1-3*

(A) A inflorescence shoot of *tso1-1* mutant. (B) A T2 chimera of the *tso1-1* plant, showing wild type branches arising from a *tso1-1* mutant background. (C) A T3 plant derived from seeds collected from the wild type branch of the T2 chimera shown in B. (D-G) T3 plants of *tso1-3* transformed with the CRISPR construct. (D) A T3 plant showing typical *tso1-3* phenotype; severely reduced fertility and very small siliques. (E) A T3 *tso1-3* plant heterozygous for a CRISPR-mediated *myb3r1* mutation. (F) A T3 *tso1-3* plant homozygous for the CRISPR-mediated *myb3r1* mutation. (D, E, and F are sibling plants). (G) Close-up of the siliques made by plants in (D) (top), (E) (middle), and (F) (bottom). (H) Sequence of *MYB3R1* targeted by the gRNA and mutations generated by CRISPR in different *tso1-1* T2 chimera and *tso1-3* T3 plants.

### 2.3.5 Mutations in *MYB3R1* suppress *tsol-1* root phenotype

The TSO1-GR inducible system made it possible to obtain *tsol-1* homozygous seeds and subsequently observe *tsol-1* mutant roots upon germination on agar. We found that *tsol-1* mutant exhibited significantly reduced root length (Figure 2.6 A). In contrast, the *tsol-3* allele did not exhibit this root defect (Figure 2.6 A). To investigate the underlying reason for the short root phenotype, we examined root cell organization through confocal microscopy of how many days old ? roots stained with propidium iodide (PI), which stains cell wall. The root meristem size is defined by the number of cells in the cortex cell file in the meristematic zone (MZ) (Figure 2.6B arrowheads, quantified in Figure 2.6 C). Within the cortex cell file (the second cell layer from the epidermis), the position where the next cortex cell is twice the size of the previous ones (marked by the top arrowhead) delimits the upper boundary of the MZ while the quiescent center (QC) denotes the lower end of the MZ (and marked by the bottom arrowhead). We found that *tsol-1* roots had significantly reduced number of cells in the root meristematic zone and thus reduced meristem size (Figure 2.6 B, C). The root of *tsol-1* mutant does not lack any cell types in the root and the stereotypical division of the cortex/epidermis initials divided properly (Figure 2.6.B lower panels). The QC cells did not terminate prematurely (Figure 2.6.B lower panels). Conversely, precocious differentiation of the root epidermis cells was observed (Figure 2.6 B arrows). These phenotypes indicate that the short root and reduced MZ phenotype of *tsol-1* is likely due to precocious transition from proliferation to differentiation, rather than stem cell defects.

We asked whether the *myb3r1* mutations, identified as suppressors of *tsol-1* shoot phenotype, also suppress the *tsol-1* root phenotype. Indeed, *tsol-1; myb3r1* (induced by CRISPR) developed roots with length and meristem size comparable to wild type (Figure 2.6 B, C). Therefore, mutations in *MYB3R1* suppress *tsol-1* both in shoots and in roots. These data strongly suggest that *MYB3R1* acts in all processes that require *TSO1*.

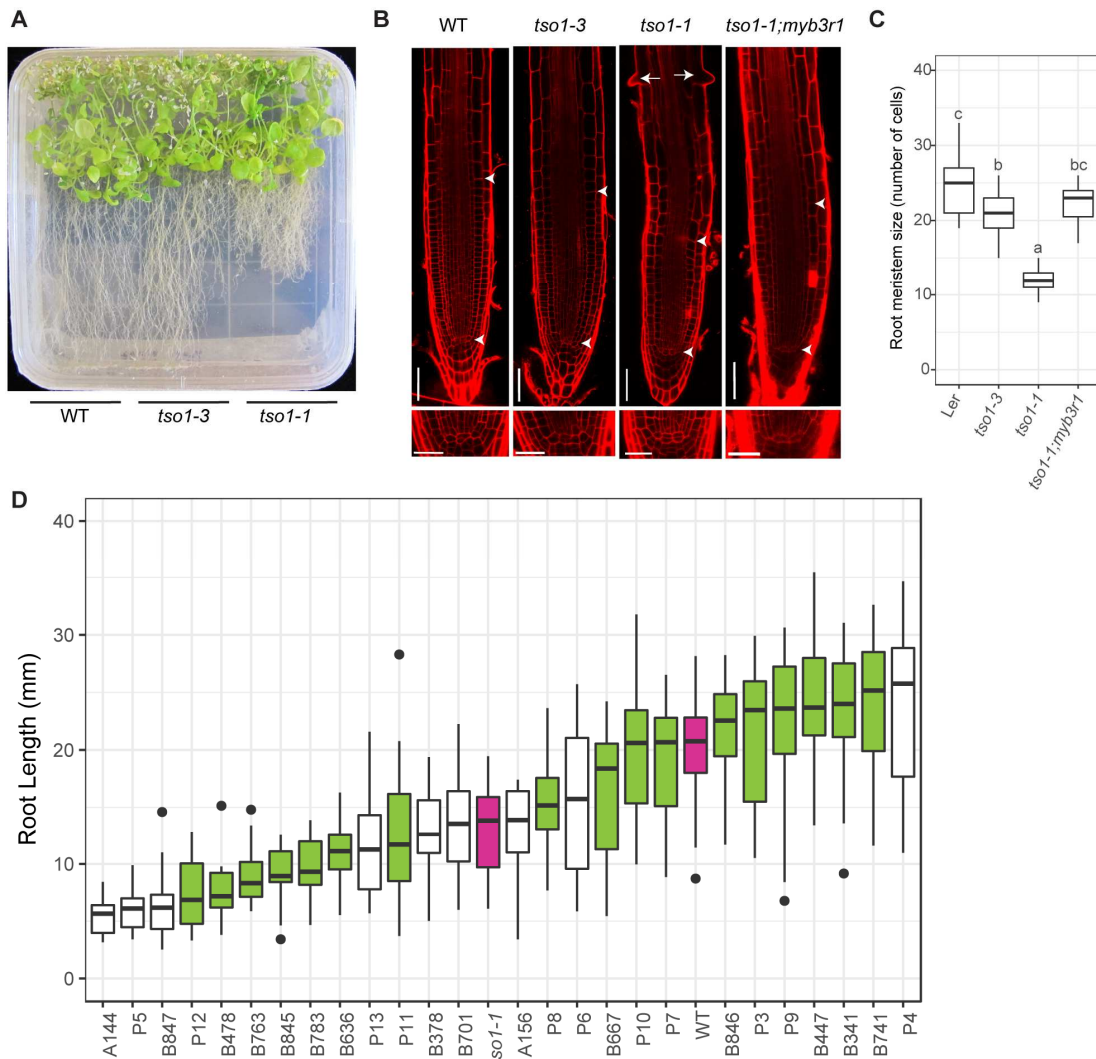


**Figure 2.6 The *tso1-1* root phenotype can be suppressed by *myb3r1* mutations**  
**(A)** WT(Ler), *tso1-3* and *tso1-1* seedlings at 42 days post germination (dpg) on a half strength MS media plate. **(B)** Confocal images of root apical meristem of WT(Ler), *tso1-3*, *tso1-1*, and *tso1-1; myb3r1* (progenies of plants in Figure 2.5 C) (7dpg). Propidium iodide (PI) staining (red) was performed for observing cell outlines. Arrowheads delimit the boundary of meristematic zone (MZ). Arrows indicate precocious differentiation of root hair cell in *tso1-1*. Lower panel shows the stem cell niche of the root. Bars = 50um (upper panels) and 25 um (lower panels). **(C)** Quantification of root MZ size using cell number in the meristematic zone (n=10~15 plants). Different letters indicate statistically significant difference (p<0.01, one way ANOVA and Tukey test). **(D)** Box plot of root length measured from WT(Ler), *tso1-1* and suppressors isolated in the screen (n=15~58 plants). WT(Ler) and *tso1-1* are labeled pink as reference points and *myb3r1* mutants are labeled green.

### 2.3.6 Mis-expression of *MYB3R1* was found in *tsol-1* mutant SAM

To investigate the mechanism underlying the observed *TSO1-MYB3R1* genetic interaction, we examined the *MYB3R1* gene expression in *tsol-1* mutants. A promoter *MYB3R1::GUS* reporter was previously used to study *MYB3R1* expression (Haga et al. 2007). This reporter was introduced into *tsol-1* and showed both increased and ectopic GUS staining in the shoot apex when compared with wild type (Figure 2.7 A, B). This reveals that *MYB3R1* mRNA is abnormally expressed in *tsol-1* background and this ectopic and over-expression of MYB3R1 likely mediates the *tsol-1* phenotype. These data suggest the simplest model that TSO1 normally represses the expression of *MYB3R1*.

To understand the genetic interaction of *TSO1* and *MYB3R1* in the developmental context of the SAM, we generated translational reporters of *TSO1* and *MYB3R1*. Specifically, a 4.1kb *TSO1* genomic sequence including native 1kb promoter was used for the translational reporter *pTSO1::TSO1-GFP*. This *pTSO1::TSO1-GFP* reporter rescued *tsol-1* mutants and thus could inform us where TSO1 protein is made and functions. We studied multiple lines in which the *tsol-1; pTSO1::TSO1-GFP*, and they all showed very weak GFP signal at SAM, suggesting *TSO1* gene expression or protein level is relatively low. This made confocal microscopy at the SAM rather challenging. To enhance the GFP signal, we fused the same genomic fragment of TSO1 with *NLS-3xEGFP* (Takada and Jürgens 2007) coding sequence to produce *pTSO1::TSO1-NLS-3xEGFP* (*gTSO1-3xEGFP* for short) reporter. Since TSO1 is a nuclear protein, the added nuclear localization signal should not interfere

with TSO1 function. a 6.4 kb genomic fragment of *MYB3R1* was used to construct the *pMYB3R1::MYB3R1-NLS-3xEGFP* (*gMYB3R1-3xEGFP* for short) reporter. We are in the process of confirming the functionality of these 3xEGFP reporters.

In the *gTSO1-NLS-3xGFP* (*Ler*) line, GFP signal can be observed throughout the SAM, including the fast dividing meristem cells and also differentiating flower primordium (Figure 2.7.E). Interestingly, the GFP signal shows a sporadic pattern reminiscent of genes/proteins under cell cycle regulation, suggesting TSO1 protein level may be under cell cycle regulation. In contrast, in the *gMYB3R1-NLS-3xEGFP* (*Ler*) line, GFP signal can be observed in almost every cell (Figure 2.7.C upper panel) with similar intensity. This is consistent with previous observation that *MYB3R1* expression do not change during cell cycle in cultured tobacco cells (Haga et al. 2007). In *tso1-1* mutant SAM, the tissue organization is disrupted, which made it difficult to distinguish meristem zones and floral primordia. Nonetheless, GFP signal conferred by *gMYB3R1-NLS-3xEGFP* transgene can be observed ubiquitously (Figure 2.7 C lower panel). The nuclear GFP signal shows extreme variation of nuclei size and shape, consistent with previously observed cytokinesis and nuclei defects in *tso1-1* SAM (Liu, Running, and Meyerowitz 1997). These reporter lines showed that TSO1 and *MYB3R1* expressions overlap and are both expressed in proliferating and differentiating tissues. These expression patterns are largely consistent with available gene expression data (*Arabidopsis* eFP browser) of *TSO1* and *MYB3R1* (Figure 2.7F).

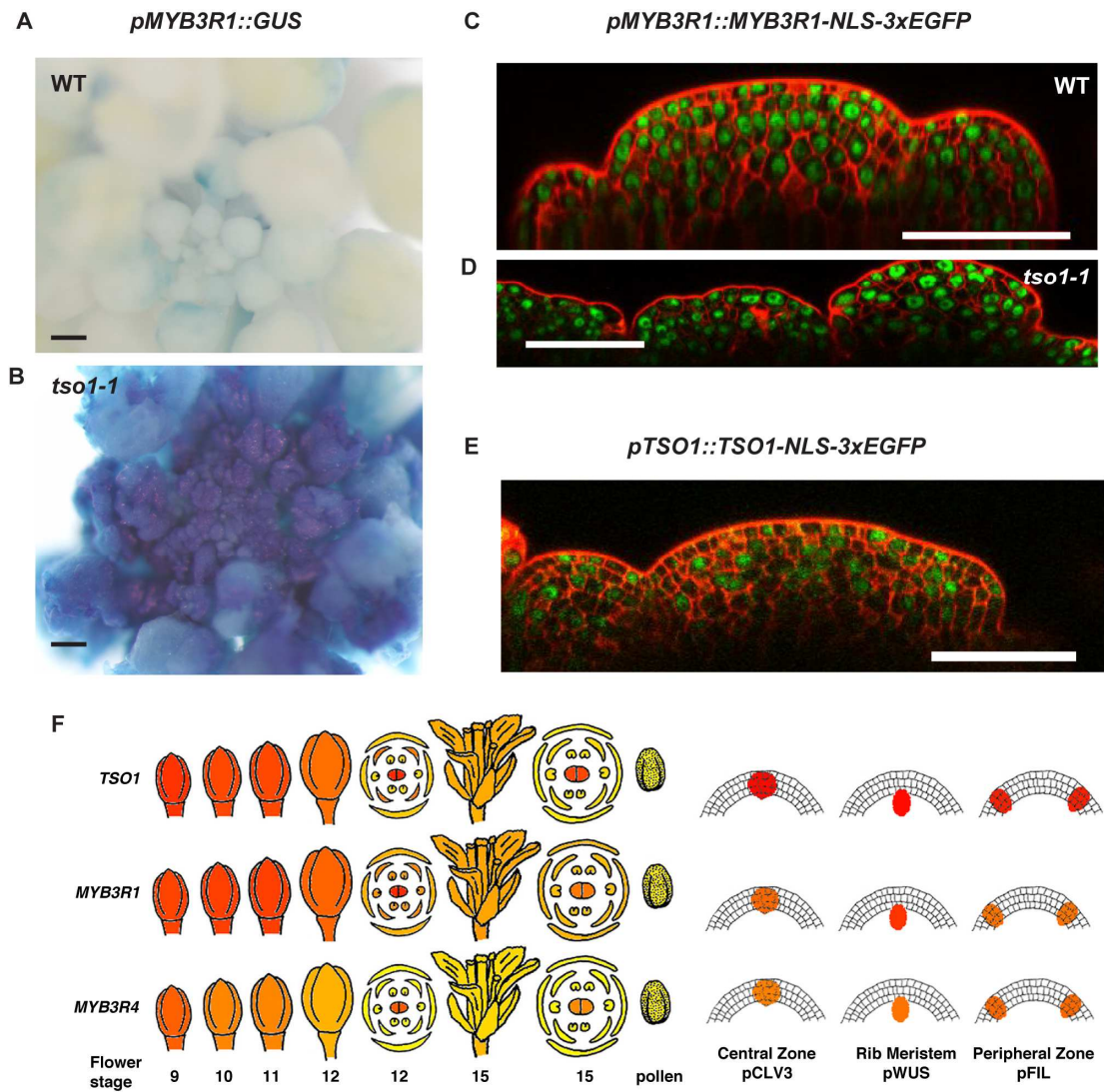


**Figure 2.7 Comparisons of *TSO1* and *MYB3R1* expression at the SAM**  
**(A-B)** *pMYB3R1::GUS* expression in wild type (Ler) **(A)** and in *tso1-1* **(B)** inflorescence. The GUS signal is both ectopically expressed throughout the inflorescence and at significantly high levels. The plant in **(A)** and **(B)** are siblings harboring the same *pMYB3R1::GUS* line and stained in X-gluc for the same amount of time. **(C-D)** *pMYB3R1::MYB3R1-NLS-3xEGFP* expression in wild type (Ler). **(C)** and in *tso1-1* **(D)** SAM. The plant in **(C)** and **(D)** are siblings harboring the same *pMYB3R1::MYB3R1-NLS-3xEGFP* line. **(E)** *pTSO1::TSO1-NLS-3xEGFP* expression in wild type (Ler). **(F)** eFP image showing similar expression pattern of *TSO1*, *MYB3R1*, and *MYB3R4* in young floral buds, pollen, and inflorescence meristem. Bars= 200  $\mu$ m **(A-B)** and 50  $\mu$ m **(C-E)**.

### 2.3.7 Mis-expression of *MYB3R1* mediates *tsol-1* mutant RAM phenotype

Because mutations in *MYB3R1* also rescue the short root phenotype of *tsol-1*, we investigate if *MYB3R1* is mis-expressed at the RAM. The *pMYB3R1::GUS* reporter described above showed an expression pattern similar to the pattern described previously by Haga et,al. The GUS signal can be observed in the vasculature tissue above the transitional zone (Figure 2.8 A). Very weak signal could also be detected at the meristematic zone (Figure 2.8 A). When introduced into *tsol-1* mutant, the *pMYB3R1::GUS* showed enhanced signal at the RAM comparing to wild type (Figure 2.8 A). Furthermore, the GUS signal seems to extend into the meristematic zone in *tsol-1* mutant (Figure 2.8 A). This reporter line revealed both overexpression and ectopic expression of *MYB3R1* at the RAM, consistent with what's observed at SAM.

To understand the genetic interaction of *TSOI* and *MYB3R1* in the developmental context of the RAM, we investigate the transcription/translational activity of *MYB3R1* and *TSOI* at the RAM. The *gMYB3R1-3xEGFP* translational reporter showed GFP pattern largely similar to that shown by *pMYB3R1::GUS* reporter (Figure 2.8 B). In addition to the vasculature, GFP signal can observed in epidermal cells above the transition zone (Figure 2.8 B). relatively weak GFP signals can also be observed in the ground tissue in the meristematic zone. The difference of GUS and 3xEGFP reporter pattern are likely due to difference in resolution.

The *pTSOI::TSOI-GFP* reporter showed GFP signal in the nuclei of all cell types in the root meristematic zone (Figure 2.8 C). No GFP signal was observed in the

columella cells and cells above the transition zone (Figure 2.8 C). This meristematic zone specific expression pattern shown by the *pTSO1::TSO1-GFP* reporter is consistent with *TSO1* expression pattern revealed by the “root map” tissue specific gene expression data (Brady et al. 2007). By transcriptome profiling of dissected series of cross sections of the *Arabidopsis* root, Brady et, al generated gene expression map of the root and performed gene clustering based on the expression pattern along the longitudinal axis. *TSO1* transcripts are present at high level in the root meristematic zone (clustered in Longitudinal Pattern 4 and 10) (Figure 2.8 D).

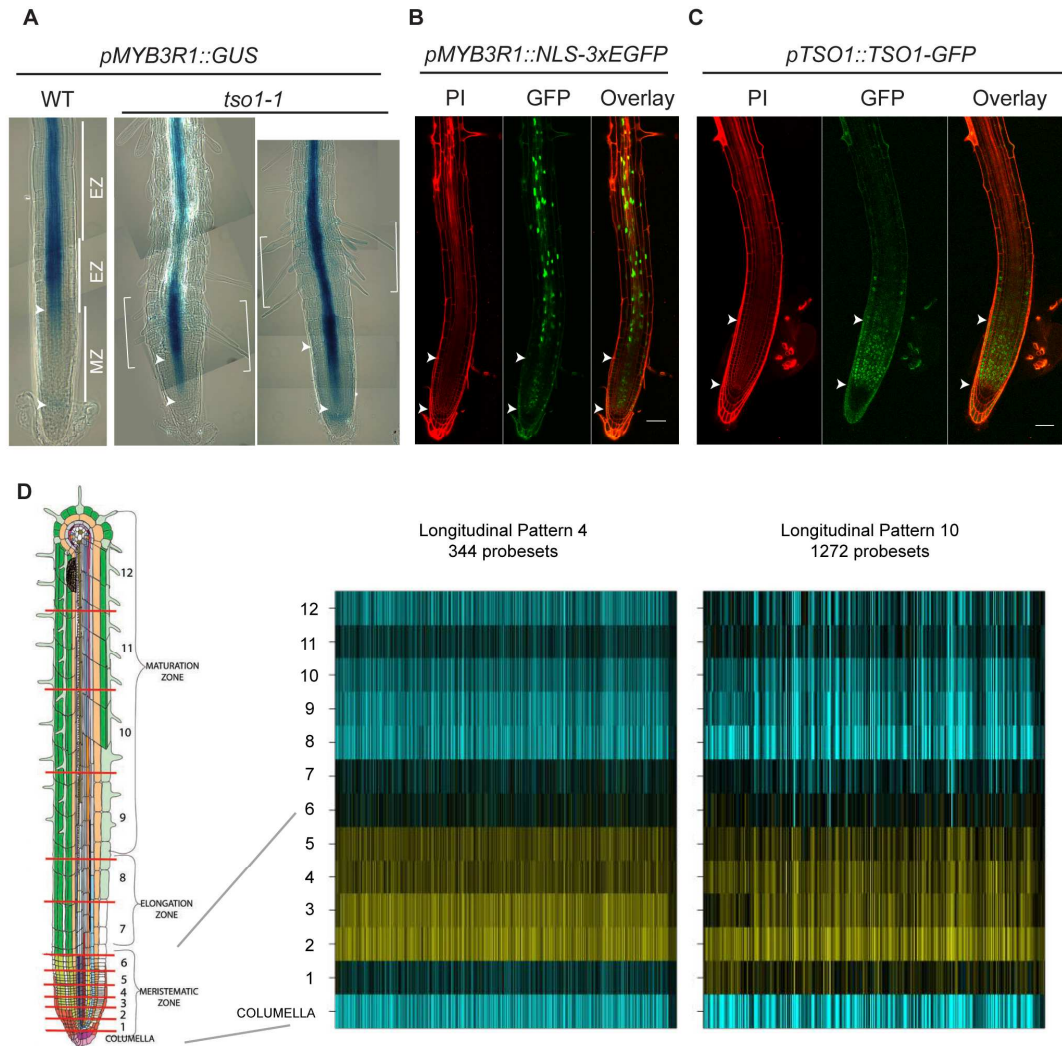


### Figure 2.8 *TSO1* and *MYB3R1* expression at the RAM

(A) *pMYB3R1::GUS* expression in wild type and *tso1-1* root (7dpg). Arrowheads indicate the boundary of the meristematic zone. Brackets indicate strong GUS signal accompanied by burst of root hair cell formation. (B) *pMYB3R1::NLS-3xEGFP* expression in the root. (C) *pTSO1::TSO1-GFP* expression in the root. In RAM, *TSO1* and *MYB3R1* appear to exhibit complementary patterns of expression, supporting a negative regulatory relationship between *TSO1* and *MYB3R1*. PI: Propidium iodide staining. Bars = 50um (B and C). (D) Heatmap of genes showing longitudinal expression pattern 4 and 10 in the high-resolution gene expression map study of Brady et al. 2007. *TSO1* is among the genes clustered in cluster 4 and 10. In the Brady et al. 2007 study, series cross sections of the root were collected and subjected to transcriptome profiling using ATH1 DNA microarray. Genes showing distinct expression pattern along the longitudinal axis of the root are clustered by fuzzy k-means clustering. Red lines on the root legend (left) denote the sections. Sections are labeled with “COLUMELLA” and numbers 1-12 on the root legend and the heatmaps on the right.

Interestingly, *TSO1* expression domain in root is largely complementary to *MYB3R1* expression domain revealed by the transcription and translational reporters (Figure 2.8). While *TSO1* is expressed in the meristem zone, *MYB3R1* is expressed above the transition zone. *TSO1* and *MYB3R1* show little overlap expression in the meristematic zone. In *tso1-1* mutant, the *MYB3R1* expression extended into meristematic zone. These expression pattern suggest that *TSO1* normally represses *MYB3R1* expression to limit its expression to differentiating tissue in the root.

Our gene expression data from the reporter lines showed elevated and ectopic expression of *MYB3R1* in *tso1-1* mutant both in SAM and RAM. Combined with the genetic interaction where *myb3r1* mutations rescued *tso1-1* phenotype both at SAM and RAM, we hypothesize a shared regulatory module: *TSO1* repress *MYB3R1* expression both at RAM and SAM to coordinate cell proliferation and differentiation. In roots, *TSO1* represses *MYB3R1* in the MZ to prevent cells from entering differentiation. When *TSO1* is mutated, *MYB3R1* is ectopically expressed in MZ, causing earlier and ectopic differentiation of roots. In SAM, *TSO1* however, the situation is more complicated as *MYB3R1* is both a partner and a target of *TSO1* regulation. Further, the difference between promoter fusion and translational fusion of *MYB3R1* in SAM suggests additional levels of regulation beyond transcriptional regulation.

### **2.3.8 Overexpression of *MYB3R1* is not sufficient to cause *tsol-1* mutant phenotype**

If *tsol-1* phenotype is mediated by mis-expression of *MYB3R1*, we ask if overexpression of *MYB3R1* is sufficient to cause *tsol-1* mutant phenotype. To test this model, we overexpressed *MYB3R1(cDNA)* in wild type (*Ler*) by introducing the *35S::MYB3R1* construct into *Ler* plants. The resulting plants did not show any phenotype (data not shown), suggesting that overexpressing *MYB3R1* alone is not sufficient to cause meristem or fertility defects observed in *tsol-1* mutants. We further tested this hypothesis using the TSO1 weak allele *tsol-3* as a sensitized background. The resulting *tsol-3; 35S::MYB3R1* plants also did not show any phenotypic difference from *tsol-3* plants (data not shown), suggesting that simply over-expressing MYB3R1 transcripts is not sufficient to cause the various defects observed in *tsol-1* mutants. Perhaps, increased MYB3R1 products alone can not cause any effect in the absence of simultaneous increase of MYB3R1 partners (which maybe increased simultaneously in *tsol-1* background). Alternatively, post-transcriptional or post translational regulation of MYB3R1, is also regulated directly or indirectly by TSO1, may be necessary to cause increased and constitutive MYB3R1 activity.

### **2.3.9 MYB3R1 phospho mimic enhanced *tsol-3* phenotype**

Based on the above result, we hypothesize that one way MYB3R1 is regulated post-transcriptionally is the phosphorylation at the serine residues. We queried the *Arabidopsis* Protein Phosphorylation Site Database (PhosPhAt 4.0)(Heazlewood et al. 2008; Durek et al. 2010) for phosphorylation sites detected for MYB3R1 protein. The serine at position 656 (Umezawa et al. 2013) and 709 (X. Wang et al. 2013) were

found to be phosphorylated in previous large scale phosphoproteomic studies. (level of conservation of the protein domain, sequence). To test the functional relevance of the phosphorylation of on these two sites, we modified *pMYB3R1::MYB3R1-GFP* constructs to change serine 656 and 709 into aspartic acid to produce phospho mimics S656D and S709D respectively. The resulting *pMYB3R1::MYB3R1-GFP-S656D* (gMYB3R1-S656D for short) and *pMYB3R1::MYB3R1-GFP-S709D* (gMYB3R1-S709D for short) were introduced into the *tso1-3* mutant background. We hypothesize that the phospho mimics of functionally relevant serine residues would confer constitutively active MYB3R1 and thus may cause a phenotype similar to *tso1-1*. The *tso1-3* mutants may offer a sensitized background for observing the effect of phosphomimics. While the S709D phospho mimic did not have any obvious phenotypic effect on *tso1-3*, the S656D phosphomimics enhanced the floral organ developmental defects, particularly carpel development, and fertility defect of *tso1-3* (Figure 2.9 B C D), but did not cause SAM fasciation (Figure 2.9 lower panel inflorescence). Our data suggest the serine 656 and its phosphorylation plays a positive role in MYB3R1 function regulation. This notion is supported by the *myb3r1-13* (A317) suppressor allele, a nonsense mutation that removes the C-terminus of MYB3R1 where serine 656 resides (Figure 2.4 D). As a result, *myb3r1-13* is a loss-of-function allele. Taken together, MYB3R1 serine 656 appears to subject to regulation by phosphorylation, which positively regulates MYB3R1 activity and enhances *tso1-3* floral organ developmental defect.

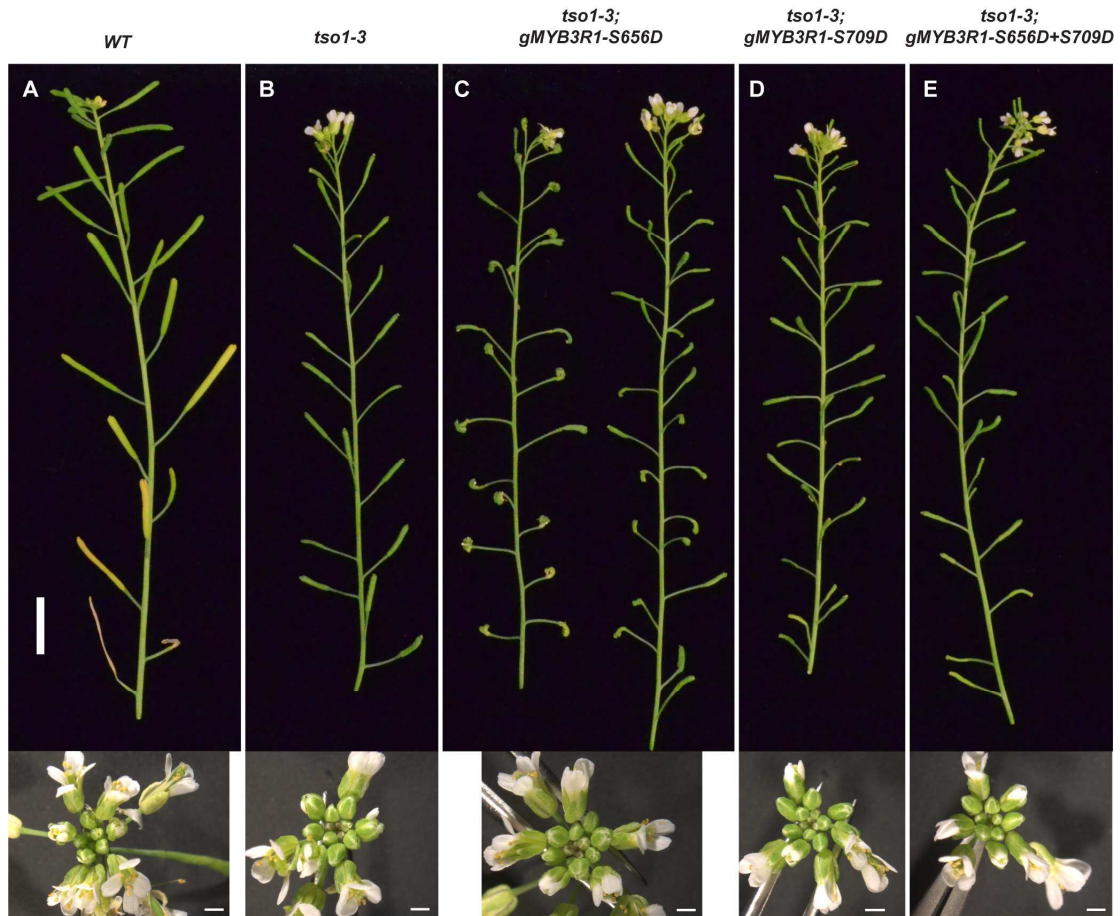


**Figure 2.9 MYB3R1 phospho mimic S656D enhanced *tso1-3* mutant**

The main shoot and inflorescence of WT(Ler) (A), *tso1-3* (B), *tso1-3*; *gMYB3R1-S656D* (C), *tso1-3*; *gMYB3R1-S709D* (D), *tso1-3*; *gMYB3R1-S656D+S709D* (E). Bars = 1cm (upper panel) and 1mm (lower panel). Two independent transgenic lines were shown for *tso1-3*; *gMYB3R1-S656D* (Note the reduced fertility (shorter seed pods) and malformed carpels).

The above results showed that loss-of-function alleles of *MYB3R1* suppress *tso1* mutants while putative gain-of-function *MYB3R1* enhances *tso1* mutants, suggesting that TSO1-MYB3R1 forms a regulatory module and are functionally tied together.

### 2.3.10 MYB3R1 physically interact with TSO1

Since *TSO1* and *MYB3R1* encode the homologs of DREAM complex components, and *TCX5* (*Arabidopsis TSO1* homolog) and *MYB3R3* has been shown to form a protein complex in promoting G2/M cell cycle gene expression, we test the hypothesis of a *TSO1*-*MYB3R1* protein complex by co-immunoprecipitation.

Our collaborators Dr. Hongli Lian and Pengbo Xu carried out the co-immunoprecipitation experiments.

Overexpression constructs *35S::YFP-MYB3R1* and *35S::Flag-TSO1* were transiently co-expressed in tobacco cell and immunoprecipitates were subjected to western blot.

Both transgenes were expressed and fusion protein could be detected in western

(Figure 2.10 Input). We found that *TSO1* did physically interact with *MYB3R1*

(Figure 2.10 IP, showing two replicates). This data suggests the biochemical nature of the *TSO1*-*MYB3R1* regulatory module is a *TSO1*-*MYB3R1* protein complex.

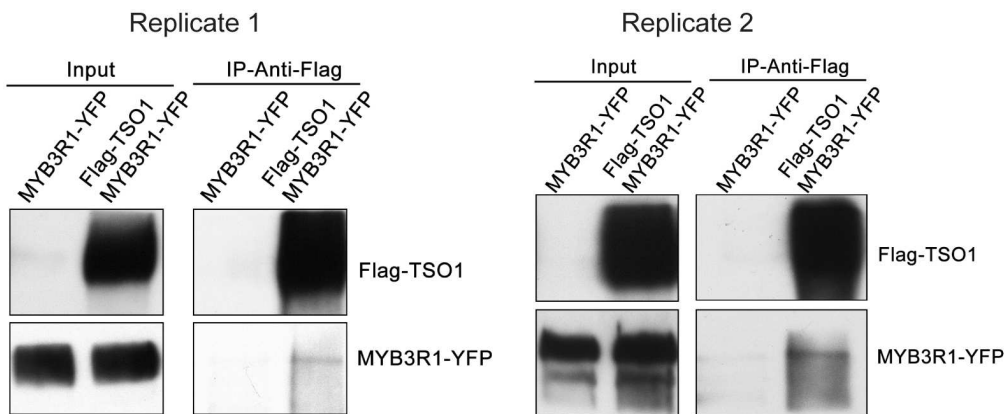


**Figure 2.10 TSO1 physically interact with MYB3R1**

Immunoprecipitation (IP) was performed with anti-Flag antibody using protein extract from tobacco leaves transiently expressing *35S::Flag-TSO1* and *35S::YFP-MYB3R1*. Tobacco leaves transiently expressing only *35S::YFP-MYB3R1* was used as control. Co-IP of *TSO1* and *MYB3R1* was examined by western blots using anti-GFP antibody. Protein extract before IP was used as input in replicate 1. Homogenized tissue directly boiled in loading buffer was used as input in replicate 2.

### 2.3.11 *myb3r4* loss-of-function mutation cannot suppress *tso1-1* phenotype

The closest homolog of *MYB3R1* in *Arabidopsis* is *MYB3R4*; these two genes were previously shown to play redundant function in promoting the expression of G2/M phase cell cycle genes in stomata in *Arabidopsis* leaves (Haga et al. 2011). However, none of the suppressor mutations maps to *MYB3R4*, suggesting that *MYB3R4* may differ from *MYB3R1* in its interaction with TSO1. Alternatively, *MYB3R4* may somehow reside in a region of chromosome that is resistant to mutagen. To test if mutations in *MYB3R4* could also suppress *tso1-1*, we designed CRISPR-Cas9 system to target the 2nd exon of *MYB3R4*. Several T2 plants that are homozygous for CRISPR generated mutations in *MYB3R4* were isolated. Among them, two plants are *tso1-1; myb3r4* double homozygous mutants and they are indistinguishable from *tso1-1* single mutant (Figure 10.A B E). This result demonstrates that unlike *myb3r1* loss-of-function mutations, *my3r4* loss-of-function mutations do not suppress *tso1-1*.

To test if *MYB3R4* functions redundantly with *MYB3R1* in the interaction with *tso1*, we introduced the *MYB3R4* CRISPR-Cas9 construct into a weakly suppressed *tso1-1* line, B12. The B12 suppressor line is the *tso1-1; myb3r1-5* double mutant. As described above, the *myb3r1-5* is a hypomorphic allele that partially impaired *MYB3R1* function. If *MYB3R4* functions redundantly with *MYB3R1* in suppressing *tso1-1*, *myb3r4* mutation should further suppress the defect of B12. In T2 plants, we isolated *tso1-1; myb3r1-5; myb3r4CRISPR* triple mutant (Figure 2.10 D). Compared with B12 (*tso1-1; myb3r1-5*), the triple mutant showed smaller stature and reduced fertility. The smaller stature of the triple mutant is reminiscent of *myb3r1-1; myb3r4-*

*l* double mutant reported previously (Haga et al. 2011). However, the triple mutant set little seeds. Thus, the CRISPR-induced bi-allelic mutations in *MYB3R4* did not further suppress the fertility defect of B12. These data suggest that *MYB3R1* and *MYB3R4* do not perform redundant function with respect to the interaction and function with *TSO1*.

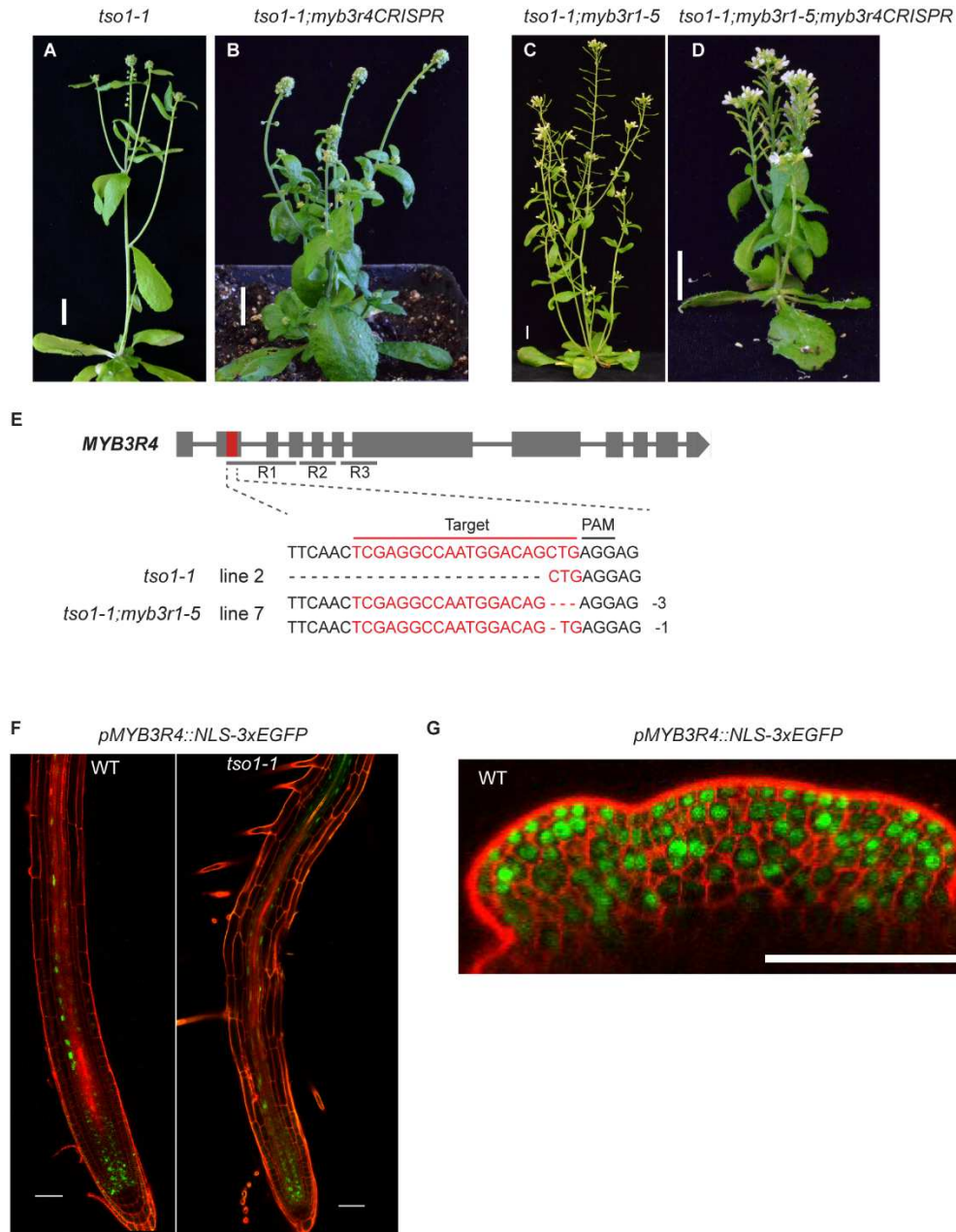


**Figure 2.11 MYB3R4 is not part of the TSO1-MYB3R1 module**  
**(A)** A *tso1-1* plant. **(B)** A *tso1-1; myb3r4CRISPR* plant. The specific mutations in MYB3R4 caused by CRISPR is shown in E (*tso1-1* line2). **(C)** A *tso1-1; myb3r1-5* plant. **(D)** A *tso1-1; myb3r1-5; myb3r4CRISPR* plant. Specific change in MYB3R4 by CRISPR is shown in E (*tso1-1; myb3r1-5* line7). **(E)** MYB3R4 gene structure and mutations created in this study. R1R2R3 coding regions are underlined. The CRISPR target sequence in the 2<sup>nd</sup> exon of MYB3R4 is shown. Corresponding mutant phenotypes are shown in **(B)** and **(D)**. **(F)** *pMYB3R4::NLS-3xEGFP* expression in wild type (Ler) and *tso1-1* root. This suggest that TSO1 may not repress MYB3R4 expression at least in root. **(G)** *pMYB3R4::NLS-3xEGFP* expression in wild type

(WT) SAM. Propidium iodide staining (red) was performed to show cellular outlines in roots in (F) and (G). Bars = 1cm (A-D) and 50um (F-G).

Although MYB3R1 and MYB3R4 are similar in amino acid sequence, their non-redundant nature may be due to distinct expression pattern. A transcription reporter *pMYB3R4-NLS-3xEGFP* was made and the GFP signal distribution was observed at SAM and RAM (Figure 2.10 F G). At the SAM, *MYB3R4* showed sporadic expression pattern throughout the proliferating and differentiating tissue. This pattern is consistent with previous observation that *MYB3R4* expression changes during cell cycle in cultured tobacco cells (Haga et al. 2007). *MYB3R4* expression pattern did not change significantly in *tsol-1* mutant RAM compared to wild type (Figure 2.10 F). Thus, we did not observe significant difference between *MYB3R1* and *MYB3R4* expression pattern. We speculate the difference in their ability to repress *tsol* mutants is due to their intrinsic function.

## 2.4 Discussion

### 2.4.1 *TSOI* and *MYB3R1* form a regulatory module functioning in multiple developmental processes

Our results show that beside its previously described regulatory role at SAM, *TSOI* also plays a role in regulating RAM. *tsol-1* mutant shows significantly reduced root length due to reduced Meristematic Zone size and early differentiation. Therefore, *TSOI* appears to play opposite roles in SAM and RAM: *TSOI* promotes differentiation and represses proliferation at SAM, while promotes proliferation and repress differentiation at RAM. This phenomenon is not unique to *TSOI* because factors such as plant hormone cytokinins and *HD-ZIP III* transcription factors also

play opposite roles in SAM and RAM. The opposite effects of *TSO1* at SAM and RAM strongly suggest a genetic connection between *TSO1* and factors like cytokinins and *HD-ZIP III* transcription factors which merit further investigation.

Our study, for the first time, functionally links *TSO1* to *MYB3R1* in plants and revealed a critical role of *MYB3R1* in SAM and RAM, which were not known before. Strong alleles of *myb3r1* mutants can suppress *tso1-1* almost completely, suggesting that almost all defects in *tso1-1*, including defects in SAM and RAM, are mediated through *MYB3R1*. As a transcription factor/chromatin factor, *TSO1* may regulate many genes involved in meristem homeostasis and cell cycle progression. The surprising finding that mutations in a single gene, *MYB3R1*, could suppress almost all aspects of *tso1* defects suggests that *MYB3R1* is critically involved in all processes regulated by *TSO1*.

*tso1-3* allele is a non-sense mutation and shows a weak phenotype limited to reduced fertility. Mutations in *MYB3R1* created by CRISPR also suppress *tso1-3*'s fertility defects. Thus, *MYB3R1* also plays a role in regulating reproductive development, possibly the development of male and female gametes (see Appendix I: Analysis of male meiosis and germline defects of *tso1-3*).

#### **2.4.2 TSO1-MYB3R1 likely function as a plant DREAM complex**

*TSO1* encodes the homolog of *LIN54*, an animal DREAM complex core component. The DREAM complex core recruit RB and E2F/DP to repress cell cycle gene expression at G0/quiescence to prevent cells from entering the S-phase. During G2/M

transition, the DREAM complex disassociates with the repressor RB/E2F and recruit B-Myb to activate G2/M phase gene expression. Thus, the DREAM complex is deemed the master coordinator of cell cycle genes expression. The animal ortholog of *MYB3R1*, *B-Myb*, is a target of DREAM complex, being repressed by DREAM, at G0 phase of the cell cycle. But at G2/M transition, B-Myb is incorporated into the DREAM complex and acts to promote G2/M phase gene expression. Mutations in *LIN54*, the animal homolog of *TSO1*, disrupt the DREAM complex core and compromise the G1/S checkpoint which lead to unchecked expression of cell cycle genes (Schmit, Cremer, and Gaubatz 2009; Kittler et al. 2007; Matsuo et al. 2012). During G2/M phase, mutations in the DREAM complex core can impair B-Myb function and lead to cytokinesis defects (Knight, Notaridou, and Watson 2009; Reichert et al. 2010). *Arabidopsis* possesses almost all DREAM complex component homologues (Table 1.1) suggesting the possibility of a DREAM-like complex in plants. Indeed, putative DREAM complex has been shown by proteomic analysis from young seedlings consists of RBR1, E2Fs, MYB3R3, ALYs and TCX5. Yet the proteomic study lacked developmental context and did not indicate the function for the complex.

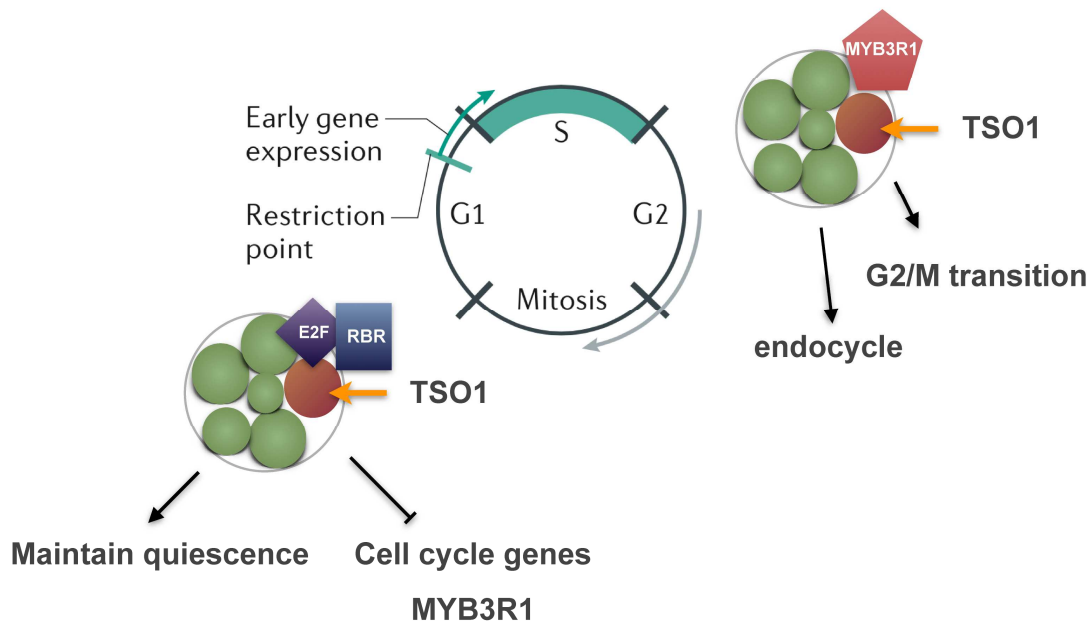


### Figure 2.12 Working model

We hypothesize that TSO1-MYB3R1 regulatory module function as a plant DREAM-like complex. TSO1 as part of the complex core, represses cell cycle gene including *MYB3R1* expression to maintain quiescence (G0). Proper MYB3R1 function depends on TSO1 and the complex core to promote late cell cycle genes for G2/M transition or enter into endocycle.

Using genetics and biochemistry, we demonstrated that TSO1 and MYB3R1 function together. Our data strongly suggests that TSO1 and MYB3R1 may function in a plant DREAM-like complex. If an analogous DREAM complex exists, where TSO1 is part of the complex core while MYB3R1 is both a target and a component of the complex, it explains well the observations and the meristem defects reported here.

At the SAM, *tso1-1* mutant showed over proliferation of meristem cells accompanied by overexpression of *MYB3R1* (Figure 2.7). This is because the defective DREAM core complex no longer represses *MYB3R1* as well as other cell cycle genes, causing uncontrolled meristem cell proliferation (Figure 2.12).

Cytokinesis defects were previously observed at the *tsol-1* SAM cells (Liu et al., 1997), where partially formed cell wall stubs failed to separate daughter cells. The cytokinesis defects of *tsol-1* is similar to the cytokinesis defects of stomata cells in *my3r1; myb3r4* double mutants, which were shown to be caused by failure in *KNOLLE (KN)* activation (Haga et al. 2007). *KN* encodes Syntaxin-related protein important for secretion of Golgi derived vesicles to form cell wall materials (Lukowitz et al., 1996). Therefore, the similar cytokinesis phenotype of *tsol-1* and *myb3r1; my3r4* is consistent with that MYB3R1 and/or MYb3R4 may need to associate with a functional DREAM complex core in order to activate G2/M phase genes such as *KN*.

This proposed model also provide explanation as to why mutating both TSO1 and MYB3R1 shows close-to-normal phenotype. Our data suggest that TSO1 and MYB3R1 function are interdependent. Losing TSO1 resulted in hyper active MYB3R1 to drive cell cycle, but also impair MYB3R1 function at G2/M. When the over-proliferation is suppressed by knocking out *MYB3R1*, the relatively normal cell cycle progression may allow redundant factors to fix cytokinesis defects. Further supporting the notion is the evidence that *Drosophila myb* mutant adult lethality can be suppressed by mutations in the MuvB core component mip130 (Beall et al. 2004), showing that mutating interdependent DREAM complex components can show almost normal phenotype.

At RAM, *tsol-1* mutant showed reduced proliferation and early differentiation accompanied by overexpression of *MYB3R1*. The transition of proliferation to differentiation at root is driven by the cells exiting mitotic cycle and entering endocycles. We hypothesize that TSO1 represses *MYB3R1* at RAM to inhibit entry into endocycle and maintains RAM size.

The above proposed model highlights the integration of the *TSO1-MYB3R1* module into different cell cycle phases in the context of different developmental processes.

#### **2.4.3 Insights of *MYB3R1* function and regulation**

Our saturated mutagenesis screen resulted in 13 new *myb3r1* mutant alleles. Several alleles were isolated multiple times from independent suppressors harboring the exact same mutation. 12 of the new alleles are caused by mutations in the DNA binding repeats of MYB3R1. Consider the relatively large gene body, the density of mutations in the DNA binding domain demonstrates its essential role for MYB3R1 function.

5 missense mutations that changes amino acids all resides in the R2R3 repeats. This is consistent with structural knowledge of animal Myb proteins that the R2R3 repeats are in direct contact with DNA. Suppressor B667 (C125Y in R2 repeat) showed that a redox sensing cysteine residue is functionally conserved from animals to plants.

These data lend support to previous knowledge of MYB3R1 DNA binding domain structure (Heine, Hernandez, and Grotewold 2004).

The only *myb3r1* allele that resides outside the DNA binding domain, *myb3r1-14*, causes a premature stop codon that removed the C-terminal region containing the serine 656. Our phospho mimic data suggest that this serine residue is likely phosphorylated and the phosphorylation is required for MYB3R1 activity. This revealed one post-translational regulatory mechanism of MYB3R1. It remains to be tested if MYB3R1 is regulated by cyclin-CDKs and if serine 656 is the substrate of cyclin-CDKs.

Intriguingly, by mining a high-resolution gene expression map of *Arabidopsis* root (Li et al. 2016), we discovered that *MYB3R1* has 5 splicing isoforms. Isoform 3 and 5 showed cell type specific enrichment: isoform 3 is enriched in epidermal cells and isoform 5 is enriched in QC cells. Although the functional relevance of these isoforms remains to be explored, we observe bursts of epidermal cell differentiation into root hair cells accompanied by high *MYB3R1* expression (Figure 2.8 A). Our mutation alleles *myb3r1-3* and *myb3r1-7* likely produce truncated proteins that mimic the predicted protein product of isoform 3 and 5 respectively. Thus, these *myb3r1* alleles provide valuable tools for further inquiries into *MYB3R1* regulation.

#### **2.4.4 MYB3R1 may play a unique role among R1R2R3 MYB proteins in Arabidopsis**

MYB3R1 and MYB3R4 were previously considered redundant factors in promoting G2/M phase cell cycle genes. Here we show that they are very different and may have distinct roles regarding meristem patterning. While mutations in *MYB3R1* alone could suppress all aspects of *tsol-1* mutant phenotype, *MYB3R4* mutations did not exert any

effect on *tsol-1* phenotype, even when combined with the weak *myb3r1-5* allele.

MYB3R1 has been shown to be both activator and repressor type of MYB3R protein (Kobayashi et al. 2015). The activator type MYB3R4 single mutant do not show G2/M gene expression change. Only in *myb3r1;myb3r4* double mutant, G2/M gene expression is reduced causing cytokinesis defects. Similarly, double mutant of the repressor *myb3r3;myb3r5* do not show G2/M gene expression change (shown by qPCR and reporter genes) unless combined with *myb3r1* mutant. These data suggest that MYB3R1 plays a commanding role among MYB3R proteins. This may explain why mutating *MYB3R1* was able to rescue both over proliferation (G1/S control) and cytokinesis (G2/M) defects of *tsol-1*.

*Drosophila* only has one Myb and it is both an activator and repressor of cell cycle genes. It seems that MYB3R1 functions similarly to the *Drosophila* Myb, and the other 4 *Arabidopsis* MYB3R proteins adopted specific activation or repression function. It remains to be tested if single MYB3R1 could fulfill the function of all five *Arabidopsis* MYB3R proteins, and also if *Drosophila* Myb gene could complement *Arabidopsis myb3r1* mutant (test could be done using *tsol-1;myb3r1* double mutant, since *myb3r1* single mutant do not have phenotype).

## Chapter 3: Identification of *REVOLUTA*, a *HD-ZIP III* transcription factor, as a downstream target of TSO1

### 3.1 Introduction

The iterative generation of aerial organs of flowering plants relies on the proper patterning of the shoot apical meristems (SAMs), microdomains that house the stem cell populations at the aerial growing tips. The stem cells are maintained in the central zone (CZ) and the stem cell daughters then enter periphery zone (PZ) where cells divide rapidly and acquire cell fate upon positional cues. Lateral organ primordia generated from the PZ acquire adaxial/abaxial (ad/ab) polarity based on their inherited position related to the meristem: the adaxial (ad) side is facing the SAM, while the abaxial (ab) side is facing away from the SAM. The ad/ab polarity of differentiating lateral organs also feeds back to the meristem, where the adaxial environment promotes stem cell activity, while abaxial environment antagonizes it. Thus, the proper patterning of SAM requires coordination between cell proliferation and differentiation, as well as the balance between stem cell activity and lateral organ ad/ab polarity.

One of the key modules that regulate the ad/ab cell fate is the bidirectional negative feedback circuit between the *HD-ZIP III* gene *REVOLUTA* (*REV*) and the miR165/166. *REV* is expressed at the adaxial side of the lateral organs and represses miR165/166 gene expression to restrict miR165/166 expression only at the abaxial side (Merelo et al. 2016). On the other hand, miR165/166 forms a gradient originating from the abaxial side and represses *HD-ZIP III* gene expression post-transcriptionally

at the abaxial side (Mallory et al. 2004; Emery et al. 2003). It was previously shown that dominant mutations in these *HD-ZIP III* genes were caused by mutations in a conserved region targeted by the miR165/166. The mutated miR166/165 binding site within the *HD-ZIP III* sequence made *HD-ZIP III* mRNA resistant to the miR166/165-mediated degradation, leading to adaxialization of leaves (Emery et al. 2003; Zhong and Ye 2004b; McConnell et al. 2001; McConnell and Barton 1998; Ochando et al. 2008). Knocking down miR165/166 also lead to adaxialization of lateral organs (Emery et al. 2003; McConnell et al. 2001; Yan et al. 2012). Therefore, the *HD-ZIP III* - miR165/166 regulatory circuit, together with other antagonistic mechanisms, provides the positional information along the ad/ab axis to direct adaxial or abaxial cell fate acquisition and maintenance (Kuhlemeier and Timmermans 2016). Established early during embryogenesis, the *HD-ZIP III* - miR165/166 circuit is involved in the patterning of multiple stem cell niches including shoot, root apical meristems and vascular stem cell niche in *Arabidopsis*. At the SAM, gain-of-function alleles of *HD-ZIP III* genes often exhibit enlargement or ectopic formation of meristems (McConnell et al. 2001; Zhong and Ye 2004a), suggesting that proper level of *HD-ZIP III* activity is crucial for maintaining SAM size.

The *Arabidopsis TSO1* gene plays an essential role in coordinating stem cell proliferation with floral organ differentiation at the SAM. The *tso1-1* allele has fasciated shoot meristems with over proliferating stem cells and failure of floral organ differentiation (Z. Liu, Running, and Meyerowitz 1997). Further, *tso1-1* exhibited a bushy phenotype revealing a reduced apical dominance. How does TSO1, a CXC

domain containing transcription factor, regulate and coordinate these different developmental processes is not well understood. In chapter II, I described a genetic screen that identified the TSO1-MYB3R1 regulatory module at the shoot and root apical meristem that coordinates proliferation with differentiation. My results shown in chapter II revealed that TSO1 and MYB3R1 likely form a protein complex to negatively regulate target genes including MYB3R1, cell cycle genes, and other as yet unidentified genes. However, how does the TSO1-MYB3R1 cell cycle regulatory module get incorporated in the plant meristem tissue context and interact with known SAM regulators remains elusive. Uncovering the additional TSO1 protein complex components and/or target genes may provide insights to the underlying mechanism of TSO1 function at SAM and help explain the pleiotropic defects in *tso1* mutants.

The identification of 32 *myb3r1* suppressor alleles in chapter II indicated that the mutagenesis screen is reaching saturation and would unlikely lead to additional new genetic loci. In this chapter, I report a second mutagenesis screen that led to the identification of several dominant enhancers of *tso1*. This screen took advantage of a weak suppressor of *tso1-1*, B12, which harbors a missense mutation in *MYB3R1*. The weakly suppressed *tso1-1* background allowed us to screen for enhanced phenotypes of *tso1* mutants. The enhancer screen was previously not possible as *tso1-1* showed very strong phenotypes including complete sterility.

Here, we report the characterization of a dominant enhancer, E2, from these second genetic screen. We showed that E2 is a *REVOLUTA* gain-of-function mutant allele,

which enhances meristem fasciation and organ formation defects of *tsol-1*. Our results suggest that *TSOI* normally represses the expression of *REV*. Since, *REV* is known to promote *STM* expression and axillary meristem formation, the bushy phenotype of *tsol-1* is likely due to elevated *REV* expression in *tsol-1* mutants. In addition, it may also explain meristem fasciation of *tsol-1*. The genetic interaction between *TSOI* and *REV* revealed by this study not only helped to explain the pleiotropic *tsol-1* mutant phenotype but also *TSOI*'s crucial role in repressing *HD-ZIP III* genes in different developmental context.

### **3.2 Material and methods**

#### **Plant material and growth conditions**

*Arabidopsis thaliana* ecotype Landsberg *erecta* (*Ler*) was used as the wild type. All mutants are in the *Ler* background and were described previously: *tsol-1* (Liu et al. 1997), *tsol-1*+/*sup-5* (Sijacic et al. 2011) and *tsol-3* (Hauser et al. 1998). *tsol-3*+/*sup-5* (Chapter II).

Plants were grown on Metromix soil (Griffin) under a 16 hour light-8 hour dark cycle at 25°C. Sterilized seeds were germinated on half-strength Murashige and Skoog (1/2 MS) medium containing 1% (w/v) sucrose and 0.6% (w/v) phyto agar.

#### **EMS mutagenesis**

Seeds from 10 B12 backcrossed F2 individuals (total 0.12g) were pooled. Seeds were treated with 0.2% EMS solution overnight and rinsed with water for 4 hours before spreading on soil.

## **Molecular cloning**

*REV* translational reporter *pREV::VENUS* was kindly provided by Dr. Meyrowitz (Heisler et al. 2005). To make *REV* genomic construct carrying the E2 mutation, *REV* genomic fragment was released from *pREV::VENUS* vector by BamHI and NcoI digestion and cloned into pCR/8/GW/TOPO vector (Invitrogen) to produce *gREV*-TOPO vector. The fragment between EcoNI and HindIII cutting sites that encompasses the miR165/166 targeting site in the *gREV*-TOPO vector was then replaced with amplified fragment from the E2 enhancers. For *REV* gene editing, gRNA was designed to target the 1st exon of *REV*. Primers ATTGGTACACAGCTGAGCAAGTCG and AAACCGACTTGCTCAGCTGTGTAC were annealed and ligated into pHEE401E (Z.-P. Wang et al. 2015) vector by Golden Gate cloning (Engler and Marillonnet 2014).

## **Microarray experiments and data analysis**

Total RNAs were isolated from inflorescences of three *tsol-1* and three WT plants and were used in microarray assay as three biological replicates. The microarray assay was performed at Biopolymer/Genomic Core Facility, School of Medicine, University of Maryland, Baltimore. Wild type inflorescences (with open flowers removed) and *tsol-1* inflorescences were harvested at the same time. Three biological replicates were collected for each genotype. 150 ng of total RNA from each sample was used for aRNA target preparation with the 3' IVT Express Kit (Affymetrix, Ca,

USA). The probes were hybridized with the *Arabidopsis* ATH1 Genome Arrays using The GeneChip Hybridization, Wash, and Stain Kit (Affymetrix, CA, USA).

The microarray data was collected in the form of preprocessed and normalized CEL files and expression measures were calculated with justRMA using RMA (Irizarry et al. 2003). Differential expression was determined with a moderated t-statistic using Empirical Bayes methods (Smyth 2004). Corrections for multiple testing were done using the False Discovery Rate (FDR) method (Benjamini and Hochberg 1995). Genes for which the fold-change between *tsol-1* and wild type was greater than 1.5 (FDR-adjusted  $P \leq 0.05$ ) were designated as “down-regulated” in *tsol-1* or “up-regulated” in *tsol-1*.

The “up-regulated” and “down-regulated” in *tsol-1* gene lists were further filtered to remove genes that were expressed only in “late” stage floral organs (these organs are absent in the *tsol-1* mutants). The AtGenExpress (Schmid et al. 2005) provided microarray data sets for floral stages 1-6, 9, 10-11, and 12. The mean value of three biological replicates of stage 9, 10-11, and 12 was respectively compared with the mean value of three biological replicates of early floral stages 1-6. We designated genes as being “early” (1.5x up-regulated in stages 1-6 vs any of the stages 9-12 with, as before, FDR-adjusted  $P \leq 0.05$ ), “late” (the reverse) or “neither”. Genes belonging to both “up-regulated”, “down-regulated” in *tsol-1* and “early” were identified using an R script.

Gene Set Enrichment Analysis was performed on two gene sets: first, genes that were both “up-regulated” in *tsol-1* and part of the “early” set as defined above (Table 3.1), and second, genes that were both “down-regulated” in *tsol-1* and part of the “early” set as defined above (Table 3.2). This Gene Set Enrichment Analysis of GO BP categories was performed using a hypergeometric test (Falcon and Gentleman 2007; Hahne et al. 2010). Intersections between gene sets were plotted using the UpsetR package (Conway, Lex, and Gehlenborg 2017). All analyses described in this section were done using the R language.

### **RNA extraction and quantitative real-time RT-PCR**

RNA were extracted from inflorescence tissue using NucleoSpin RNA Plant kit (MACHEREY-NAGEL). First strand cDNA was synthesized with iScript cDNA synthesis kit (BioRad). qPCR was carried out using Sso Fast Evagreen supermix (BioRad) using primers REV.qPCR.F:CCAAGCTGTGAATCTGTGGTC, REV.qPCR.R:CGATCTTTGAGGATCTCTGCA (Y. Liu et al. 2014). STM.qPCR.F:GGCCTTACCCTTCGGAGCAA, STM.qPCR.R:GGTGAGGATGTGTTGCGTCCATT (Y. Wang et al. 2014). PP2A.F:TAACGTGGCCAAAATGATGC, PP2A.R:GTTCTCCACAACCGCTTGGT.(Lieberman et al. 2015)

### 3.3 Results

#### 3.3.1 Isolation of genetic modifiers of *tso1-1*; *myb3r1-5* (*B12*)

Chapter II reported the discovery of the *TSO1-MYB3R1* regulatory module that operates at the *Arabidopsis* shoot and root meristems. *myb3r1-5* is a relatively weak suppressor of *tso1-1*. Unlike strong *myb3r1* mutant alleles that suppressed both meristem fasciation and sterility of *tso1-1*, *myb3r1-5*, a weak loss-of-function allele, does not completely suppress the fertility defects of *tso1-1*. Hence, *tso1-1*; *myb3r1-5* double mutant is almost wild type but may be sensitive to additional genetic changes that may compromise the “*TSO1* pathway”. Therefore, this double mutant can be used as a sensitized genetic background for a new round of mutagenesis to screen for enhancers of *tso1-1*; *myb3r1-5*. For simplicity, this double mutant, *tso1-1*; *myb3r1-5*, is called *B12* in the remainder of this chapter.

Using *B12* as a sensitized background, we carried out an EMS mutagenesis to identify enhancer or suppressor mutations of *B12* by examining meristem or/and fertility defects. Figure 3.1 illustrates the mutagenesis screen scheme. About 2000 M1 plants were obtained. Although most suppressors or enhancers are recessive and only exhibit phenotypes in the M2 generation, some suppressors and enhancers were dominant and exhibited phenotypes at the M1 generation. I screened M1 generation and identified 3 dominant suppressors and 13 dominant enhancers (Figure 3.1). Because *B12* also contains the *TSO1-GR* construct, the dominant enhancers can be rescued by DEX treatment to obtain seeds.

For the screening of the M2 generation, seeds from 8-15 M1 plants were pooled together and planted. Six additional suppressors and 49 enhancers were isolated in the M2 generation. In total, 9 suppressors and 62 enhancers were identified from this second screen using *B12* (Figure 3.1).

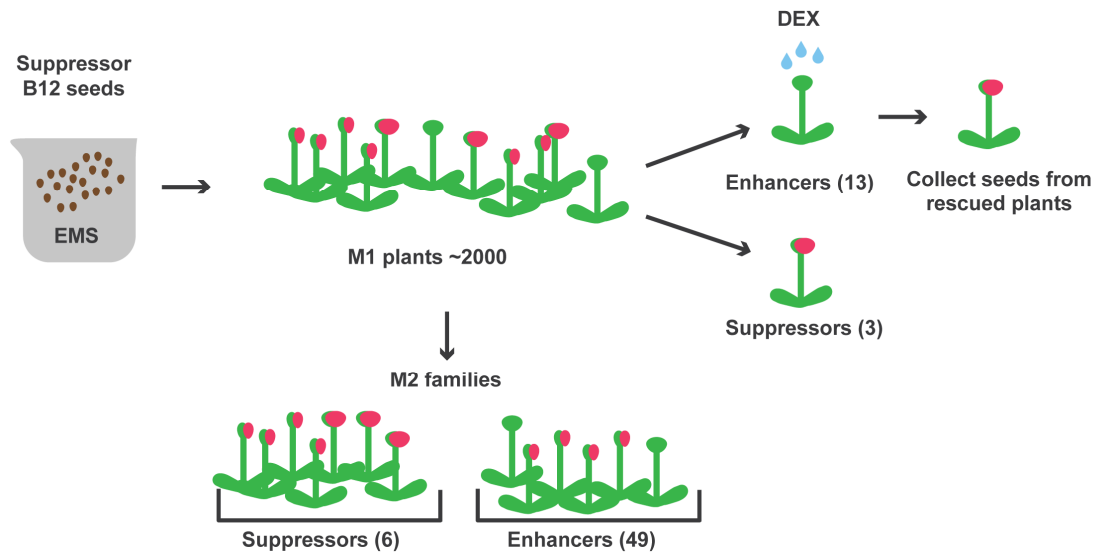


**Figure 3.1 Diagram summarizing the EMS mutagenesis screen**

*B12* (*tsol-1; myb3r1-5*) seeds were treated with EMS and gave rise to ~2000 M1 plants. By screening the M1 population, 13 enhancers were identified that showed meristem fasciation and sterility (denoted by green apex); they were treated with DEX to get seeds. Three suppressors with improved fertility (denoted by big red apex) were isolated as well. For M2 population, seeds were pooled from 8-15 M1 plants and germinated to give rise to M2 plants. Six suppressors and 49 enhancers were isolated by screening the M2 plants.

**3.3.2 REVOLUTA gain-of-function mutation enhances *B12* phenotype**

Two dominant enhancers E2/+ and E9/+ showed small siliques without seeds (Figure 3.2A) and fasciated inflorescence meristems with many more floral buds per shoot (Figure 3.2B). Additionally, their leaves are sometimes trumpet-shaped (Figure. 2C). Homozygous E2 and E9 M2 plants showed stronger defects in fasciation, sterility, and trumpet-shaped leaves (Figure 3.3 B,C). The progeny of E2/+ segregated in a

ratio of 31/126 (24.6%) strong phenotype; 54/126 (42.9%) medium phenotype and 41/126 (32.5%) background *B12* phenotype (Chi-squared test p-value=0.125), confirming the dominant nature of the E2 enhancer.

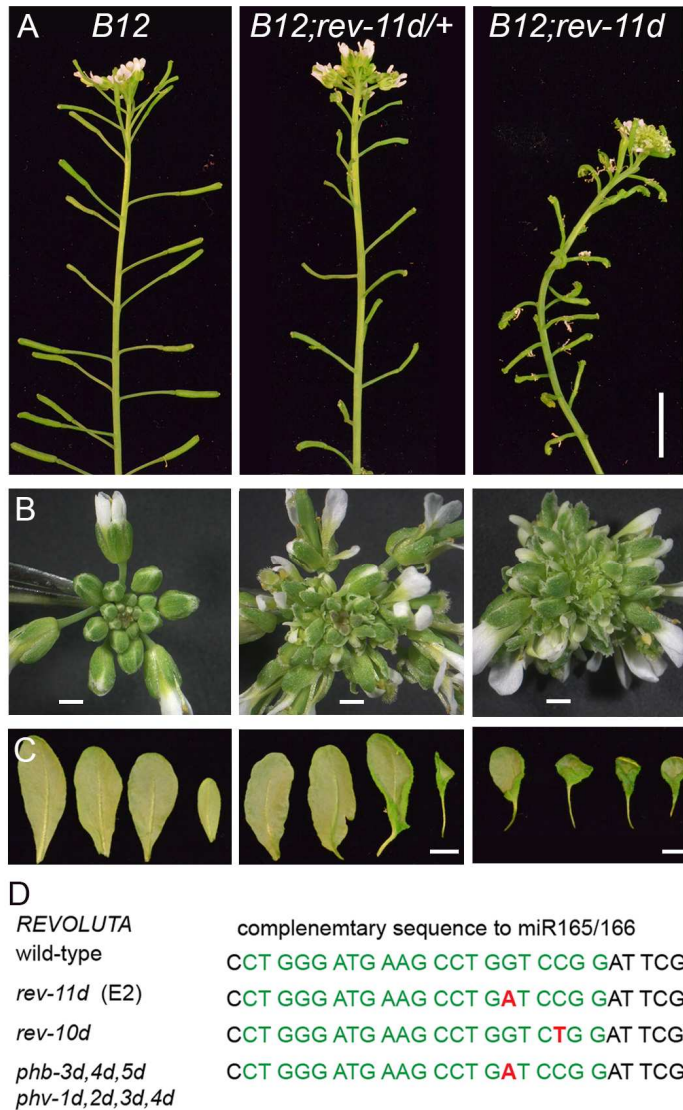


**Figure 3.2 A gain-of-function allele in the *REVOLUTA* gene enhances *B12* phenotype**

(A) Phenotype of *B12*; +/+, *B12*; *rev-11d*/+ heterozygous and *B12*; *rev-11d/rev-11d* homozygous plants. In the *B12* background, *rev-11d* (the E2 enhancer) caused enhanced fertility defect shown by smaller siliques (middle). *B12*; *rev-11d/rev-11d* plants showed even stronger phenotypes including even shorter siliques or curled siliques due to defects in carpel development (right). Scale bar = 1cm.

- (B)** *B12; rev-11d/+* plants showed fasciated inflorescence with more floral buds than the *B12* inflorescence (middle). *B12; rev-11d/rev-11d* plants too showed inflorescence fasciation. Scale bar = 1mm.
- (C)** Rosette leaves with abaxial side facing up. Curling (an indicator of adaxialization of the leaf) is obvious in *B12; rev-11d/+* and *B12; rev-11d/rev-11d* plants. Scale bar = 1cm.
- (D)** *REV* DNA sequence at the miR165/166 target site; the specific sequence complementary to miR165/166 is labeled in green. The *rev-11d* (E2) mutation is shown in red beneath the WT sequence. Previously published mutations in the *HD-ZIP III* family (McConnell et al. 2001; McConnell and Barton 1998) are shown beneath the *rev-11d* (E2) sequence.

The leaf phenotype of these enhancer mutants resembled gain-of-function mutants in the *HD-ZIP III* gene family. To determine if the E2 and E9 are gain-of-function mutations in the *HD-ZIP III* genes (*PHABULOSA*, *PHAVOLUTA*, *REVOLUTA* (*REV*), *INCURVATA4* (*CORONA/ATHB15*) and *ATHB8*), we PCR amplified a 1Kb region of all five *HD-ZIP III* genes encompassing the miR165/166 binding site from E2 and E9 and sequenced the PCR products. A G-to-A mutation, was found in the *miR165/166* targeting site of *REV* in both E2 and E9 (Figure 3.2D). This mutation likely makes the *REV* mRNA resistant to the miRNA165/166 degradation, although it also causes an amino acid substitution (G189D) in the START domain of the *REV* protein. Hence, we renamed E2 and E9 as *rev-11d*, despite that E2 and E9 were isolated independently from one another. The ability of *rev-11d* to confer increased *REV* function due to its immunity to miRNA165/166 is supported by that several dominant alleles of the *HD-ZIP III* family members *PHB* and *PHV* (*phb-3d,4d,5d* and *phv-1d,2d,3d,4d*) had the identical G to A change at the miRNA target sites (Figure 3.2D)(McConnell et al. 2001; McConnell and Barton 1998). Therefore, the E2 and E9 enhancer mutations are mutants of the *REV* at the *miR165/166* target site.

### 3.3.3 Synergistic interaction between *rev-11d/+* and *B12* at the shoot apical meristem

To determine if *rev-11d* indeed enhances *B12* instead of just being additive with *B12*, we examined *rev-11d/+* mutant phenotype in the absence of *tso1-1*. Specifically, Dexamethasone (DEX) was supplied to the *B12; rev-11d/+* plants; DEX treatment allowed TSO1-GR to enter nucleus and rescue *tso1-1*. The resulting DEX treated plant should be no longer defective in the *tso1* locus and should exhibit *myb3r1-5; rev-11d/+* phenotype only. Indeed, DEX treated plants no longer exhibited fasciated inflorescence and the silique was fully developed and fertile (Figure 3.3A). Similarly, the *B12 (tso1-1;myb3r1-5)* alone in the absence of *rev-11d/+* also showed normal inflorescence and almost full length silique (Figure 3.2A left). Therefore, only when *B12* and *rev-11d/+* were combined (ie, in the *B12; rev-11d/+* plants) (Figure 3.2A middle, Figure 3.3A, Mock), the inflorescence was fasciated and the siliques were curled and infertile, strongly supporting a synergistic genetic interaction between *B12* and *rev-11d/+*.

*rev-11d* homozygous plants have a very strong phenotype including strong meristem fasciation, infertility, and trumpet-leaves (Figure. 2A right and 3B), addition or removal of *tso1-1* (by MOCK or DEX treatment) failed to show any changes in the severity of the phenotype (Fig. 3B), indicating that *rev-11d* homozygous mutants are not sensitive to *B12* due to its already strong gain-of-function phenotypes. Hence, the synergistic genetic interactions can only be revealed when *REV* function is partially affected.

*tsol-1*, in the absence of *myb3r1-5*, also exhibited a strong phenotype (Chapter I, II). We tested if *rev-11d/+* could further enhance *tsol-1*. We crossed *rev-11d; B12 (tsol-1; myb3r1-5)* with wild type (Ler) and screened for *tsol-1; rev-11d/+* plants in the F2 population. The resulting *tsol-1; rev-11d/+* showed an inflorescence phenotype identical to *tsol-1* single mutant as well as absence of silique development due to failure of carpel development in *tsol-1* (Figure 3.3C), suggesting that *tsol-1* is insensitive to *rev-11d/+* due to its already strong defects in meristem and fertility.

*B12* consists of *myb3r1-5* and *tsol-1*. *myb3r1-5* single mutant and other hypomorphic and null alleles of *MYB3R1* normally do not have any obvious phenotype. To determine if synergy is observed between *rev-11d/+* and *myb3r1-5* (in the absence of *tsol-1*), we obtained *myb3r1-5; rev-11d/+* by screening the same F2 population described above. *myb3r1-5; rev-11d/+* plants, like mock treated *B12, rev-11d/+*, did not exhibit any meristem fasciation, nor reduced fertility (Figure 3.3D). This data suggests that *myb3r1-5; rev-11d/+* double mutant do not cause meristem fasciation in the absence of *tsol-1*.

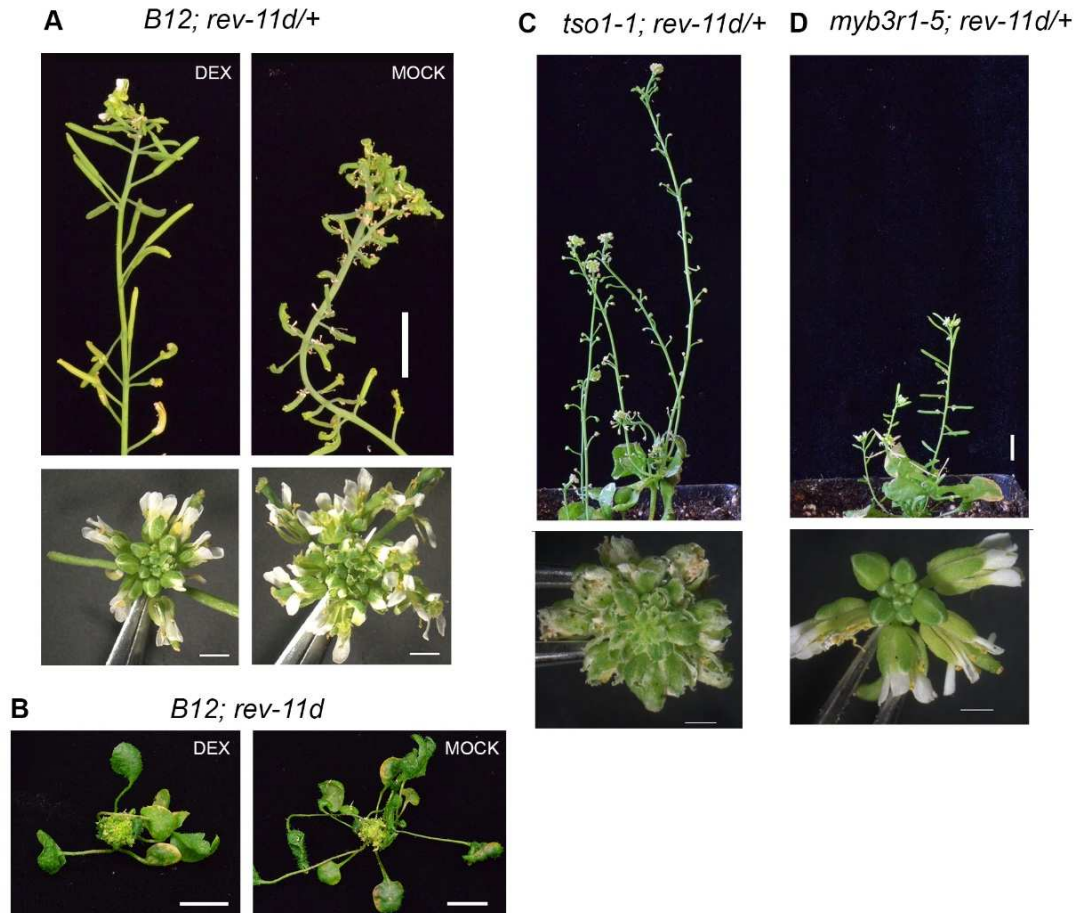


**Figure 3.3 Demonstration of synergistic interaction between *B12* and *rev-11d/+***  
**(A)** *B12; rev-11d/+* treated with DEX rescued *tso1-1* and did not show any enhanced phenotype when compared with *B12; rev-11d/+* without the DEX treatment (mock). Scale bar = 1 cm (upper panel) and 1 mm (lower panel).  
**(B)** *B12; rev-11d/rev-11d* plants treated with DEX showed similar phenotype to *B12; rev-11d/rev-11d* plants without the DEX treatment (mock). Scale bar = 1 cm.  
**(C)** *tso1-1; rev-11d/+* plants showing a phenotype similar to *tso1-1* single mutants. Scale bar = 1 cm.  
**D.** *myb3r1-5; rev-11d/+* plants are similar to wild type in the inflorescence and silique length. Scale bar = 1 cm.

In summary, the genetic synergy is only observed when *tso1-1* phenotype is partially suppressed by *myb3r1-5* and when *rev-11d* is partially affected as a heterozygote.

*myb3r1-5* mutation likely attenuates *tsol-1* mutant phenotype to allow the enhancement effect of *rev-11d/+* to be uncovered.

*tsol-3* is a weak *tsol* allele showing normal SAM patterning with reduced fertility. To determine if *tsol-3* and *rev-11d/+* also show synergistic interaction, we crossed the *B12/+*, *rev-11d/+* plants to the *tsol-3* plants. The *tsol-3; rev-11d/+* plants from the resulting progeny will be examined in July 2017.

Our results demonstrated a synergistic genetic interaction between *B12* and the *REV* gain-of-function mutation (*rev-11d/+*), suggesting that *TSO1* and *REV* likely function in the same pathway to regulate proper meristem size and fertility. Induction of *TSO1* wild type function by DEX in *B12; rev-11d/+* was able to rescue the meristem fasciation and fertility defects, suggesting that wild type *TSO1* can repress *rev* gain of function.

#### **3.3.4 Genome wide identification and analysis of TSO1 downstream targets by DNA microarray**

If *TSO1* and *REV* function in the same pathway, what is their regulatory relationship? Since *TSO1*-*MYB3R1* complex is often thought as a negative regulator, one possible interpretation is that *TSO1*-*MYB3R1* normally represses *REV* transcription as well as other genes involved in meristem development and cell cycle regulation. To gain a genome-wide understanding of *TSO1*-regulated genes and processes, a former postdoc in the Liu lab, Paja Sijacic, conducted a microarray experiment. RNAs were extracted from inflorescence tissues (consisting of only unopened flowers) of wild

type (*Ler*) and *tso1-1*, respectively, in triplicates; they were made into cDNA probes and hybridized to the ATH1 microarray containing approximately 24,000 *Arabidopsis* genes on the Chip. A former graduate student, Charles Hawkins, then did the data analysis. Differentially expressed (DE) genes between WT inflorescence and *tso1-1* inflorescence were identified (see Methods). Up-regulated genes in *tso1-1* mutants were of particular interests as they may represent genes normally repressed by *TSO1*. On the contrary, down-regulated genes in *tso1-1* may simply due to missing floral organs in *tso1-1*. Therefore, genes expressed at later stages of flower development (stages 9-12; (Schmid et al. 2005)) were filtered out from the *tso1*-down and -up list to reduce these indirectly affected genes (Table 3.1 and Table 3.2).

Gene ontology (GO) enrichment analysis was conducted among the *tso1-1* up and down-regulated genes (after filtering) (Table 3.1 and 3.2). The resulting enriched GO terms are listed in Table 3.3 and 3.4. Top 10 ranked GO terms are shown in Figure 4A and B. Consistent with the *tso1-1* mutant phenotype (Liu et al., 1995), genes involved in “maintenance of meristem identity”, “DNA replication initiation”, “cytokinesis by cell plate formation” were significantly enriched among *tso1-1* up-regulated genes, suggesting up-regulation of transcription programs favoring cell division and stem cell maintenance (Figure 3.4A, Table 3.3). Interestingly, genes involved in “polarity specification of adaxial/abaxial axis” were significantly enriched in *tso1-1* up-regulated genes, suggesting *TSO1* perhaps normally represses ad/ab polarity genes (Figure 3.4A, Table 3.3). In contrast, genes responsible for tissue differentiation processes like “sexual reproduction”, “secondary cell wall biogenesis”

and “anther development” are enriched among the *tsol-1* down-regulated genes (Figure 3.4B, Table 3.4). Taken together, our genome-scale transcriptome analysis of *tsol-1* mutant revealed that *TSO1* represses meristem genes and adaxial/abaxial polarity genes while at the same time promotes differentiation.

*REV* is among the *tsol-1* up-regulated gene list (Figure 3.4C); *REV* expression was increased by 1.6-fold (p-value = 0.004). Other members of the *HD-ZIP III* gene family, *PHV* and *PHB*, also showed increased expression in *tsol-1*, with *PHV* showing statistically significant increase (1.32-fold change, p-value = 0.002) (Figure 3.4C). Therefore, our data support that *TSO1* normally acts to repress the transcription of *REV* and *PHV* during inflorescence development.

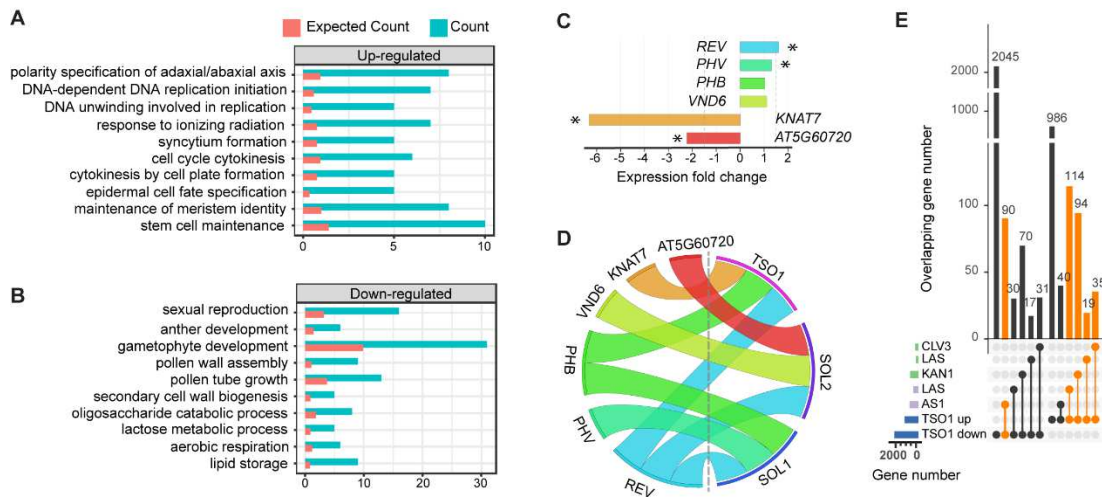


**Figure 3.4 Summary of *TSO1* microarray and yeast-one-hybrid data**  
**(A)** Top 10 ranked GO categories (biological process) enriched among genes upregulated in *tsol-1*. **(B)** Top 10 ranked GO categories (biological process) enriched among genes downregulated in *tsol-1*. Only GO categories with gene count > 5 and hypergeometric test p-value < 0.01 were selected and ranked by odds ratio. GO categories represented by similar sets of genes were combined to avoid redundant listing. **(C)** Transcript fold change for the six target genes shown in A based on our microarray data comparing WT inflorescence to *tsol-1* inflorescence. Minimum cut off is at +/- 1.5-fold indicated by the dashed lines. Asterisks indicate significant

expression changes ( $p$ -value  $< 0.01$ ). Bars are colored according to the target gene name shown in (D). (D) Circos graph summarizing yeast-one-hybrid results by mining large scale yeast-one-hybrid screens (Taylor-Teeples et al. 2014; Gaudinier et al. 2011). One-to-one relationship between TSO1, SOL1, and SOL2 transcription factors (right of the dotted line) to the promoter of their respective target genes (left of the dotted line) is indicated by colored ribbon. Shown are all target genes found by the screens to be bound by TSO1, SOL1 and SOL2.

(E) Overlapping gene numbers (Y-axis) between differentially expressed (DE) genes in *tsol-1* mutant and genes expressed at specific subdomains of the shoot apex. CLV3, LAS, and KAN1 (green bars) represent three different subdomains defined by their respective expression (Yadav et al 2014). Number of genes specifically expressed in respective subdomains are indicated by the green bars to the left. Similarly, number of LAS and AS1 subdomain (purple bars) expressed genes are indicated to the left (Yu et al., 2014). Number of genes up- or down-regulated in *tsol-1* mutants are indicated by blue bars to the left. X-axis and the matrix beneath indicate the intersection/overlap between two specific data sets indicated by filled circles connected by a line. The sizes of the intersections (number of overlapping genes between the two datasets) were plotted as bar graph above the matrix columns. Statistically significant over-representation of sub-domain genes among the *tsol-1* up or down DE genes are indicated as orange bars (hypergeomorphic test  $p$ -value  $< 0.05$ ).

### 3.3.5 TSO1 and TSO1 homologs directly bind to the promoters of *HD-ZIP III* genes

To determine if TSO1 directly represses *REV*, we mined a large-scale yeast-one-hybrid dataset (Taylor-Teeples et al. 2014). The promoters of fifty genes implicated in root xylem cell specification were screened against 467 root-xylem-expressed transcription factors using a high throughput yeast-one-hybrid assay. TSO1, SOL1 and SOL2 are among the 467 transcription factors tested. TSO1 and its homologs SOL1 and SOL2 were found to bind to the *REV* promoter (Figure 3.4D) (Taylor-Teeples et al. 2014; Gaudinier et al. 2011). The data indicate the possible redundancy between TSO1 and its family members SOL1 and SOL2 in regulating *REV* expression. However, TSO1 and its homologs may regulate *REV* in different tissues or developmental stages. A change of *REV* expression in *tsol-1* microarray in inflorescence suggests that *TSO1* plays a major role in regulating *REV* during

inflorescence development. In addition to *REV*, TSO1 and its homologs SOL1 and SOL2 appear to bind the promoters of other *HD-ZIP III* genes, *PHB* and *PHV* (Figure 3.4D), consistent with increased expression of *PHV* in *tso1-1* (Figure 3.4C). To sum up, TSO1 and its family members, SOL1 and SOL2, may directly regulate *HD-ZIP III* gene expression by binding to the promoters of these *HD-ZIP III* genes.

In the yeast one-hybrid study, *REV* was discovered as a major hub in the gene regulatory network for secondary cell wall synthesis (Taylor-Teeple et al. 2014; Gaudinier et al. 2011). *REV* promoter was found to be bound by 35 transcription factors (Table 3.6). In addition to TSO1, *REV* promoter is bound by another putative DREAM complex component E2Fc, a cell cycle regulator in the conserved RB/E2F complex, suggesting that *REV* may be negatively regulated by the DREAM-like complex consisting of TSO1 and E2Fc. TSO1/SOL2/SOL1 and E2Fc are the only plant DREAM-like complex components tested in the above yeast-one-hybrid study.

In addition to *HD-ZIP III* family members, the yeast-one-hybrid data also revealed *KNOTTED ARABIDOPSIS THALIANA7 (KNAT7)*, a class II KNOX transcription factor, as another regulatory target of *TSO1* (Figure 3.4D). However, we detected significant down-regulation of *KNAT7* in *tso1-1* microarray (-6.32 fold change, p-value = 6.14E-08) indicating TSO1 as possibly a direct positive regulator of *KNAT7*. *KNAT7* and *BELLI-LIKE HOMEODOMAIN 6 (BLH6)* were previously shown to form a heterodimer that binds the *REV* promoter and represses *REV* expression during secondary cell wall synthesis in root (Y. Liu et al. 2014). Therefore, *TSO1* may

positively regulate *KNAT7*, a repressor of *REV*. This feed-forward regulatory loop between TSO1 and *REV* further ensures the repression of *REV*.

*VASCULAR-RELATED NAC-DOMAIN 6 (VND6)/NAC101* is a gene, whose promoter was bound by SOL2 (Taylor-Teeples et al. 2014) (Figure 3.4D). *VND6* encodes a major factor in xylem cell fate determination and has the ability to transdifferentiate other cell types to xylem cells (Yamaguchi et al. 2010; Ohashi-Ito, Oda, and Fukuda 2010). *VND6* expression did not show significant change in *tsol-1* mutant (Figure 3.4C), perhaps reflecting a specific SOL2-VND6 interaction in root tissues only and suggesting a possible function of *SOL2* in regulating xylem formation through *VND6*.

Another direct target of SOL2 revealed by yeast-one-hybrid is *AT5G60720* (Taylor-Teeples et al. 2014), which showed significant down-regulation in the *tsol-1* mutant (-2.23 fold change, p-value= 1.91E-05) (Figure 3.4C). *AT5G60720* encodes a protein of unknown function, and showed high expression in the root xylem. Its functional relevance to TSO1 remains to be tested.

### **3.3.6 Genome-wide comparisons between *tsol-1* differentially expressed (DE) genes and SAM expressed genes.**

To understand the altered transcription landscape of *tsol-1* mutant, we ask if DE genes in *tsol-1* show a shift of gene expression profile characteristic of specific subdomains of the SAM. Each subdomain of the SAM has distinct function and possesses a unique transcription landscape (Yadav et al. 2014, 2009; Tian et al.

2014). Using meristem subdomain specific promoters to drive GFP, Yadav et al. applied fluorescent activated cell sorting to isolate subpopulations of cells at the SAM. Transcription profiling of these subpopulations of cells identified subdomain specific genes. Following three populations of cells are relevant to this study: stem cells in the Central Zone of SAM defined by the p*CLV3*::GFP reporter, the cells at the adaxial domain and organ boundary defined by the p*LAS*::GFP, and the cells at the organ abaxial region, Peripheral Zone, and organ outer boundary defined by the p*KANI*::GFP. To determine if fasciated *tso1-1* mutant SAM is due to over-representation of specific subdomains, we compared DE genes in *tso1-1* with above mentioned subdomain (*CLV3/LAS/KANI*) specific genes (Yadav et al. 2014) by gene set enrichment analysis. Genes that are up-regulated in *tso1-1* inflorescence showed significant enrichment (ie. over-representation) of *CLV3*, *LAS* and *KANI*- subdomain specific genes (hypergeometric test p-value <0.001) (Figure 3.4E). Hence, all subdomains of SAM are over represented among the *tso1-1* up-regulated genes, suggesting that *tso1-1* meristem fasciation results from over-proliferation/growth of all subdomains of the SAM (including adaxial, abaxial and boundary regions) and that *TSO1* may directly or indirectly repress the expression of these genes.

We carried out similar analysis with an independent data set derived from transcription profiling of meristem-organ boundary (*LAS*) and developed leaf (*ASI*) cells from young seedlings (Tian et al. 2014). In this study, specific subdomains were isolated using the ribosome TRAP-seq method (Mustroph et al., 2009; Jiao and Meyerowitz, 2010). Similar to the analysis above, the meristem-organ boundary

(*LAS*) specific genes are significantly enriched among the *tso1-1* up-regulated gene set. In contrast, seedling leaf tissue (*ASI*) specific genes were significantly enriched among the *tso1-1* down-regulated gene set (Figure 3.4E). Therefore, *tso1-1* mutants appear to over-express meristem genes while at the same time reduce the expression of differentiation genes such as those for leaf differentiation, supporting the notion that TSO1 normally represses meristem genes while promotes tissue differentiation.

### **3.3.7 *REV* may mediate the pleiotropic meristem defects of *tso1-1***

Does *REV* up-regulation in *tso1-1* background contribute to *tso1-1* mutant phenotype?

*REV* is well known to promote adaxial identity and meristem formation. Loss of *REV* resulted in early termination of SAM and lack of axillary meristem (AM) (Otsuga et al. 2001; Talbert et al. 1995). In contrast, gain-of-function mutations of *REV* produced bushy plants with fasciated meristems in certain genetic background (Zhong and Ye 2004a). A recent study showed that *REV* promotes the meristem identity gene *STM* expression by directly binding to the *STM* promoter in axillary meristem and inflorescence tissue (Shi et al. 2016). Therefore, increased or ectopic *REV* in *tso1-1* may lead to increased or ectopic *STM* expression and meristem fasciation. Indeed, *STM* is up-regulated by 0.45-fold in *tso1-1* mutant (Figure 3.4C).

In addition to meristem fasciation, the *tso1-1* mutants produced more secondary shoots than wild type, giving rise to the bushy phenotype (Figure 3.5C). These meristem defects of *tso1-1* is reminiscent of that of *REV* gain-of-function mutants (Zhong and Ye 2004a). If these phenotypes are mediated by *REV-STM* over-

expression, it should be reversed by combining *tsol-1* with a *rev* loss-of-function mutation.

To test this hypothesis, we designed CRISPR-Cas9 system to target the 1st exon of *REV* and introduced the construct into *tsol-1*<sup>+/+</sup>*sup-5* heterozygous background (Figure 3.5A). In the T1 line 2 (*tsol-1*<sup>+/+</sup>*sup-5*), a CRISPR induced homozygous G-to-A mutation changed a conserved valine in the homeobox domain (Prigge and Clark 2006) into aspartic acid (V34D) (Figure 3.5A). The line 2 plants showed fewer axillary branches on the main shoot and no axillary meristem in the axil of some cauline leaves (Figure 3.5D). This phenotype is characteristic of hypomorphic *rev* mutant alleles (Otsuga et al. 2001; Talbert et al. 1995). Thus, the V34D mutation in line 2 likely produced a hypomorphic *rev* allele (termed *rev-12*) that is ideal for testing our hypothesis. In the T2 generation, *tsol-1*<sup>+/+</sup>*sup-5*;*rev-12* plants showed similar phenotypes as the *tsol-1*<sup>+/+</sup>*sup-5*;*rev-12* plants from T1 generation. Surprisingly, the *tsol-1*;*rev-12* plants in T2 showed reduced branching on the main shoot and produced no secondary branches. Furthermore, the shoot meristems terminated, usually between two downward curling leaves.

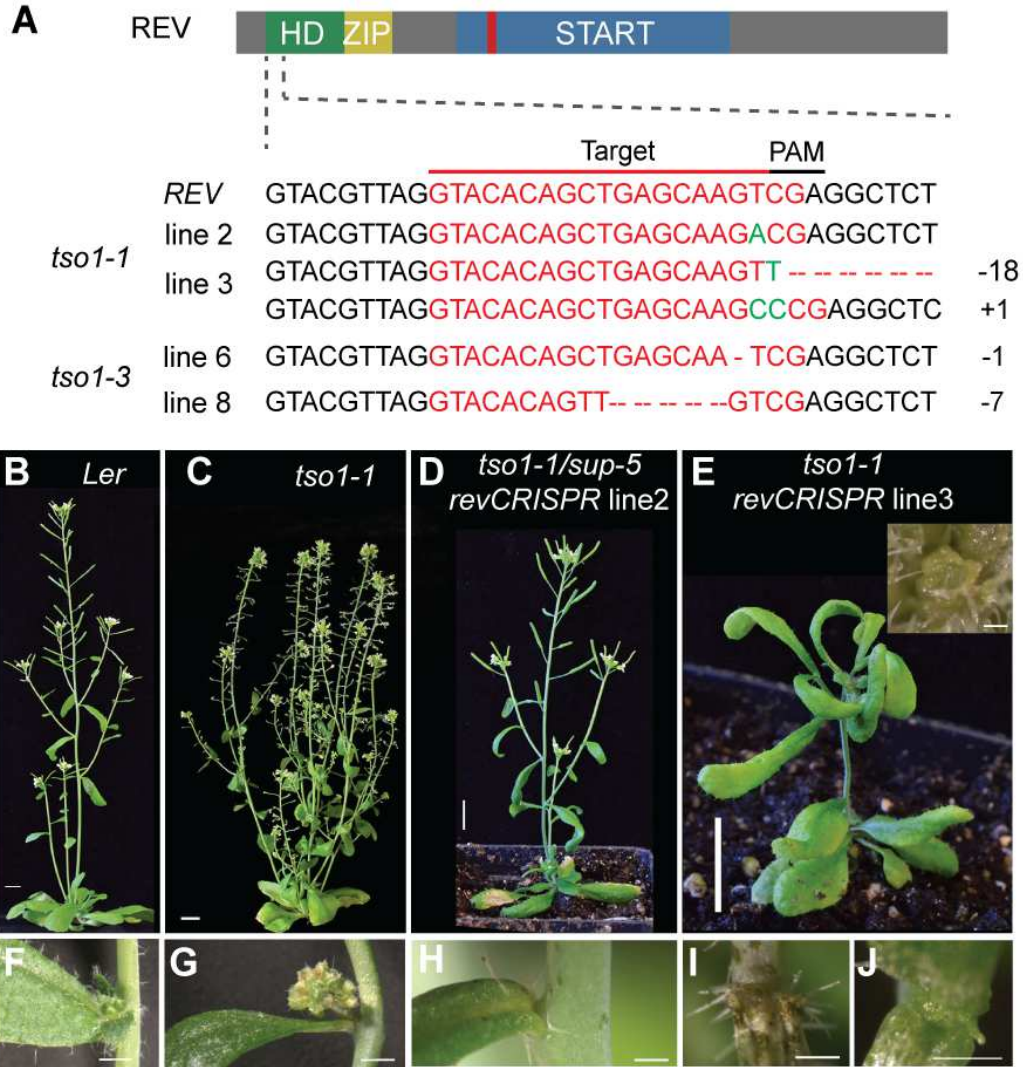


**Figure 3.5 REV overexpression underlies *tso1-1* AM phenotype**

**A.** Diagram of REV protein domains and details of the CRISPR induced mutation. REV protein consists of a homeodomain (green), leucine zipper domain (yellow), and a putative sterol binding START domain (blue). The miR165/166 target sequence (red) is within the START domain. sgRNA was designed to target the 1<sup>st</sup> exon of REV. The specific CRISPR-induced mutations in various backgrounds are highlighted beneath the target sequence.

**(B)** A wildtype plant (*Ler*). **(C)**, A typical *tso1-1* plant. **(D)** A *tso1-1/+sup-5;revCRISPR line2* plant. The *revCRISPR line2* mutation is a A-to-T mutation (green) shown in (A), changing of a conserved valine (V34D) in the homeobox domain. Sequence analysis confirmed homozygosity of the mutation. **(E)** A *tso1-1; revCRISPR line3* plant. This line contains CRISPR-induced bi-allelic mutations in REV; the sequence is shown in (A).

**(F)** A close-up image showing an axillary meristem of wild type (*Ler*) in the leaf axial. **(G)** A close-up image showing an axillary meristem of *tso1-1* in the leaf axial.

(H) A close-up image showing an absence of axillary meristem in the leaf axial of a *tso1-1*<sup>+/+</sup>*sup-5*;*rev*CRISPR line2. (I) A close-up image showing an absence of axillary meristem in the *tso1-1*;*rev*CRISPR line3. (J) A terminating meristem between two apical leaves of the plant in (E). Scale bar = 1cm (B to G) and 0.5mm (H, I, J).

In another T1 line 3 (*tso1-1*), the CRISPR-Cas9 induced bi-allelic mutations in the *REV* gene (Figure 3.5A). The complex mutations appear to result from a combination of insertion and deletion. One allele in line 3 has 1bp insertion followed by 19bp deletion that led to a total 18bp deletion that deleted residues 34-39 (VEALER) from the homeobox domain. The other allele in line 3 has 1bp deletion followed by 2bp insertion that resulted in a shifted reading frame and premature stop codon in exon 1. This bi-allelic mutation line (line 3) likely knocked out *REV* gene completely and is also homozygous for the *tso1-1*, leading to *tso1-1*; *rev* double homozygous mutant. The *tso1-1*; *rev* line 3 plant also showed early termination of SAM (Figure 2.5K) and lacked any axillary meristem (Figure 2.5E, J), supporting the results from plants from line 2.

These results indicate that ectopic *REV* expression is mediating the bushy (extra AM) phenotype of *tso1-1* as *rev* loss-of-function mutation is epistatic to *tso1-1* by suppressing the bushy phenotype of *tso1-1*. Yet the *rev* loss-of-function alleles did not simply revert the AM phenotype back to wildtype-like, but led to further AM reduction and SAM termination. The strong phenotype of meristem termination in *tso1-1*; *rev* double mutants revealed the synergistic interaction between *TSO1* and *REV* in promoting meristem formation, and the complex underlying genetic network

that might be involved. And levels of *TSO1* and *REV* function balances the meristem activity.

To further test the genetic interaction between *rev* and the weak *tso1-3* allele, we transformed *tso1-3<sup>+/+</sup>sup-5* plant with the same CRISPR-Cas9 construct targeting *REV*. In line 6 (*rev-13*) and line 8 (*rev-14*) (T2 generation), CRISPR induced deletions led to frameshift (Figure 3.5). The *rev-13* and *rev-14* alleles on their own showed similar phenotypes to that of *rev-12* and previously described *rev* loss-of-function alleles, suggesting that the mutations in *rev-13* and *rev-14* significantly reduced *REV* function. Combining *rev-13* and *rev-14* alleles with *tso1-3* showed additive effects (Figure 3.6), suggesting that there is no genetic interaction between *REV* loss-of-function alleles and *tso1-3*.

### **3.4 Discussion**

#### **3.4.1 B12 as a sensitized background for identifying enhancers of *tso1* mutation**

In this study, we took advantage of a weak *myb3r1* allele, which partially suppressed *tso1-1* and provided an ideal genetic background with a mild but specific phenotype for us to conduct genetic screen to look for enhancers or suppressors. Compared with other *myb3r1* strong loss-of-function alleles which fully rescued *tso1-1* phenotype, the *myb3r1-5* allele in *B12* carried a missense mutation, which is likely a hypomorphic allele and hence only partially suppressed *tso1-1* phenotype. Thus, in the *B12* background, the *TSO1-MYB3R1* pathway is partially functional and more sensitive to mutations that compromise the *TSO1-MYB3R1* pathway. Indeed, most genetic modifiers isolated in this screen are enhancers (62 out of 71). We

hypothesized several scenarios that may underlie the nature of the suppression or enhancement: (1) suppressor mutations in the *MYB3R1* gene that further disrupt *MYB3R1* function; (2) enhancer mutations that cause loss-of-function mutations in a DREAM complex component; (3) mutations in genes regulated by TSO1 or MYB3R1 could be identified as enhancers or suppressors depending on if they are repressed or activated by TSO1 or MYB3R1; (4) mutations in proteins that interact with MYB3R1 could be isolated as enhancer or suppressors. This study represents the analysis of the first enhancer from this screen and identified a mutant allele in *REV*, belonging to the (3) scenario listed above. Analysis of the remaining enhancers/suppressors will further reveal the genetic framework of the TSO1 pathway.

#### **3.4.2 TSO1 maintains meristem size partly by repressing *REV* gene expression.**

Ectopic *REV* expression has been shown to disrupt the ad/ab polarity in leaves, floral organs and also stem vascular bundles (Emery et al. 2003; Zhong and Ye 2004a). The gain-of-function *REV* alleles also have the ability to promote SAM fasciation in certain genetic backgrounds (Zhong and Ye 2004a). In the B12 background, *rev-11d/+* allele caused meristem fasciation and sterility, and the phenotypes were absent when DEX was applied to rescue the *tso1-1* mutation, indicating that the observed phenotype requires *tso1-1* (Figure 3.2A). Similarly, when *rev-11d/+* was removed, the B12 alone did not exhibit these phenotypes. The experiments in Figure 3.2 and 3.3 suggest that it is the synergistic genetic interaction between *B12* and *rev-11d/+* that led to the enhanced phenotype. Hence, this represents the first genetic and functional connection found between *TSO1-MYB3R1* and *REV* and as a result

connecting *TSO1-MYB3R1* to the adaxial identity. This linkage between *TSO1* and adaxial identity could be highly significant as it for the first time suggests that *TSO1*'s effect on SAM may be mediated by its effect on adaxial identity. Since overexpression of *TSO1* did not show any tissue polarity or meristem patterning defects (data not shown), *TSO1* function likely requires co-factors that are under spatial-temporal regulation.

The synergistic interaction between *tso1-1* and *rev-11d/+* could be explained as following. In *rev-11d/+* background, *REV* mRNA is stabilized due to its resistance to miR166/165. However, *TSO1-MYB3R1* wild type complex is able to repress *REV* transcription to keep *REV* mRNA level still below critical threshold. In *B12* background, *TSO1-MYB3R1* complex activity is partially compromised, leading to elevated *REV* transcription; combined with the resistance to miR165/166 due to *rev-11d* mutation, the mutant *REV* mRNA level is now above the threshold level to cause meristem fasciation and infertility.

It is still unclear how *TSO1-REV* module also regulates fertility. The *tso1-1* allele fails to develop floral organs. The *REV* gain-of-function alleles display carpel tissue adaxialization in certain background, but the fertility is unaffected (Zhong and Ye 2004a). In *B12/+* background, *rev-11d/+* displayed normal floral organs and fertility. Only in *B12* background, where *tso1-1* and *myb3r1-12* exist as homozygous, *rev-11d/+* caused floral organ adaxialization and sterility. This genetic interaction may reveal a novel role of *REV* in regulating fertility.

In conclusion, the identification of the *TSO1-REV* regulatory module provided much needed insights into how *TSO1* and its homologs regulate meristem. They may restrict meristem size and new meristem initiation by restricting adaxial environment or by indirectly restricting *STM* expression. Furthermore, this *TSO1-REV* module likely functions at SAM to regulate SAM size and in AM to regulate lateral shoot branches.

### **3.4.3 Model**

In light of the discovery of the *TSO1-REV* regulatory relationship at the shoot apical meristem and axillary meristem, we propose a model of *TSO1-REV* interaction. The TSO1 protein complex that includes MYB3R1 binds *REV* promoter and represses *REV* expression. In addition, the TSO1 complex may promote the expression of *KNAT7*, a known repressor of *REV* (Y. Liu et al. 2014). This TSO1 complex could be extended to include *TSO1* family genes, *SOL1* and *SOL2*, and the regulatory module could be extended to include the repression of other members of the *HD-ZIP III* genes. With the combinations of tissue specific expression of TSO1 family genes or *HD-ZIP III* genes, tissue specific modules could be formed to pattern meristem in different tissue and stage context.

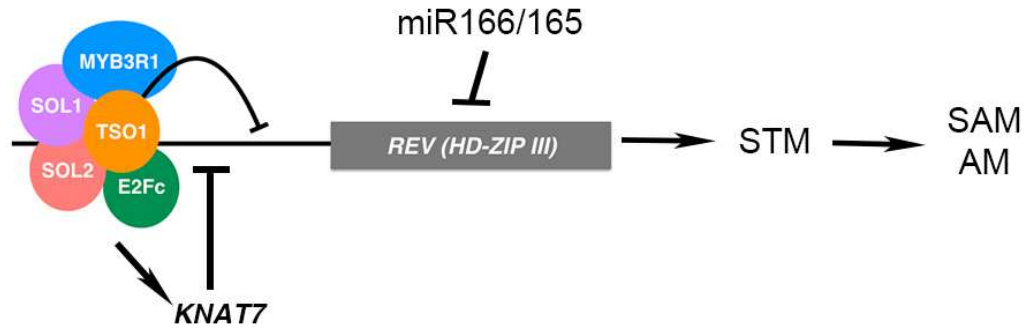


**Figure 3.6 A Model illustrating the *TSO1-REV* pathway in regulating meristems**  
 Working model for *TSO1-REV* pathway in regulating meristem patterning. The putative plant DREAM-like complex consisting TSO1, MYB3R1 and E2Fc binds *REV* promoter and represses *REV* expression at meristems. The DREAM-like complex also represses *REV* by promoting the expression of *KNAT7*, a known repressor of *REV*. The compromised *REV* regulation caused by *B12* is likely due to defects in both direct regulation and indirect regulation through *KNAT7*. TSO1 homologs SOL1 and SOL2 either function redundantly with TSO1, or form tissue specific complex with different combinations of TSO1/SOL1/SOL2 to regulate *HD-ZIP III* genes. The effect of *HD-ZIP III* mis-regulation maybe mediated by altered expression of *STM*, a positive regulator of SAM and AM.

The *TSO1-HD-ZIP III* regulatory model could provide mechanistic explanation to the pleiotropic meristem defects of *TSO1* mutants. The *tso1-1* mutant has over proliferation of SAM and AM, and reduced RAM size (Chapter II), reminiscent of *HD-ZIP III* gain-of-function mutant phenotypes (Ioio et al. 2012; Zhong and Ye 2004b). Elevated *HD-ZIP III* gene expression in *tso1-1* could lead to ectopic expression of *STM* at the SAM and AM which in turn leads to meristem fasciation. Intriguingly, *REV* has been shown to directly activate *WUS* expression together with the cytokinin response factors, B-type ARRr during plant tissue regeneration (Zhang et al. 2017). In contrast, at the root apical meristem, *PHB* activates the cytokinin biosynthesis gene *IPT7* to promote cell differentiation and control the root meristem size. Gain-of-function *phb-1d/+* allele leads to reduced RAM size and early differentiation (Ioio et al. 2012). Thus, ectopic expression of *HD-ZIP III* genes could

be the underlying molecular contributor to the meristem defects of *tsol-1* mutant. It remains to be tested if overexpression of *HD-ZIP III* genes mediates *tsol-1* root phenotype. Hence, the *TSO1-HD-ZIP III* regulatory model suggests a conserved regulatory module consisting of *TSO1/SOL1/SOL2-HD-ZIP III* in regulating plant stem cell populations.

## Chapter 4: A144, a novel suppressor of *tso1-1*

### 4.1 Introduction

Through our genetic screen in the *tso1-1* mutant background, we isolated a novel suppressor A144 that is distinct from the *myb3r1* suppressor alleles. The A144 mutation suppressed both the strong *tso1-1* allele and the weak *tso1-3* allele. The causative mutation of A144 was subsequently mapped to the gene *AT1G49170*. *AT1G49170* encodes a small protein (126 aa) with a domain of unknown function (DUF167). The DUF167 is a conserved protein domain exist across plants and animals. Our data revealed the *Arabidopsis* DUF167 protein plays a role in meristem regulation and possibly cell cycle regulation. In this chapter, I present the functional characterization of *AT1G49170*.

### 4.2 Material and method

#### Plant material and growth condition

Refer to Chapter II

#### Vector construction and Genotyping

To produce translational reporter, the 2.3kb genomic fragment of *AT1G49170* including 1.5kb promoter sequence was amplified from *Ler* genomic DNA with primers GAAGATTTTCCTTTTCTTGGCCG and GGTAGGTTTTGATGCTTGGG and ligated into pCR-GW8-TOPO. After sequencing confirmation, the fragment was recombined into pMDC107 (Curtis and Grossniklaus 2003) and pGreenII-NLS-3xEGFP (Takada and Jürgens 2007) to produce translational reporter. The genomic fragment was also recombined into pEarleyGate 303 (Earley et al. 2006) to produce

c-terminal cMyc tag fusion for protein pull down assay. Vectors were introduced into wild type *Ler* or A144 suppressor by floral dipping via *Agrobacterium tumefaciens* (GV3101).

To construct CRISPR vector for *AT1G49170* gene editing, gRNA was designed to target the 1st exon. Primers ATTGAAAGAAGACCAAATCGGCGG and AAACCCGCCGATTTGGTCTTCTTT were annealed and ligated into the BsaI cutting site of pHEE401E vector (Wang et al. 2015). The underlined sequences provide overhangs allowing for ligation. The construct was introduced into *tso1-1/sup-5* and *tso1-3/sup-5* plants via *Agrobacterium* by floral dipping.

The A144 mutation T40I destroyed a BccI restriction site and generated a CAPs marker. PCR using primers ATGGCTCCGACGAAGAAAGGAA and ACAGAGCTCATGTACTCGAGAAGAG followed by BccI digestion was used to genotype the A144 mutation.

### **Suppressor screen and complementation tests**

Refer to Chapter II

### **Mapping by sequencing**

Refer to Chapter II

### **Microscopy**

Refer to Chapter II

### **Phylogenetic analysis of DUF167 proteins in plants and animals**

Full-length amino acid sequences of DUF167 genes encoded by *AT1G49170* and *AT5G63440* were used for BLAST search in *Arabidopsis thaliana* (taxid:3702), *Zea mays* (taxid:4577), *Physcomitrella patens* (taxid:3218), *Caenorhabditis elegans* (taxid:6239), *Drosophila* (taxid:7215), *Danio rerio* (taxid:7955), *Mus musculus* (taxid:10090), *Homo sapiens* (taxid:9606) reference proteins database. The *E. coli* DUF167 protein (Swiss-Pro ID, P52060), whose 3D protein structure has been solved, was also included in the analysis. A total of 19 protein sequences were identified and aligned with MUSCLE (Edgar 2004) with default parameters in the MEGA7 software (Kumar, Stecher, and Tamura 2016). The phylogenetic tree was constructed using the Neighbour-joining method (Saitou and Nei 1987). The evolutionary distances were computed using the Poisson correction method (Zuckermandl and Pauling 1965).

### **Protein 3D structure of AT1G49170 modeling**

The amino acid sequence of AT1G49170 (total 126 residues) were used to query the Phyre2 engine (Kelley et al. 2015). The model with the highest confidence score derived from structure of the *E. coli* YggU protein (PDB ID:1YH5) (Aramini et al. 2003) was selected for further investigation and shown in Figure 4.4.

## **4.3 Results**

### **4.3.1 Isolation and phenotypic characterization of suppressor A144**

In an effort to screen for EMS-induced mutations that suppress *tsol-1* mutant phenotypes, we identified a large number (45) of suppressor mutations by screening

an M2 population of *tsol-1; 35S::TSO1-GR* plants. In Chapter II, we showed that 32 of these suppressor mutations resided in the *MYB3R1* gene. However, A144 (Figure 4.1A) is distinct from *myb3r1*. First, A144 was crossed with 16 other *myb3r1* suppressors, and was shown to complement them (Figure 4.1B), suggesting that A144 defines a different gene from *MYB3R1*. Second, unlike *myb3r1* mutants, the fertility defect of *tsol-1* is only partially suppressed by A144 (Figure 4.2A). Like *myb3r1*, the meristem fasciation phenotype is completely suppressed (Figure 4.2A). Third, A144 did not suppress the short root phenotype of *tsol-1* (Figure 4.2D). A144 plants were crossed with the parental line *tsol-1; 35S::TSO1-GR* to generate F1 (*A144/+; tsol-1; 35S::TSO1-GR*), which showed the *tsol-1* phenotype, indicating that A144 is recessive.

To reliably determine the phenotype of *tsol-1; A144* double mutant, we would like to remove the TSO1-GR transgene as well as other background mutations from the A144 background. *A144* plants from the mapping population was backcrossed to the *tsol-1/sup-5* plants, and the *tsol-1/tsol-1; A144/A144* plants were re-isolated in the F2 population. The A144 mutation again rescued the meristem fasciation phenotype as well as the infertility phenotype (Figure 4.2A). The number of flowers in each inflorescence, as a proxy for meristem size, is comparable to wild type plants (Figure 4.2C). The fertility defects of *tsol-1* were partially rescued indicated by an elongated silique but shorter than wild type (Figure 4.2A).

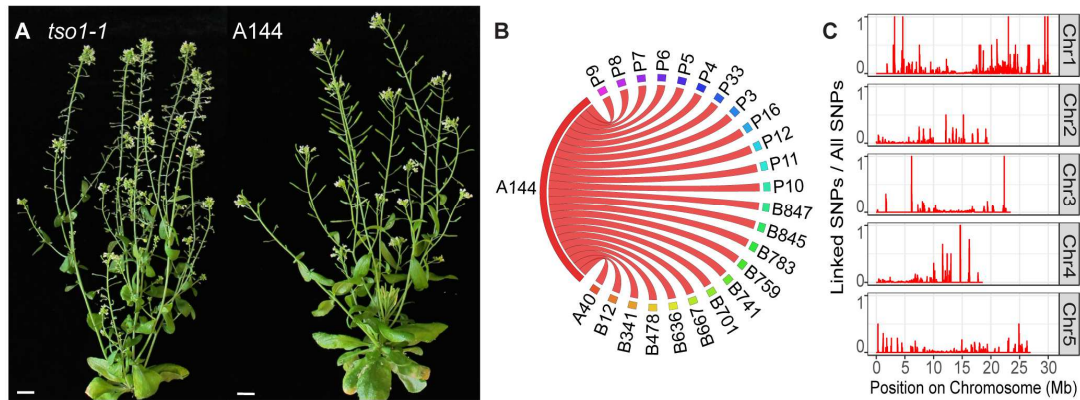


**Figure 4.1 Isolation of A144, a novel suppressor of *tso1-1***

(A) Left: A *tso1-1* mutant plant. Right: A144 suppressor isolated from the EMS screen described in Chapter II. Note the fuller siliques indicating partially restored fertility as well as smaller inflorescence heads due to suppression of meristem fasciation. (B) Circos graph illustrating complementation tests done between A144 and 16 other suppressors (all *myb3r1* alleles) isolated in the same screen. All crosses yielded F1 plants with *tso1-1* phenotype, suggesting that A144 complemented these 16 other suppressor mutations. (C) Genome wide SNP mapping of an F2 population pointed the A144 mutation to the lower arm of *Arabidopsis* chromosome 1. Y-axis plot the ratio of SNPs linked with the suppressed phenotype over all SNPs detected in a 100,000bp sliding window. X-axis denotes position on the chromosomes.

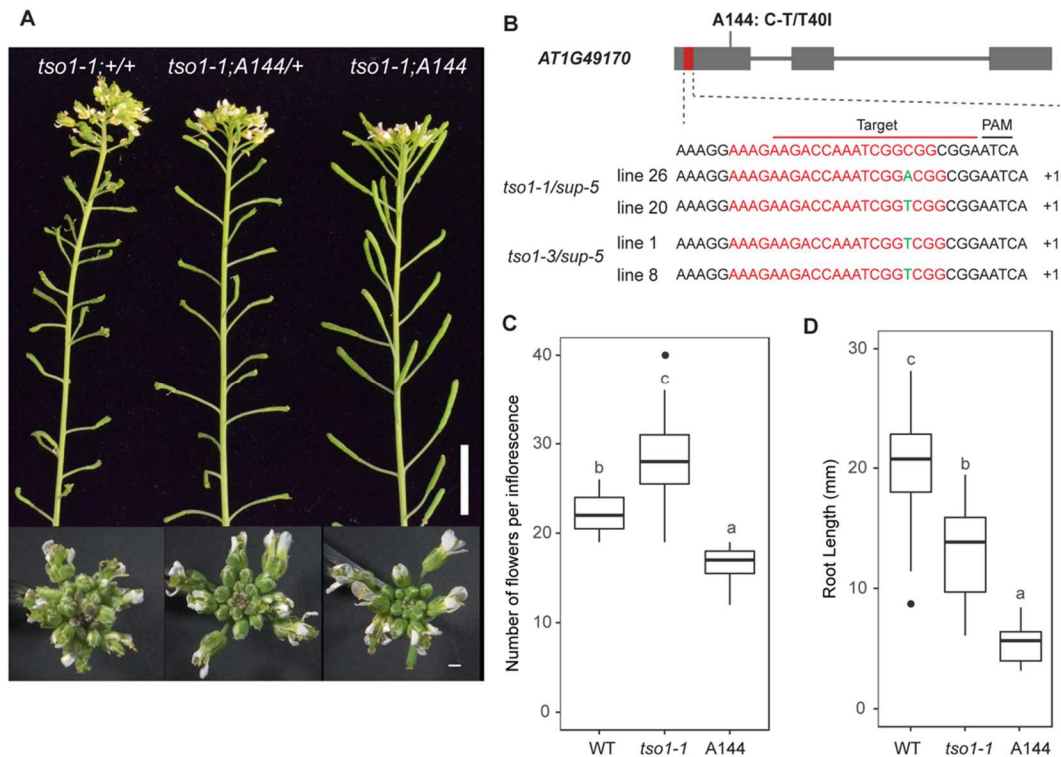


**Figure 4.2 A144 suppresses the meristem fasciation but not short root defect of the *tso1-1* allele**

(A) Phenotype of *tso1-1*, *tso1-1*;A144/+, *tso1-1*;A144 and *tso1-1*;AT1G49170CRISPR plants. Note the longer silique and smaller inflorescence meristem in *tso1-1*; A144. (B) AT1G49170 gene structure and mutations created in this study. The A144 mutation generated by EMS mutagenesis is denoted above the first exon. CRISPR system designed to target the sequence in the 1<sup>st</sup> exon (red) generated mutations in both *tso1-1* and *tso1-3* mutants that leads to premature stop codon. (C) Boxplot showing flower count per inflorescence as a proxy of meristem size (n=15 for each genotype). Different letters indicate statistically significant difference (p<0.01, one way ANOVA and Tukey test). (D) Boxplot of root length measurement at 7dpj for WT (*Ler*) (n=55), *tso1-1* (n=35), and A144 (n= 27). Different letters indicate statistically significant difference (p<0.01, one way ANOVA and Tukey test).

To assess if the suppressor effect of A144 is allele-specific to *tso1-1*, we tested a different *tso1* allele, *tso1-3*. *tso1-3* is caused by a nonsense mutation resulting in a truncation between the two CXC domains. *tso1-3* mutation only exhibits reduced fertility phenotype and lacks meristem phenotype. A144 suppressor was crossed to the *tso1-3*/sup-5 heterozygous plant and the A144/A144; *tso1-3*/*tso1-3* plants were

identified in the F2 population through allele-specific genotyping (Figure 4.3). The resulting plant also showed rescue of the fertility defect (Figure 4.3).

In all, our genetic data demonstrated that the A144 mutation suppressed the meristem fasciation and fertility defects caused by *tso1-1* or *tso1-3*. However, A144 does not suppress the short root phenotype of *tso1-1* mutant (Figure 4.2D).



**Figure 4.3 A144 suppresses the fertility defect of the *tso1-3* allele**  
Phenotype of *tso1-3*, *tso1-3;A144/+*, and *tso1-3;A144* plants. Note the longer siliques in suppressed plants. Scale bar for shoot = 1cm. Scale bar for inflorescence top view = 1mm.

#### **4.3.2 A144 is defective in *ATIG49170* coding for a small protein with unknown function.**

To determine the molecular nature of A144, we crossed A144 with *tsol-1*; *35S::TSOI-GR* parental line to generate a mapping population. This F2 population has 538 non-suppressed and 100 suppressed plants. DNA from 50 suppressor plants were pooled and sequenced at about 20X coverage. Mapping was done using method described in Chapter II. Candidate mutations were mapped to the lower arm of chromosome 1 (Figure 4.1C) and three of them caused amino acid changes (in gene *ATIG48650*, *ATIG49170* and *ATIG54940*).

The lack of a second allele of A144, in contrast to over 32 alleles of *MYB3R1* in the same screen, led us to postulate that either A144 encodes a small gene, or A144 bears a very special and unusual mutation instead of a simply loss-of-function mutation. Among the three candidate genes, *ATIG49170* encodes a small protein with 126 amino acids and is of unknown function. A nucleotide change from C-to-T led to the T40I missense mutation located in the protein domain of unknown function DUF167 (Figure 4.2B). Little is known about this protein domain and its sequence relevance. Gene *ATIG48650* encodes a RNA helicase and is expressed at the shoot and root meristem (Data from *Arabidopsis* eFP browser). The mutation in *ATIG48650* caused a Ser(S) to Phe(F) change outside any conserved protein domain. Gene *ATIG54940* is not expressed at the shoot apical meristem (Data from *Arabidopsis* eFP browser). Hence we focused our analysis of the candidate gene *ATIG49170*.

To validate that *At1G49170* is indeed the gene whose mutation suppress *tso1-1*, CRISPR was designed to target the 1<sup>st</sup> exon of gene *AT1G49170* and the construct was transformed into *tso1-1/sup-5* plants. In T1 generation, *tso1-1/sup-5* plants with CRISPR induced mutations were isolated. In line line 26 and 20, 1 bp insertions lead to shifted reading frame hence early stop codon (Figure 4.2B). We will analyze the *tso1-1;AT1G49170* plants in the next generation to test if loss of function mutations in *AT1G49170* can result in the suppression of *tso1-1*. This would provide insight as to the nature of the A144 mutation.

*tso1-3/sup-5;AT1G49170* mutants were also generated de novo through CRISPR gene editing (Figure 4.2B). We await the *tso1-3;AT1G49170* double mutant plants from the next generation to test if the genetic interaction between *TSO1* and *AT1G49170* is allele specific.

To determine if single mutation in *AT1G49170* (in the absence of *tso1* mutation) exhibit any phenotype, we searched literature and found that a *AT1G49170* T-DNA knock out line *at1g49170-1* (T-DNA insertion in the first exon) did not show any phenotype at the shoot nor at root (Baldwin et al. 2013). We are in the process of isolating single mutants of *AT1G49170* with the A144 allele and the CRISPR alleles to confirm results described by Baldwin et al. (2013).

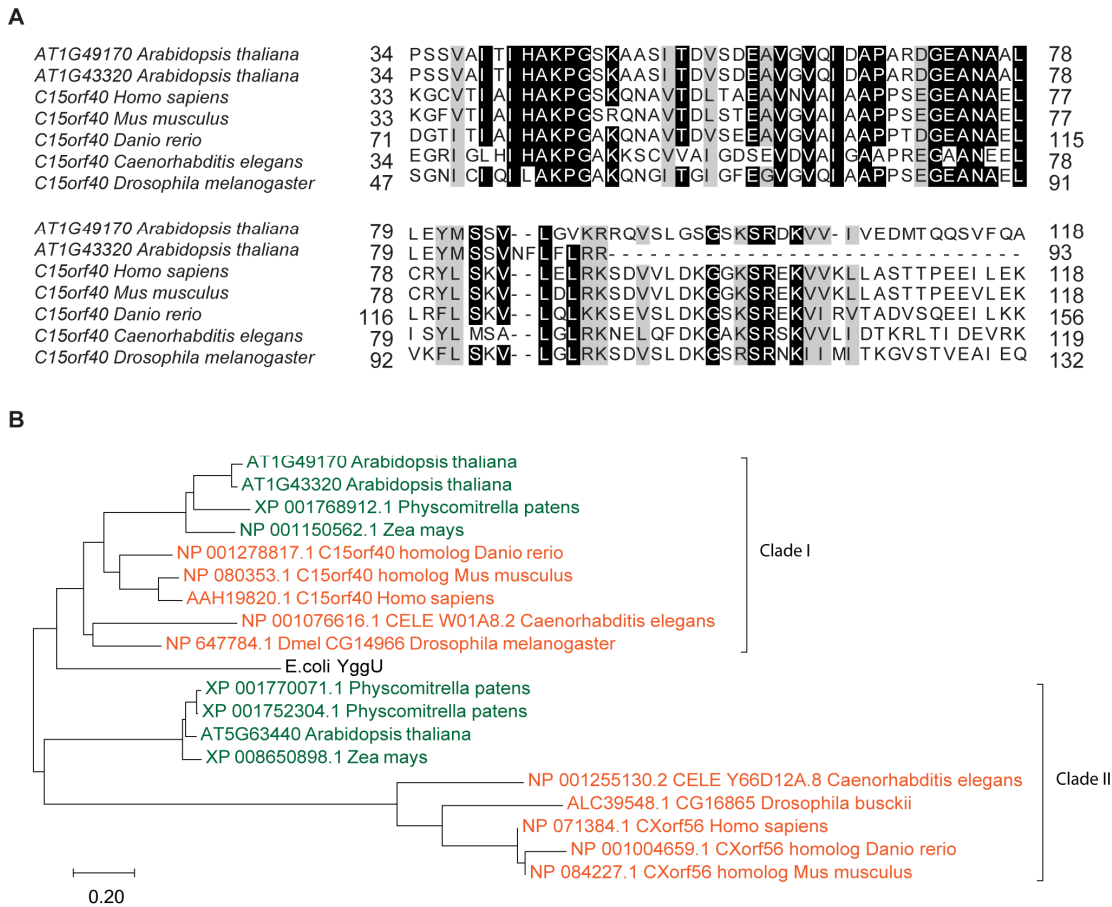


**Figure 4.4 Phylogeny of *AT1G49170*, a conserved DUF167 gene from prokaryotes to eukaryotes**

**(A)** Protein sequence alignment of *AT1G49170* and orthologues from plant and animal species. Highly conserved residues were shaded in black while similar residues were shaded in gray. Amino acids positions are denoted beside the sequence.

**(B)** Phylogenetic tree of 19 DUF167 proteins from representative plant (green), animal (orange) species and bacteria. The evolutionary history was inferred using the Neighbor-Joining method (Saitou and Nei 1987). The optimal tree with the sum of branch length = 6.14372292 is shown. The tree is drawn to scale, with branch lengths in the same units as those of the evolutionary distances used to infer the phylogenetic tree. The evolutionary distances were computed using the Poisson correction method (Zuckerkanndl and Pauling 1965) and are in the units of the number of amino acid substitutions per site. The analysis involved 19 amino acid sequences. All positions containing gaps and missing data were eliminated. There were a total of 60 positions in the final dataset. Evolutionary analyses were conducted in MEGA7 (Kumar et al. 2016).

### 4.3.3 *AT1G49170* function and expression

Little is known about DUF167 proteins. Three genes in the *Arabidopsis* genome, *AT1G49170*, *AT1G43320* and *AT5G63440*, encode proteins with DUF167 domain. Single and double mutants of *AT1G49170* and *AT5G63440* (Col-o ecotype) do not show any morphological phenotype under normal growth conditions (Baldwin et al. 2013). *AT1G49170* and *AT5G63440* are distant paralogs that diverged in the eukaryotic common ancestor (Baldwin et al. 2013) and likely have distinct functions. Phylogenetic analysis of DUF167 proteins from representative plant and animal organisms revealed that the DUF167 proteins form two clades that may have diverged before the plant animal common ancestor. In the animal organisms analyzed, each genome encodes a single ortholog of *AT1G49170* (Figure 4.4B).

Sequence alignments of the *Arabidopsis AT1G49170* with several animal orthologs revealed that the isoleucine residues flanking the A144 mutation site T40 are highly conserved (Figure 4.4A). Yet, the threonine T40 is not conserved. If the T40I substitution lead to suppression of *tsol-1* phenotype, we speculate that the spacing of the isoleucine residues is essential for the function of the DUF167 domain and isoleucine specifically is disfavored at the T40 position. 3D structure of *AT1G49170* protein modeled by Phyre2 server based on the *E. coli* ortholog YggU protein (Yee et al. 2002; Kelley et al. 2015) produced a single globular structure with a hydrophobic tunnel (Figure 4.5). The isoleucine at 39 and 41 are sticking into the tunnel while the threonine at position 40 is protruding to the opposite direction. The hydrophobic pocket structure with essential hydrophobic residues are often evolved in recognition of hydrophobic ligands like lipids.

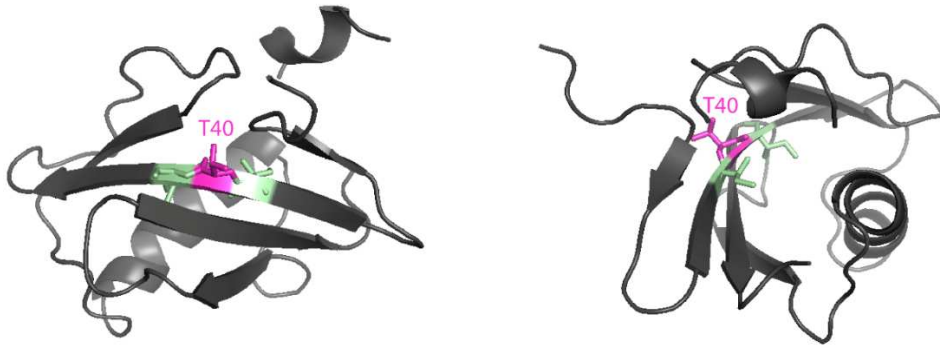


**Figure 4.5 Modeled AT1G49170 protein structure**

AT1G49170 protein structure modeled by Phyre2 (Kelley et al. 2015) based on the prokaryote YggU (Swiss-Pro ID, P52060) (PDB ID:1YH5) (Aramini et al. 2003) protein structure. Residue T40 is highlighted in pink and residues I39, I41 were highlighted in green. Left: view of beta sheets focused on the T40 residue that is mutated in A144. Right: view of the hydrophobic tunnel.

To understand the function of *AT1G49170* in the meristem tissue context, we generated a translational reporter fusing a 2.3 kb genomic fragment of *AT1G49170* to GFP coding sequence. The reporter was introduced into A144 suppressor and complemented A144 mutation (reverted suppressor phenotype back to *tsol-1-like*), suggesting that the fusion construct is functional and further support that the causative mutation of A144 resides in *AT1G49170*.

To determine the protein subcellular localization, we first looked at the root meristem where the tissue is free of chloroplast autofluorescence. When the reporter was introduced to wild type plants (*Ler*), weak GFP signal was observed in all cell types at the root apical meristem and also differentiated root cells (Figure 4.6B). The GFP signal primarily localized in the nuclei but could also be detected in the cytoplasm (Figure 4.6B).

To enhance the signal of the translational reporter, the same 2.3 kb genomic fragment was also used to produce a reporter fused with a nuclear localization signal and 3 copies of GFP (*NLS-3xEGFP*). This construct was introduced into A144 suppressor and did not complement the mutant phenotype. We reasoned that the added nuclear localization signal and bulky 3 copies of GFP may have impaired intra and inter cellular movement that's required for *AT1G49170* protein function. Nevertheless, the *pAT1G49170::AT1G49170-NLS-3xGFP* (*pAT1G49170-3xGFP* for short) reporter line may be used to indicate where this gene is transcribed. At the SAM, GFP signal was detected upon primordium inception at i1 and persist in the later stage primordium. GFP signals seem to be stronger in the L1 and L2 layers and peaked at P3 at the primordium growing tip (Figure 4.6B). Interestingly starting from P4, GFP signals are diminished at the primordium tip while maintained at the flanking region. After the lateral organ is fully established at P6, GFP signals become prominent in adaxial tissue (Figure 4.6B). It seems that *AT1G49170* is under spatial-temporal regulation at the SAM. Its expression is lower in the stem cell proper but higher in emerging primordia. As the primordia develops, the GFP signal retreats from the growing tip toward the periphery of the growing bud. The functional significance of this dynamic regulation of *AT1G49170* remains to be explored. In general, the expression pattern of *AT1G49170* overlaps with the fast dividing cell population in the periphery zone and young flower primordium and overlaps with the expression pattern of *TSO1* (Chapter II). Thus, the expression pattern of *AT1G49170* support our hypothesis that *AT1G49170* may play a role in meristem patterning.

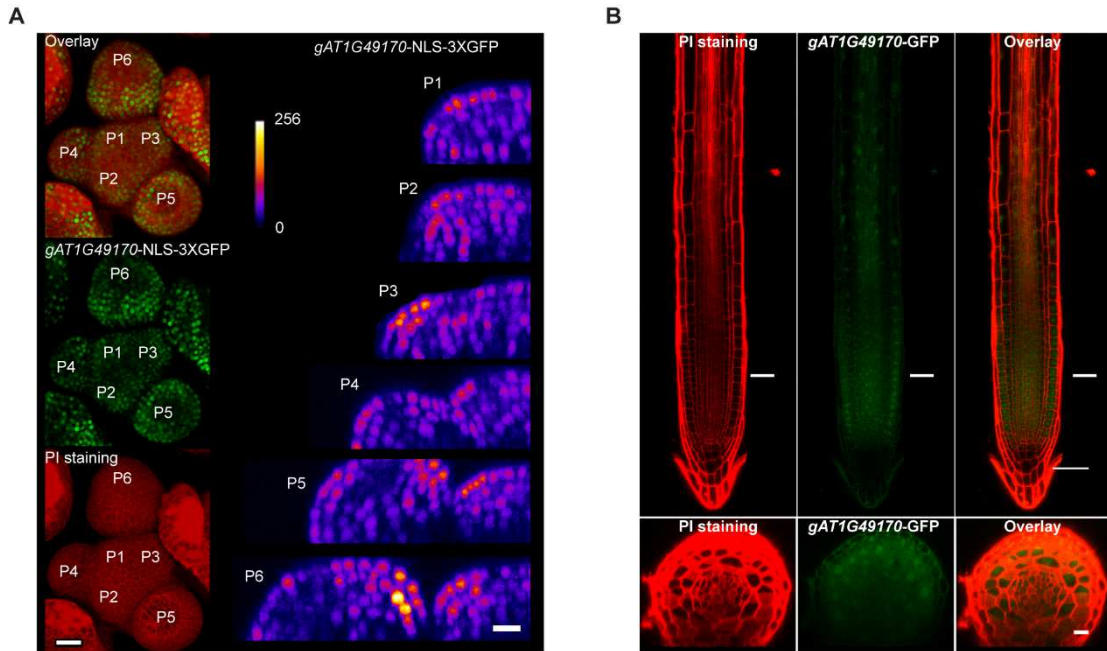


**Figure 4.6 *AT1G49170* is expressed at the shoot and the root apical meristem**  
**(A)** *AT1G49170* expression pattern in the SAM based on transcription fusion to *NLS:3xEGFP*. Membrane was labeled with propidium iodide (PI) (red) and *gAT1G49170-3xEGFP* expression is shown in green (left panel) or using the Fire lookup table in ImageJ (right panel). Scale bar = 20  $\mu$ m. Longitudinal optical sections (5 $\mu$ m thick maximal intensity projection of orthogonal views) through 6 successive primordia of a representative shoot apical meristem expressing *gAT1G49170-3xEGFP* (right panel) (Scale bar = 10 $\mu$ m). **(B)** *AT1G49170* expression pattern (shown by translational reporter) in the RAM. Membrane was labeled with PI and *gAT1G49170-GFP* expression is shown in green. Medium longitudinal section was shown in the upper panel (Scale bar = 50 $\mu$ m). 5 $\mu$ m thick maximal intensity projection of orthogonal views was taken from line denoted to produce cross optical sections (lower panel). (Scale bar = 10 $\mu$ m)

#### 4.4 Discussion

Through a forward genetic screen, we identified *AT1G49170* as a suppressor of *tso1* meristem fasciation and fertility defects and demonstrated that *AT1G49170* (*DUF167*) plays a role in meristem and stem cell regulation. DUF167 proteins exist broadly across plants and animals, and across single and multicellular organisms, suggesting that DUF167 proteins may be involved in biological processes in single

cell organisms and are co-opted into developmental regulation in multicellular organisms like flowering plants.

The human ortholog of *ATIG49170*, C15orf40, has multiple splicing isoforms. Isoform 1 encodes a protein of 126 amino acids. The conserved DUF167 of the two proteins (amino acids 37-105) share 55% sequence identity ( $E=7e-24$ ). C15orf40 appears to be a direct target of the master cell cycle regulator, the DREAM complex. C15orf40 promoter has been shown to be bound by DREAM complex member p130, E2F4, E2F8 and RB proteins (Table 4.1), suggesting it may play a cell cycle related role. C15orf40 expression did not show cell cycle phase specific changes (Table 4.2). There is no functional description of C15orf40 to date.

The nature of *ATIG49170* function and how does mutations in *ATIG49170* suppress *tsol-1* mutant phenotype remains elusive. Based on the information that C15orf40 is a putative target of human DREAM complex, we hypothesize that, *ATIG49170* is repressed by TSO1 and TSO1 associated DREAM-like complex in *Arabidopsis*. Ectopic or overexpression of *ATIG49170* may contribute to the *tsol-1* mutant phenotype. However, we did not detect significant change of *ATIG49170* expression level in our microarray study comparing *tsol-1* mutant and wild type plants (described in Chapter III, data not shown). It is possible that *ATIG49170* expression is under spatial-temporal control and may only express in small groups of cells. Our microarray data derived from whole inflorescence may not detect *ATIG49170* expression change due to mixing of all inflorescence cells. Alternatively, TSO1

complex may also regulate *AT1G49170* indirectly through post translational modification.

Although little is known about DUF167 protein function, a study on conserved ancient protein complexes across metazoan species discovered that the DUF167 proteins form conserved protein complexes (Wan et al. 2015). Specifically, the authors generated extensive soluble protein fractionations across diverse metazoan model organisms, and subjected these protein fractions to LC-MS/MS. Proteins that co-purify from the same fraction are deemed to have co-complex interaction. The human C15orf40 has been discovered to form conserved protein complexes in animals. Co-fractionation studies have shown that C15orf40 co purifies with human Excision Repair 1 (ERCC1) protein (Wan et al. 2015). The *Drosophila* C15orf40 and ERCC1 orthologs also co-purify from the same protein fraction, suggesting that C15orf40 and ERCC1 physically interact (Wan et al. 2015). ERCC1 (RAD10 in yeast) plays essential roles in the base-excision DNA repair pathway. A conserved co-complex interaction was inferred between *AT1G49170* and *AT3G05210* in *Arabidopsis* (Wan et al. 2015). C15orf40 has also been found to co-purify with Methyltransferase Like 1 (METTL1) in human and mouse (Wan et al. 2015). METTL1 is a methyltransferase that catalyzes the 7-methylguanosine modification of tRNA (Alexandrov, Martzen, and Phizicky 2002). Base on this finding, a conserved co-complex interaction between *AT1G49170* and *AT5G24840* was inferred in *Arabidopsis* (Wan et al. 2015). These discoveries shed light on the cellular processes

that DUF167 proteins may be involved in and provided hypotheses for future inquiries regarding *ATIG49170* functions.

## Chapter 5: Conclusions and future directions

In conclusion, we identified major players in the *TSO1* pathway through the forward genetic approach. Multiple alleles of the *MYB3R1* gene provided strong evidence that all aspects of *TSO1* function are mediated by *MYB3R1*, which is likely a direct target of *TSO1*. The biochemical data also suggest a molecular mechanism of direct physical interaction between TSO1 and MYB3R1. Together, my data showed that *MYB3R1* can be regulated by *TSO1* at the transcriptional level and indirectly at the post-translational level. And TSO1 and MYB3R1 may form a DREAM-like complex to coordinate cell proliferation with differentiation.

One essential and unique aspect of TSO1 and MYB3R1 is that they are not expressed in a specific domain at the shoot apical meristem. They are expressed broadly across the meristem showing a sporadic pattern that is characteristic of cell cycle genes. Mutations in these genes can drastically alter the course of meristem development accompanied with cytokinesis defects. My data highlight the crucial role of TSO1-MYB3R1 in integrating the cell cycle regulation within the meristem tissue context. Thus, to fully understand how the TSO1-MYB3R1 module works, it is crucial to resolve TSO1-MYB3R1 expression with higher spatial-temporal resolution.

The shoot apical meristem cells operate in a population mode driven by dynamic auxin and cytokinins movement and signaling. As the progeny cells of stem cells get pushed out toward the periphery of the meristem, they adopt different rules that set the cell division plane (Shapiro et al. 2015). Thus, cell divisions need to be

coordinated with the positional information. Observing *TSO1* and *MYB3R1* expression with relation to auxin signaling reporter and auxin transporter PIN localization may provide valuable insights into the spatial coordination. On the other hand, meristem cells also exhibit different length of cell cycle and cell cycle phases. These temporal regulations may underlie the intricate patterns generated by the collective cell divisions and timely switching from proliferation into differentiation mode. Thus, using live imaging to characterize the cell cycle progression of meristem cells with respect to *TSO1*-*MYB3R1* protein dynamic would provide insights into how the coordination is achieved. Cell proliferation dynamics at the RAM has been characterized by comparing the ratio of histone variants H3.1/H3.3 by Otero and colleagues (Otero et al. 2016). The same tool could be used to characterized cell cycle (pahse) dynamics at the SAM. Finally, and most importantly, the dynamic expression of *TSO1* in comparison to *MYB3R1* merits further investigation. For example, observations on whether *TSO1* expression proceeds a reduction of *MYB3R1* expression or cell division would provide insights of *TSO1* function at cell cycle resolution. With the advent of confocal imaging technology, and software that could segment and trace dividing cells overtime, these goals are very much attainable.

Imaging approaches and single-cell proteomics could also address the technical challenges that I have faced when detecting the *TSO1*-*MYB3R1* protein complex in vivo. Since these genes are expressed at a low level and may be sensitive to redox condition, isolating large intact protein complexes from sonication and cell wall lysis has been challenging.

*TSO1* plays opposite roles at shoot and root apical meristem. This seemingly paradoxical phenotype is not surprising because other factors, eg. Auxin, cytokinins, and *HD-ZIP III* genes have also been shown to play opposite roles at the shoot and root. If the same factor plays opposite roles at different context, it provides intriguing opportunities to understand the fundamental difference in tissue organization and genetic regulation. Through an enhancer screen, I discovered the genetic interaction between *REV* gain-of-function mutation with a sensitized *tso1* mutant background and *TSO1* represses *REV* expression by directly binding *REV* promoter. This finding established the connection between *TSO1* and *HD-ZIP III* gene family at the SAM. My preliminary data showed that *rev* loss-of-function mutations have no effect on the *tso1-1* root phenotype, because *tso1-1; rev* roots showed *tso1-1* short root phenotype. It remains to be tested if other *HD-ZIP III* family mutants, especially *phb*, suppresses *tso1-1* mutants at the root, since *PHB* has been shown to play a more prominent role at the root among the *HD-ZIP III* family genes

The *TSO1-MYB3R1* module presents a tantalizing unifying scheme of meristem cell regulation. And the regulation is rooted in proper cell cycle control at specific developmental context. *TSO1* and its family members have been shown to play a role in stomata meristemoid patterning (unpublished data from Burgmann lab at Stanford). It remains to be tested if *TSO1* is involved in patterning the third stem cell niche in addition to the shoot and root meristem, the procambium, that generates vasculature tissue. Since *HD-ZIP III* genes are known to play roles in patterning the procambium

meristem, *TSO1* may regulate vasculature tissue patterning upstream of *HD-ZIP III* genes.

One important question regarding the TSO1-MYB3R1 module is why mutating both *TSO1* and *MYB3R1* shows a wild type-like phenotype. Although genetic suppression is not uncommon, further investigation of the TSO1-MYB3R1 module at the systems level and regulatory network level may shed light on the complex system that maintains meristem homeostasis. This approach can reveal the potential gene redundancies that balance cell proliferation and differentiation at the meristems in the absence of TSO1-MYB3R1 in the *tso1-1; myb3r1* double mutants (suppressors). These redundant factors are not likely to be discovered from genetic screen as it requires higher order mutants that are unlikely to be produced by EMS mutagenesis.

The TSO1-MYB3R1 gene regulatory network approach can be aided by mapping and characterizing the remaining suppressors and enhancers isolated in this study. Some of these genetic modifiers of *tso1-1* showed tissue-specific suppression (A144) and enhancement (E2/*REV*) of *tso1* phenotype. Revealing the gene identity of the remaining genetic modifiers may shed light on how the TSO1-MYB3R1 module is wired in different meristem tissue context.

Furthermore, since TSO1 and MYB3R1 are conserved proteins across plants and animals and function as a protein complex, they present a likely ancient cell cycle regulatory module that existed in the single-celled common ancestor of plants and

animals. During evolution, the TSO1-MYB3R1 module seems to have evolved to regulated cell proliferation and differentiation at the meristems/meristemoid. One intriguing question is whether the TSO1-MYB3R1 module contributed to the emergence of meristems during evolution in plants. Plant meristems in the present days display astonishing capability to maintain stem cell totipotency while incur low rate of mutation, demonstrated by the resent mutation tracing of a 234-year-old Napoleon oak tree by Sarker et al., 2017 (bioRxiv preprint) that found only 17 somatic SNVs across the tree branches. It remains enigmatic what factors enables such capacity and how did they evolve during evolution.

## Appendix I: Analysis of male meiosis and germline defects of *tso1-3*

### **Section I: Brief review of *Arabidopsis* male meiosis and germline development**

*Arabidopsis*, as many flowering plants, leads a sporophyte dominant life cycle.

Haploid gametes are produced by diploid progenitor cells in reproductive organs, and resume diploid fate after fertilization that involves gamete fusion. Coordination of several cell types is required to establish the structure and function of the reproductive organs, which are anther (male), and carpel (female). During early anther development, 3 cell layers are formed surrounding microspore mother cells (MMCs) (Sanders et al. 1999). The tapetum layer is immediately connected to MMCs via plasmodesmata at stage 5 (Owen and Makaroff 1995). The tapetal cells then detach from MMCs, but support and modify the pollen at later stages.

Meanwhile, MMCs (2n) undergo meiosis.

During meiosis, DNA replicate once while cells divide twice. Meiosis is a modified cell cycle that requires mitotic cell cycle machinery and meiosis specific factors (Ma 2006). In meiosis I, homologous chromosomes pair, synapse, recombine, condense and separate. In *Arabidopsis*, recombination is initiated with generation of double stranded breaks (DBSs) by SPO11 together with several other proteins (Grelon et al. 2001; Ma 2006). Double-strand DNA break (DSB) repair is mediated by BRCA2, DMC1, and RAD51 (Siaud et al. 2004; Li et al. 2004). Recombination crossovers between homologous chromosomes and sister chromatids cohesion are physical links that are essential for proper alignment of chromosomes at the metaphase plate

and correct segregation at anaphase I. In meiosis II, sister chromatids separate to produce four newly formed haploid gametes (n).

Finally, microspores and megaspores go through further mitotic divisions and differentiation to become mature gametophyte: pollen and ovule respectively, a process termed germline development. The male germline development starts with an asymmetric division of the microspore (n) producing one small generative cell (n) enclosed within the larger vegetative cell (n). The smaller generative cell divides once more to produce two sperm cells (n). The RBR1/E2F-cyclin/CDK module controls this stereotypic series of divisions, and the termination of each lineage (Zhao et al. 2012; Z. Chen et al. 2009). At tri-cellular pollen stage, DAPI staining could reveal three nuclei: a vegetative nucleus (VN) with decondensed chromatin and two sperm nuclei with compact chromosomes. Extensive epigenetic reprogramming occurs in VN, which produces siRNAs from reactivated transposable elements (TEs) that target sperm cells (Slotkin et al. 2009). Pollens generate pollen tube upon female perception and deliver two sperm cells to complete double fertilization. One sperm fuses to the egg cell to produce the diploid zygote and the other sperm fuses to the female central cell (2n) to produce the endosperm (3n) that provides nourishment to the developing embryo.

## **Section II: Material and method**

### **Plant material**

*Ler* ecotype was used as wild type. *tsol-3* and *tsol-3/sup-5* were described in Chapter II. Plants harboring the centromere histone variant CENH3-GFP protein

fusion (Col-0 ecotype) was gifted by the Simon Chan lab (Ravi et al. 2011). Plants harboring sperm cell specific histone variant H3.3-RFP protein fusion transgene (Col-0 ecotype) was kindly shared by Xiaoning Zhang. These lines were crossed with *tsol-3* plants. In the cross progeny, *Ler* ecotype-looking plants with positive fluorescent signal were isolated and used for this study.

### **Histology**

For anther tissue sectioning, wild type (*Ler*) and *tsol-3* flowers were fixed and embedded in JB4 resin. 5 micron sections were then stained with toluidine blue.

For male meiocytes study, young flowers were fixed in ethanol-acetic acid (3:1) at room temperature for 12h. After rinsed with citrate buffer (10mM sodium citrate, pH=4.5), flower buds were digested with enzyme mix (0.3% cellulase, 0.3% macerozyme in citrate buffer) for 5min. Tissue were then macerated in 60% acetic acid followed by DAPI staining. To observe earlier meiosis events, light pressure was applied between slides and cover slides to spread chromosomes.

DAPI stained slides were observed by fluorescent or confocal microscopy.

### **Section III: Male meiosis and germline developmental defects of *tsol-3***

As described in Chapter I and II, *tsol-3* allele exhibits severely reduced fertility contributed by defects in both male and female gametes. This was further confirmed by reciprocal crosses between *tsol-3* and wild type (*Ler*) (Figure A1).

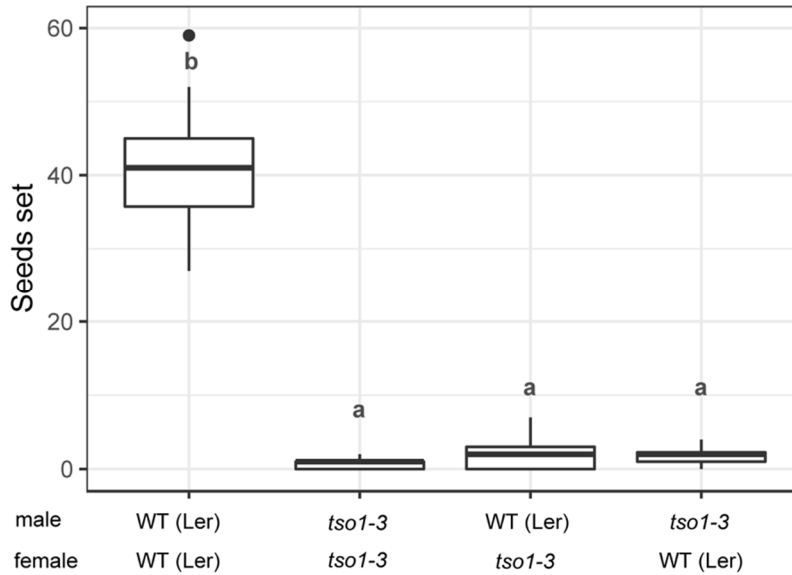


**Figure A1. Both male and female contribute to *tso1-3* fertility defects**

Seeds set quantification from reciprocal crosses between *tso1-3* and wild type (Ler). Letters denote significantly different groups (p value < 0.01, ANOVA and Tukey test).

For the easy access of male reproductive organs and greater body of existing knowledge, this study focuses on TSO1's function in male gametophyte development. *TSO1* has been shown to be expressed in reproductive organs (refer to Chater I). Here we show that *TSO1* transcripts are detected in young anther tissue and meiocytes at anther stage 5-6 (Figure A2).

Anther tissue development shows no obvious defects. At stage 5, proper layer formation is achieved and mature pollen has callose coating, indicating functional tapetum. (Figure A3)

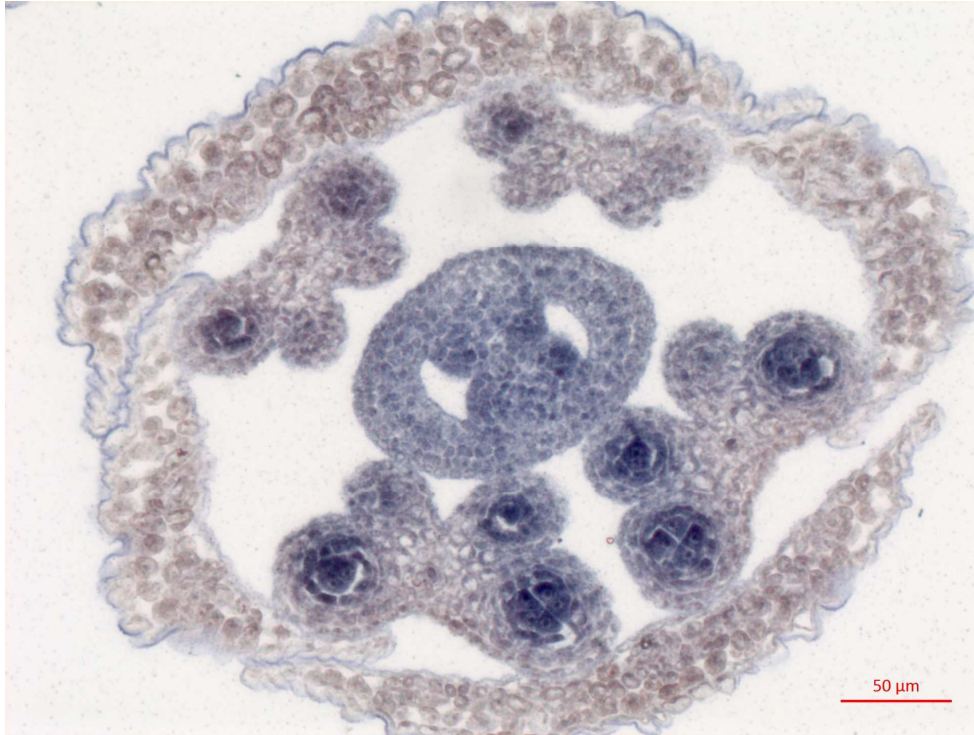


**Figure A2. *TSO1* is expressed in reproductive organs**

In situ hybridization detected *TSO1* transcript in young male and female reproductive tissue. (In situ done by Dr. Zhongchi Liu)

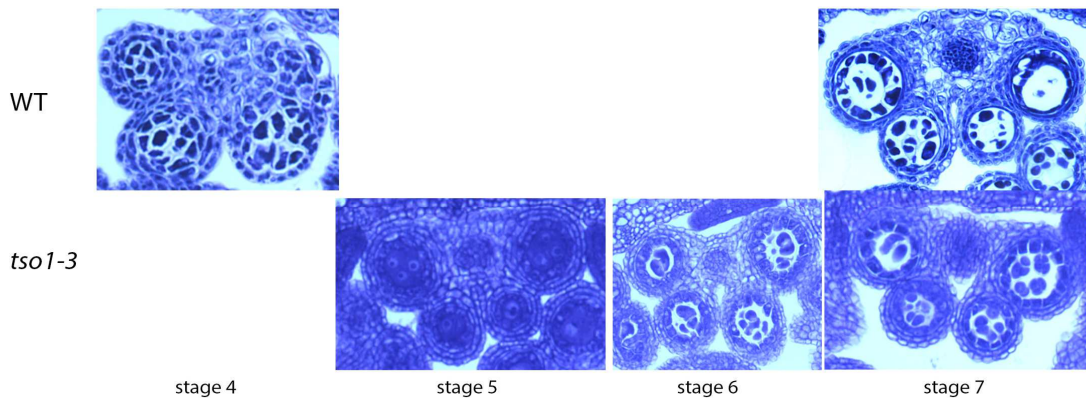


**Figure A3. Anther development of wild type and *tso1-3* flower.**

Sections of wild type (Ler) and *tso1-3* anther at stages 4 -7. Staging of anthers is done according to (Sanders et al. 1999).

Early meiosis seems normal (Figure A4E). Homologous chromosomes are able to juxtapose, synapse and condense. No chromosome fragmentation is observed, indicating functional DSBs repair machinery. Defect emerges at metaphase II (Figure A4F), where misaligned chromosomes appear at the division plane occasionally, with chromosomes lagging behind. In anaphase II, orientation of division plane is occasionally altered with mis-oriented spindle. Asynchronized chromosome separation also occurs at a low frequency (Figure A4G). At tetrad stage, about 10% of tetrads produced are with altered cell shape and DNA staining pattern, probably due to defect in meiosis II. Surprisingly, after the meiosis II, about 50% of the tetrads continued to divide for up to two more round to produce polyads (Figure A3I-L). These extra rounds of division are frequently abnormal with similar defects in meiosis II, producing cells with various sizes, shapes and different amount of DNA.

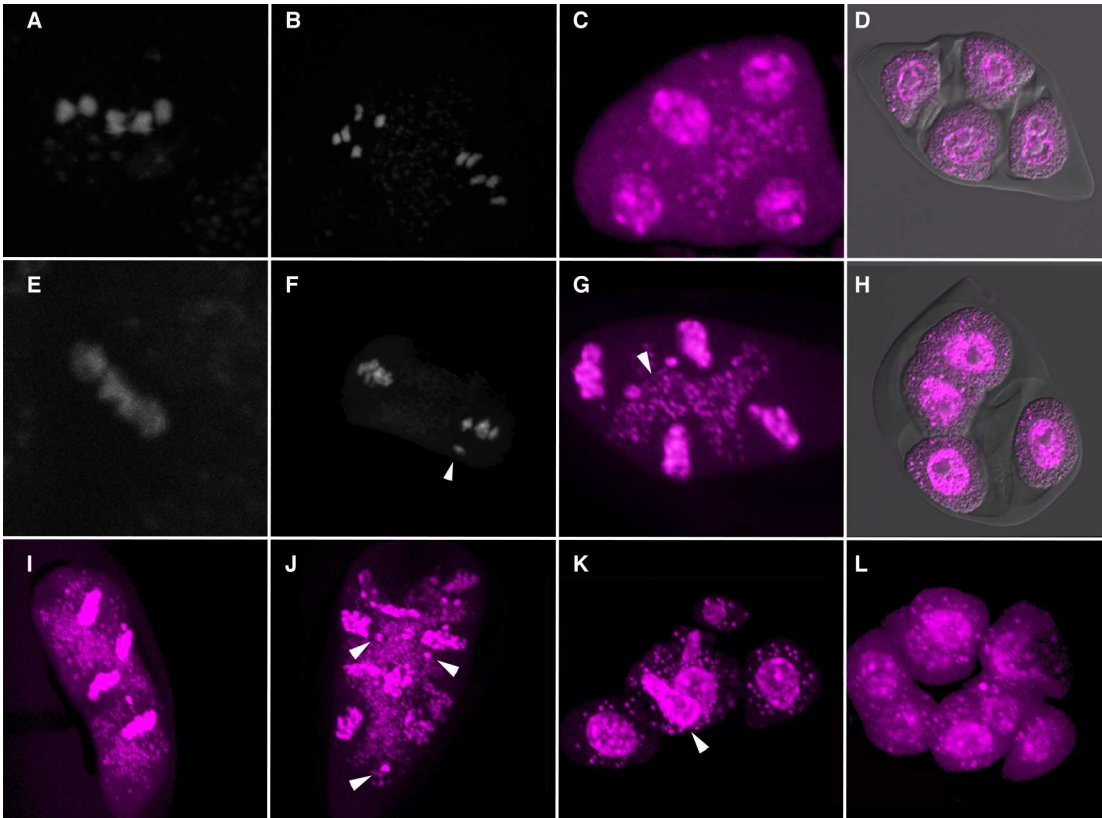


**Figure A4: *tso1-3* male meiosis progression defects**

(A-D) Wild type male meiosis. (A) Metaphase I. Five bivalents aligned at division plane. (B) Metaphase II. (C) Telophase II. (D) Tetrad with 4 newly formed microspores. (E-L) *tso1-3* meiosis. (E) Metaphase I, showing no obvious defects. (F) Metaphase II, showing one bivalents lagging behind (arrowhead). (G) Telophase, showing chromosome bridge (arrowhead). (H) A normal tetrad of *tso1-3*. (I-L) Abnormal tetrads of *tso1-3*. (I) Chromosomes aligned at division plane before an extra round of division, with chromosomes lagging behind (arrowhead). (J) Extra division leads to extra cells with scattered chromosomes (arrowheads). (K) A polyads with 6 cells. One cell shows failed cytokinesis (arrowhead). (L) A polyads with 8 cells.

I attempted to use the centromere histone variant GFP fusion (CENH3-GFP) to study the meiosis defect. This effort was hindered by that the meiosis loading of CENH3 favors the wild type copy over the CENH3-GFP made by the transgene (Ravi et al. 2011). As a result, no GFP signal was observed during meiosis. Utilizing this line requires further introgress of the *cenh3* mutant in the native locus.

Nonetheless, five centromeres could be observed in the sperm cells of the wild type and normal sized *tso1-3* pollen (Figure A5).

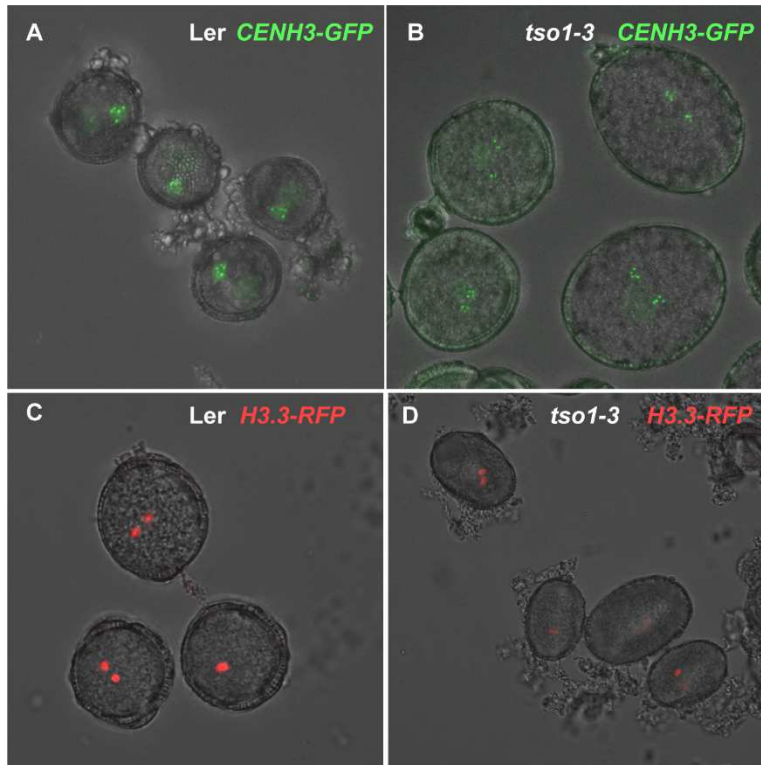


**Figure A5. Normal germline development can occur in *tso1-3* pollen.**

(A-B) Centromere histone variant CENH3 produced by *CENH3-GFP* transgene showed normal sperm cells with 5 centromeres in wildtype (Ler) (A) and *tso1-3* pollen (B). (C-D) Sperm cells marked by the *H3.3-RFP* signal in wildtype (Ler) (C) and *tso1-3* pollen (D).

During germline development, most microscopes are able to follow the stereotypical division pattern to form tricellular pollen (Figure 6 A, B show two sperm cells), indicating functioning lineage termination (differentiation) machinery. However, decondensed thin threads of chromosomes are observed occasionally especially in the vegetative nuclei (Figure A6). Taken together, defects in meiosis and germ line development process in *tso1-3* allele result in non-viable pollens with abnormal cell sizes and DNA content.

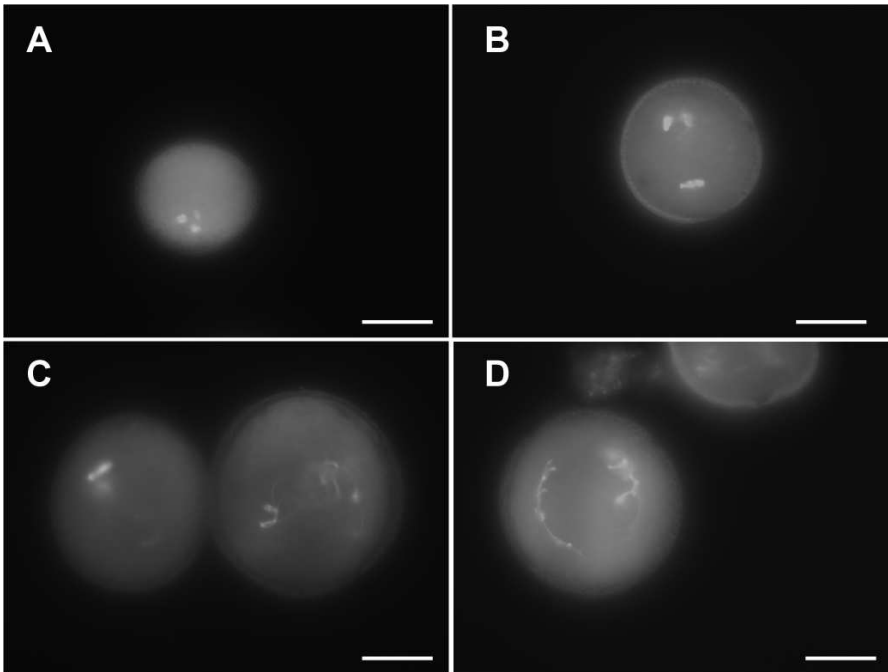


**Figure A6. Decondensed chromosomes observed in *tso1-3* pollen.**

DAPI staining of mature pollen of (A) wildtype (Ler); (B-D) and *tso1-3* pollen. Normal sized *tso1-3* pollens usually develop normal Tri-nuclear pollens. (C-D) shows *tso1-3* pollens with decondensed, threads-like chromosomes likely from sperm cells.

#### **Section IV: Brief survey of *Arabidopsis* mutant that produced polyad during male meiosis.**

In mutants of *ARABIDOPSIS THALIANA KINESIN 1 (ATK1)*, malformed spindle led to miss oriented division, imperfect alignment of chromosomes at metaphase, and synchronized segregation, and finally produced polyads (Mitsui et al. 1993; Liu, Cyr, and Palevitz 1996; C. Chen et al. 2002). However, it is unknown that how loss of kinesin function could lead to extras division.

Mutants of *Arabidopsis Skp1* homolog *Arabidopsis Skp1-like (ASK1)* also showed similar phenotype (Yang et al. 1999). Skp1 belongs to the largest E3 ubiquitin

ligases family SCF (skp1-Cullin-F-Box protein) class. SCF E3 ligases ubiquitinate a wide variety of protein substrates and target them for 26S proteasome degradation. *ASK1* mutants also showed failure of chromosome separation due to delayed sister chromatids cohesion resolution. Cohesion removal is known to be regulated by anaphase promoting complex (APC) E3 ubiquitin ligase activated by cyclin-CDK phosphorylation.

Reducing the expression of *CDC45* by RNAi caused fragmented chromosomes and polyads phenotypes (Stevens et al. 2004). The yeast CDC45 regulated mitotic DNA replication (Zou and Stillman 1998, 2000), thus CDC45 in *Arabidopsis* has been speculated to regulate pre-meiotic DNA replication (Ma 2006).

A novel protein MS5 has been shown to repress extra divisions in meiosis II (*Chaudhury 1993; Ross et al. 1997*). *MS5* encodes a novel protein with limited sequence homology to a synaptonemal complex protein in from rat.

We've shown mutations in *MYB3R1* also repress *tso1-3* mutant phenotypes (Chapter II), suggesting the TSO1-MYB3R1 module also functions at male meiosis/germline development. *myb3r1/+* can partially suppress *tso1-3* fertility defects (Chapter II) and the segregation ratio in the next generation did not deviated significantly from the 1:2:1, suggesting the suppression occurred at the somatic tissue or early in meiosis (rather than gametophytic suppression). These polyads producing mutant characterized to date presents a suite of late cell cycle genes that may be involved in the TSO1-MYB3R1 pathway in regulating meiosis.

## Reference

- Aichinger, Ernst, Noortje Kornet, Thomas Friedrich, and Thomas Laux. 2012. "Plant Stem Cell Niches." *Annual Review of Plant Biology* 63 (1). Annual Reviews: 615–36.
- Alexandrov, Andrei, Mark R. Martzen, and Eric M. Phizicky. 2002. "Two Proteins That Form a Complex Are Required for 7-Methylguanosine Modification of Yeast tRNA." *RNA* 8 (10): 1253–66.
- Amatschek, Stefan, Ulrich Koenig, Herbert Auer, Peter Steinlein, Margit Pacher, Agnes Gruenfelder, Gerhard Dekan, et al. 2004. "Tissue-Wide Expression Profiling Using cDNA Subtraction and Microarrays to Identify Tumor-Specific Genes." *Cancer Research* 64 (3): 844–56.
- Andersen, Stig Uggerhøj, Randi Groslier Algreen-Petersen, Martina Hoedl, Anna Jurkiewicz, Cristina Cvitanich, Ulrich Braunschweig, Leif Schauser, Sung-Aeong Oh, David Twell, and Erik Østergaard Jensen. 2007. "The Conserved Cysteine-Rich Domain of a tesmin/TSO1-like Protein Binds Zinc in Vitro and TSO1 Is Required for Both Male and Female Fertility in Arabidopsis Thaliana." *Journal of Experimental Botany* 58 (13): 3657–70.
- Andersen, S. U., R. G. Algreen-Petersen, M. Hoedl, A. Jurkiewicz, C. Cvitanich, U. Braunschweig, L. Schauser, S. A. Oh, D. Twell, and E. Ø. Jensen. 2007. "The Conserved Cysteine-Rich Domain of a tesmin/TSO1-like Protein Binds Zinc \itshape in Vitro and TSO1 Is Required for Both Male and Female Fertility in \itshape Arabidopsis Thaliana." *Journal of Experimental Botany* 58 (13). Soc Experiment Biol: 3657–70.
- Aramini, James M., Jeffrey L. Mills, Rong Xiao, Thomas B. Acton, Maggie J. Wu, Thomas Szyperski, and Gaetano T. Montelione. 2003. "Resonance Assignments for the Hypothetical Protein yggU from Escherichia Coli." *Journal of Biomolecular NMR* 27 (3): 285–86.
- Aroian, R. V., M. Koga, J. E. Mendel, Y. Ohshima, and P. W. Sternberg. 1990. "The Let-23 Gene Necessary for Caenorhabditis Elegans Vulval Induction Encodes a Tyrosine Kinase of the EGF Receptor Subfamily." *Nature* 348 (6303): 693–99.
- Baldwin, Katherine L., Elizabeth M. Dinh, Brian M. Hart, and Patrick H. Masson. 2013. "CACTIN Is an Essential Nuclear Protein in Arabidopsis and May Be Associated with the Eukaryotic Spliceosome." *FEBS Letters* 587 (7): 873–79.
- Beall, Eileen L., Maren Bell, Daphne Georlette, and Michael R. Botchan. 2004. "Dm-Myb Mutant Lethality in Drosophila Is Dependent upon mip130: Positive and Negative Regulation of DNA Replication." *Genes & Development* 18 (14): 1667–80.

- Beall, Eileen L., J. Robert Manak, Sharleen Zhou, Maren Bell, Joseph S. Lipsick, and Michael R. Botchan. 2002. "Role for a *Drosophila* Myb-Containing Protein Complex in Site-Specific DNA Replication." *Nature* 420 (6917): 833–37.
- Beall, E. L., P. W. Lewis, M. Bell, M. Rocha, D. L. Jones, and M. R. Botchan. 2007. "Discovery of tMAC: A *Drosophila* Testis-Specific Meiotic Arrest Complex Paralogous to Myb--Muv B." *Genes & Development* 21 (8). Cold Spring Harbor Lab: 904.
- Beitel, G. J., S. G. Clark, and H. R. Horvitz. 1990. "Caenorhabditis Elegans Ras Gene Let-60 Acts as a Switch in the Pathway of Vulval Induction." *Nature* 348 (6301): 503–9.
- Benjamini, Yoav, and Yosef Hochberg. 1995. "Controlling the False Discovery Rate: A Practical and Powerful Approach to Multiple Testing." *Journal of the Royal Statistical Society. Series B, Statistical Methodology* 57 (1). [Royal Statistical Society, Wiley]: 289–300.
- Berg, C. van den, V. Willemsen, W. Hage, P. Weisbeek, and B. Scheres. 1995. "Cell Fate in the Arabidopsis Root Meristem Determined by Directional Signalling." *Nature* 378 (6552): 62–65.
- Beug, H., A. von Kirchbach, G. Döderlein, J. F. Conscience, and T. Graf. 1979. "Chicken Hematopoietic Cells Transformed by Seven Strains of Defective Avian Leukemia Viruses Display Three Distinct Phenotypes of Differentiation." *Cell* 18 (2): 375–90.
- Biedenkapp, H., U. Borgmeyer, A. E. Sippel, and K. H. Klempnauer. 1988. "Viral Myb Oncogene Encodes a Sequence-Specific DNA-Binding Activity." *Nature* 335 (6193): 835–37.
- Bowman, J. L., and Y. Eshed. 2000. "Formation and Maintenance of the Shoot Apical Meristem." *Trends in Plant Science* 5 (3): 110–15.
- Bowman, John L., Yuval Eshed, and Stuart F. Baum. 2002. "Establishment of Polarity in Angiosperm Lateral Organs." *Trends in Genetics: TIG* 18 (3): 134–41.
- Brady, Siobhan M., David A. Orlando, Ji-Young Lee, Jean Y. Wang, Jeremy Koch, José R. Dinneny, Daniel Mace, Uwe Ohler, and Philip N. Benfey. 2007. "A High-Resolution Root Spatiotemporal Map Reveals Dominant Expression Patterns." *Science* 318 (5851). American Association for the Advancement of Science: 801–6.
- Brandt, Ronny, Mercè Salla-Martret, Jordi Bou-Torrent, Thomas Musielak, Mark Stahl, Christa Lanz, Felix Ott, et al. 2012. "Genome-Wide Binding-Site Analysis of REVOLUTA Reveals a Link between Leaf Patterning and Light-Mediated

- Growth Responses.” *The Plant Journal: For Cell and Molecular Biology* 72 (1): 31–42.
- Brand, Ulrike, Margit Grünewald, Martin Hobe, and Rüdiger Simon. 2002. “Regulation of CLV3 Expression by Two Homeobox Genes in Arabidopsis.” *Plant Physiology* 129 (2): 565–75.
- Brzeska, Katarzyna, Jan Brzeski, Jacquelyn Smith, and Vicki L. Chandler. 2010. “Transgenic Expression of CBBP, a CXC Domain Protein, Establishes Paramutation in Maize.” *Proceedings of the National Academy of Sciences of the United States of America* 107 (12): 5516–21.
- Cam, Hugh, Egle Balciunaite, Alexandre Blais, Alexander Spektor, Richard C. Scarpulla, Richard Young, Yuval Kluger, and Brian David Dynlacht. 2004. “A Common Set of Gene Regulatory Networks Links Metabolism and Growth Inhibition.” *Molecular Cell* 16 (3): 399–411.
- Ceol, C. J., and H. R. Horvitz. 2001. “Dpl-1 DP and Efl-1 E2F Act with Lin-35 Rb to Antagonize Ras Signaling in *C. Elegans* Vulval Development.” *Molecular Cell* 7 (3): 461–73.
- Chandler, John, Judith Nardmann, and Wolfgang Werr. 2008. “Plant Development Revolves around Axes.” *Trends in Plant Science* 13 (2): 78–84.
- Chaudhury, A. M. 1993. “Nuclear Genes Controlling Male Fertility.” *The Plant Cell* 5 (10): 1277–83.
- Chen, Changbin, Adam Marcus, Wuxing Li, Yi Hu, Jean-Philippe Vielle Calzada, Ueli Grossniklaus, Richard J. Cyr, and Hong Ma. 2002. “The Arabidopsis ATK1 Gene Is Required for Spindle Morphogenesis in Male Meiosis.” *Development* 129 (10): 2401–9.
- Chen, Zhong, Said Hafidh, Shi Hui Poh, David Twell, and Frederic Berger. 2009. “Proliferation and Cell Fate Establishment during Arabidopsis Male Gametogenesis Depends on the Retinoblastoma Protein.” *Proceedings of the National Academy of Sciences of the United States of America* 106 (17): 7257–62.
- Chickarmane, Vijay S., Sean P. Gordon, Paul T. Tarr, Marcus G. Heisler, and Elliot M. Meyerowitz. 2012. “Cytokinin Signaling as a Positional Cue for Patterning the Apical–basal Axis of the Growing Arabidopsis Shoot Meristem.” *Proceedings of the National Academy of Sciences* 109 (10): 4002–7.
- Conway, Jake R., Alexander Lex, and Nils Gehlenborg. 2017. “UpSetR: An R Package For The Visualization Of Intersecting Sets And Their Properties.” *bioRxiv*. doi:10.1101/120600.

- Cui, Hongchang, Mitchell P. Levesque, Teva Vernoux, Jee W. Jung, Alice J. Paquette, Kimberly L. Gallagher, Jean Y. Wang, Ikram Blilou, Ben Scheres, and Philip N. Benfey. 2007. "An Evolutionarily Conserved Mechanism Delimiting SHR Movement Defines a Single Layer of Endodermis in Plants." *Science* 316 (5823): 421–25.
- Curtis, Mark D., and Ueli Grossniklaus. 2003. "A Gateway Cloning Vector Set for High-Throughput Functional Analysis of Genes in Planta." *Plant Physiology* 133 (2): 462–69.
- Cvitanich, C., N. Pallisgaard, K. A. Nielsen, A. C. Hansen, K. Larsen, K. Pihakaski-Maunsbach, K. A. Marcker, and E. O. Jensen. 2000. "CPP1, a DNA-Binding Protein Involved in the Expression of a Soybean Leghemoglobin c3 Gene." *Proceedings of the National Academy of Sciences of the United States of America* 97 (14): 8163–68.
- Davidson, Colin J., Rabindra Tirouvanziam, Leonard A. Herzenberg, and Joseph S. Lipsick. 2005. "Functional Evolution of the Vertebrate Myb Gene Family." *Genetics* 169 (1). *Genetics*: 215–29.
- Dello Ioio, Raffaele, Kinu Nakamura, Laila Moubayidin, Serena Perilli, Masatoshi Taniguchi, Miyo T. Morita, Takashi Aoyama, Paolo Costantino, and Sabrina Sabatini. 2008. "A Genetic Framework for the Control of Cell Division and Differentiation in the Root Meristem." *Science* 322 (5906): 1380–84.
- Dubos, Christian, Ralf Stracke, Erich Grotewold, Bernd Weisshaar, Cathie Martin, and Loïc Lepiniec. 2010. "MYB Transcription Factors in Arabidopsis." *Trends in Plant Science* 15 (10): 573–81.
- Du, Hai, Zhe Liang, Sen Zhao, Ming-Ge Nan, Lam-Son Phan Tran, Kun Lu, Yu-Bi Huang, and Jia-Na Li. 2015. "The Evolutionary History of R2R3-MYB Proteins Across 50 Eukaryotes: New Insights Into Subfamily Classification and Expansion." *Scientific Reports* 5 (June): 11037.
- Durek, Pawel, Robert Schmidt, Joshua L. Heazlewood, Alexandra Jones, Daniel MacLean, Axel Nagel, Birgit Kersten, and Waltraud X. Schulze. 2010. "PhosPhAt: The Arabidopsis Thaliana Phosphorylation Site Database. An Update." *Nucleic Acids Research* 38 (Database issue): D828–34.
- Earley, Keith W., Jeremy R. Haag, Olga Pontes, Kristen Opper, Tom Juehne, Keming Song, and Craig S. Pikaard. 2006. "Gateway-Compatible Vectors for Plant Functional Genomics and Proteomics." *The Plant Journal: For Cell and Molecular Biology* 45 (4): 616–29.
- Edgar, Robert C. 2004. "MUSCLE: Multiple Sequence Alignment with High Accuracy and High Throughput." *Nucleic Acids Research* 32 (5): 1792–97.

- Emery, John F., Sandra K. Floyd, John Alvarez, Yuval Eshed, Nathaniel P. Hawker, Anat Izhaki, Stuart F. Baum, and John L. Bowman. 2003. "Radial Patterning of Arabidopsis Shoots by Class III HD-ZIP and KANADI Genes." *Current Biology: CB* 13 (20): 1768–74.
- Engler, Carola, and Sylvestre Marillonnet. 2014. "Golden Gate Cloning." *Methods in Molecular Biology* 1116: 119–31.
- Falcon, S., and R. Gentleman. 2007. "Using GOSTATS to Test Gene Lists for GO Term Association." *Bioinformatics* 23 (2): 257–58.
- Fauth, Torsten, Felix Müller-Planitz, Cornelia König, Tobias Straub, and Peter B. Becker. 2010. "The DNA Binding CXC Domain of MSL2 Is Required for Faithful Targeting the Dosage Compensation Complex to the X Chromosome." *Nucleic Acids Research* 38 (10): 3209–21.
- Fay, David S., Min Han, and Others. 2000. "The Synthetic Multivulval Genes of *C. elegans*: Functional Redundancy, Ras-Antagonism, and Cell Fate Determination." *Genesis* 26 (4): 279–84.
- Ferguson, E. L., and H. R. Horvitz. 1989. "The Multivulva Phenotype of Certain *C. elegans* Mutants Results from Defects in Two Functionally Redundant Pathways." *Genetics* 123 (1). Genetics Soc America: 109–21.
- Fischer, Martin, and James A. DeCaprio. 2015. "Does Arabidopsis Thaliana DREAM of Cell Cycle Control?" *The EMBO Journal* 34 (15): 1987–89.
- Fletcher, J. C., U. Brand, M. P. Running, R. Simon, and E. M. Meyerowitz. 1999. "Signaling of Cell Fate Decisions by CLAVATA3 in Arabidopsis Shoot Meristems." *Science* 283 (5409): 1911–14.
- Forzani, Celine, Ernst Aichinger, Emily Sornay, Viola Willemsen, Thomas Laux, Walter Dewitte, and James A. H. Murray. 2014. "WOX5 Suppresses CYCLIN D Activity to Establish Quiescence at the Center of the Root Stem Cell Niche." *Current Biology: CB* 24 (16): 1939–44.
- Gaiser, J. C., K. Robinson-Beers, and C. S. Gasser. 1995. "The Arabidopsis SUPERMAN Gene Mediates Asymmetric Growth of the Outer Integument of Ovules." *The Plant Cell* 7 (3): 333–45.
- Gaudinier, Allison, Lifang Zhang, John S. Reece-Hoyes, Mallorie Taylor-Teeples, Li Pu, Zhijie Liu, Ghislain Breton, et al. 2011. "Enhanced Y1H Assays for Arabidopsis." *Nature Methods* 8 (12). Nature Research: 1053–55.

- Gerondakis, S., and J. M. Bishop. 1986. "Structure of the Protein Encoded by the Chicken Proto-Oncogene c-Myb." *Molecular and Cellular Biology* 6 (11): 3677–84.
- Gordon, Sean P., Vijay S. Chickarmane, Carolyn Ohno, and Elliot M. Meyerowitz. 2009. "Multiple Feedback Loops through Cytokinin Signaling Control Stem Cell Number within the Arabidopsis Shoot Meristem." *Proceedings of the National Academy of Sciences of the United States of America* 106 (38): 16529–34.
- Grässer, F. A., K. LaMontagne, L. Whittaker, S. Stohr, and J. S. Lipsick. 1992. "A Highly Conserved Cysteine in the v-Myb DNA-Binding Domain Is Essential for Transformation and Transcriptional Trans-Activation." *Oncogene* 7 (5): 1005–9.
- Grelon, M., D. Vezon, G. Gendrot, and G. Pelletier. 2001. "AtSPO11-1 Is Necessary for Efficient Meiotic Recombination in Plants." *The EMBO Journal* 20 (3): 589–600.
- Grieneisen, Verônica A., Jian Xu, Athanasius F. M. Marée, Paulien Hogeweg, and Ben Scheres. 2007. "Auxin Transport Is Sufficient to Generate a Maximum and Gradient Guiding Root Growth." *Nature* 449 (7165): 1008–13.
- Guehmann, S., G. Vorbrueggen, F. Kalkbrenner, and K. Moelling. 1992. "Reduction of a Conserved Cys Is Essential for Myb DNA-Binding." *Nucleic Acids Research* 20 (9): 2279–86.
- Haecker, Achim, Rita Gross-Hardt, Bernd Geiges, Ananda Sarkar, Holger Breuning, Marita Herrmann, and Thomas Laux. 2004. "Expression Dynamics of WOX Genes Mark Cell Fate Decisions during Early Embryonic Patterning in Arabidopsis Thaliana." *Development* 131 (3): 657–68.
- Haga, Nozomi, Kiichi Kato, Masatake Murase, Satoshi Araki, Minoru Kubo, Taku Demura, Kaoru Suzuki, et al. 2007. "R1R2R3-Myb Proteins Positively Regulate Cytokinesis through Activation of KNOLLE Transcription in Arabidopsis Thaliana." *Development* 134 (6): 1101–10.
- Haga, Nozomi, Kosuke Kobayashi, Takamasa Suzuki, Kenichiro Maeo, Minoru Kubo, Misato Ohtani, Nobutaka Mitsuda, et al. 2011. "Mutations in MYB3R1 and MYB3R4 Cause Pleiotropic Developmental Defects and Preferential down-Regulation of Multiple G2/M-Specific Genes in Arabidopsis." *Plant Physiology* 157 (2): 706–17.
- Hahne, Florian, Wolfgang Huber, Robert Gentleman, and Seth Falcon. 2010. *Bioconductor Case Studies*. Springer Science & Business Media.
- Han, M., and P. W. Sternberg. 1990. "Let-60, a Gene That Specifies Cell Fates during C. Elegans Vulval Induction, Encodes a Ras Protein." *Cell* 63 (5): 921–31.

- Hauser, B. A., J. Q. He, S. O. Park, and C. S. Gasser. 2000. "TSO1 Is a Novel Protein That Modulates Cytokinesis and Cell Expansion in Arabidopsis." *Development* 127 (10): 2219–26.
- Hauser, Bernard a., Jacinto M. Villanueva, and Charles S. Gasser. 1998. "Arabidopsis TSO1 Regulates Directional Processes in Cells during Floral Organogenesis." *Genetics* 150 (1): 411–23.
- Heazlewood, Joshua L., Pawel Durek, Jan Hummel, Joachim Selbig, Wolfram Weckwerth, Dirk Walther, and Waltraud X. Schulze. 2008. "PhosphoAt: A Database of Phosphorylation Sites in Arabidopsis Thaliana and a Plant-Specific Phosphorylation Site Predictor." *Nucleic Acids Research* 36 (Database issue): D1015–21.
- Heine, George F., J. Marcela Hernandez, and Erich Grotewold. 2004. "Two Cysteines in Plant R2R3 MYB Domains Participate in REDOX-Dependent DNA Binding." *The Journal of Biological Chemistry* 279 (36): 37878–85.
- Heisler, Marcus G., Carolyn Ohno, Pradeep Das, Patrick Sieber, Gonehal V. Reddy, Jeff a. Long, and Elliot M. Meyerowitz. 2005. "Patterns of Auxin Transport and Gene Expression during Primordium Development Revealed by Live Imaging of the Arabidopsis Inflorescence Meristem." *Current Biology: CB* 15 (21): 1899–1911.
- Helariutta, Y., H. Fukaki, J. Wysocka-Diller, K. Nakajima, J. Jung, G. Sena, M. T. Hauser, and P. N. Benfey. 2000. "The SHORT-ROOT Gene Controls Radial Patterning of the Arabidopsis Root through Radial Signaling." *Cell* 101 (5): 555–67.
- Hove, Colette A. ten, Kuan-Ju Lu, and Dolf Weijers. 2015. "Building a Plant: Cell Fate Specification in the Early Arabidopsis Embryo." *Development* 142 (3): 420–30. Oxford University Press for The Company of Biologists Limited.
- Ioio, Raffaele Dello, Carla Galinha, Alexander G. Fletcher, Stephen P. Grigg, Attila Molnar, Viola Willemsen, Ben Scheres, et al. 2012. "A PHABULOSA / Cytokinin Feedback Loop Controls Root Growth in Arabidopsis." *Current Biology: CB* 22 (18): 1699–1704.
- Irizarry, Rafael A., Bridget Hobbs, Francois Collin, Yasmin D. Beazer-Barclay, Kristen J. Antonellis, Uwe Scherf, and Terence P. Speed. 2003. "Exploration, Normalization, and Summaries of High Density Oligonucleotide Array Probe Level Data." *Biostatistics* 4 (2): 249–64.
- Ito, Masaki. 2005. "Conservation and Diversification of Three-Repeat Myb Transcription Factors in Plants." *Journal of Plant Research* 118 (1): 61–69.

- Izhaki, Anat, and John L. Bowman. 2007. "KANADI and Class III HD-Zip Gene Families Regulate Embryo Patterning and Modulate Auxin Flow during Embryogenesis in Arabidopsis." *The Plant Cell* 19 (2): 495–508.
- Jackson, James P., Anders M. Lindroth, Xiaofeng Cao, and Steven E. Jacobsen. 2002. "Control of CpNpG DNA Methylation by the KRYPTONITE Histone H3 Methyltransferase." *Nature* 416 (6880): 556–60.
- Jenuwein, T., G. Laible, R. Dorn, and G. Reuter. 1998. "SET Domain Proteins Modulate Chromatin Domains in Eu- and Heterochromatin." *Cellular and Molecular Life Sciences: CMLS* 54 (1): 80–93.
- Jiang, Wenzhi, Bing Yang, and Donald P. Weeks. 2014. "Efficient CRISPR/Cas9-Mediated Gene Editing in Arabidopsis Thaliana and Inheritance of Modified Genes in the T2 and T3 Generations." *PloS One* 9 (6): e99225.
- Katzen, A. L., T. B. Kornberg, and J. M. Bishop. 1985. "Isolation of the Proto-Oncogene c-Myb from D. Melanogaster." *Cell* 41 (2): 449–56.
- Kelley, Lawrence A., Stefans Mezulis, Christopher M. Yates, Mark N. Wass, and Michael J. E. Sternberg. 2015. "The Pyre2 Web Portal for Protein Modeling, Prediction and Analysis." *Nature Protocols* 10 (6). Nature Research: 845–58.
- Kerstetter, R. A., K. Bollman, R. A. Taylor, K. Bomblies, and R. S. Poethig. 2001. "KANADI Regulates Organ Polarity in Arabidopsis." *Nature* 411 (6838): 706–9.
- Ketel, Carrie S., Erica F. Andersen, Marcus L. Vargas, Jinkyoo Suh, Susan Strome, and Jeffrey A. Simon. 2005. "Subunit Contributions to Histone Methyltransferase Activities of Fly and Worm Polycomb Group Complexes." *Molecular and Cellular Biology* 25 (16): 6857–68.
- Kinoshita, Atsuko, Shigeyuki Betsuyaku, Yuriko Osakabe, Shinji Mizuno, Shingo Nagawa, Yvonne Stahl, Rüdiger Simon, Kazuko Yamaguchi-Shinozaki, Hiroo Fukuda, and Shinichiro Sawa. 2010. "RPK2 Is an Essential Receptor-like Kinase That Transmits the CLV3 Signal in Arabidopsis." *Development* 137 (22): 3911–20.
- Kittler, Ralf, Laurence Pelletier, Anne-Kristine Heninger, Mikolaj Slabicki, Mirko Theis, Lukasz Mirosław, Ina Poser, et al. 2007. "Genome-Scale RNAi Profiling of Cell Division in Human Tissue Culture Cells." *Nature Cell Biology* 9 (12). Nature Publishing Group: 1401–12.
- Klempnauer, K. H., and J. M. Bishop. 1984. "Neoplastic Transformation by E26 Leukemia Virus Is Mediated by a Single Protein Containing Domains of Gag and Myb Genes." *Journal of Virology* 50 (1): 280–83.

- Knight, A. S., M. Notaridou, and R. J. Watson. 2009. "A Lin-9 Complex Is Recruited by B-Myb to Activate Transcription of G2/M Genes in Undifferentiated Embryonal Carcinoma Cells." *Oncogene* 28 (15). Nature Publishing Group: 1737–47.
- Kobayashi, Kosuke, Toshiya Suzuki, Eriko Iwata, Norihito Nakamichi, Takamasa Suzuki, Poyu Chen, Misato Ohtani, et al. 2015. "Transcriptional Repression by MYB3R Proteins Regulates Plant Organ Growth." *The EMBO Journal* 34 (15): 1992–2007.
- Korenjak, Michael, Barbie Taylor-Harding, Ulrich K. Binné, John S. Satterlee, Olivier Stevaux, Rein Aasland, Helen White-Cooper, Nick Dyson, and Alexander Brehm. 2004. "Native E2F/RBF Complexes Contain Myb-Interacting Proteins and Repress Transcription of Developmentally Controlled E2F Target Genes." *Cell* 119 (2): 181–93.
- Krzywinski, Martin, Jacqueline Schein, Inanç Birol, Joseph Connors, Randy Gascoyne, Doug Horsman, Steven J. Jones, and Marco A. Marra. 2009. "Circos: An Information Aesthetic for Comparative Genomics." *Genome Research* 19 (9): 1639–45.
- Kuhlemeier, Cris, and Marja C. P. Timmermans. 2016. "The Sussex Signal: Insights into Leaf Dorsiventrality." *Development* 143 (18): 3230–37.
- Kumar, Sudhir, Glen Stecher, and Koichiro Tamura. 2016. "MEGA7: Molecular Evolutionary Genetics Analysis Version 7.0 for Bigger Datasets." *Molecular Biology and Evolution* 33 (7): 1870–74.
- Langmead, Ben, and Steven L. Salzberg. 2012. "Fast Gapped-Read Alignment with Bowtie 2." *Nature Methods* 9 (4): 357–59.
- Latorre, Isabel, Michael A. Chesney, Jacob M. Garrigues, Przemyslaw Stempor, Alex Appert, Mirko Francesconi, Susan Strome, and Julie Ahringer. 2015. "The DREAM Complex Promotes Gene Body H2A.Z for Target Repression." *Genes & Development* 29 (5): 495–500.
- Laux, Thomas. 2003. "The Stem Cell Concept in Plants: A Matter of Debate." *Cell* 113 (3): 281–83.
- Laux, T., K. F. Mayer, J. Berger, and G. Jürgens. 1996. "The WUSCHEL Gene Is Required for Shoot and Floral Meristem Integrity in Arabidopsis." *Development* 122 (1): 87–96.
- Leibfried, Andrea, Jennifer P. C. To, Wolfgang Busch, Sandra Stehling, Andreas Kehle, Monika Demar, Joseph J. Kieber, and Jan U. Lohmann. 2005. "WUSCHEL Controls Meristem Function by Direct Regulation of Cytokinin-Inducible Response Regulators." *Nature* 438 (7071): 1172–75.

- Lenhard, Michael, Gerd Jürgens, and Thomas Laux. 2002. “The WUSCHEL and SHOOTMERISTEMLESS Genes Fulfill Complementary Roles in Arabidopsis Shoot Meristem Regulation.” *Development* 129 (13): 3195–3206.
- Lewis, P. W., E. L. Beall, T. C. Fleischer, D. Georlette, A. J. Link, and M. R. Botchan. 2004. “Identification of a Novel Drosophila Myb-E2F2/RBF Transcriptional Repressor Complex.” *Genes & Development* 18 (23). Cold Spring Harbor Lab: 2929.
- Lieberman, Louisa M., Erin E. Sparks, Miguel A. Moreno-Risueno, Jalean J. Petricka, and Philip N. Benfey. 2015. “MYB36 Regulates the Transition from Proliferation to Differentiation in the Arabidopsis Root.” *Proceedings of the National Academy of Sciences of the United States of America* 112 (39): 12099–104.
- Li, Heng, Bob Handsaker, Alec Wysoker, Tim Fennell, Jue Ruan, Nils Homer, Gabor Marth, Goncalo Abecasis, Richard Durbin, and Others. 2009. “The Sequence Alignment/Map Format and SAMtools.” *Bioinformatics* 25 (16). Oxford Univ Press: 2078–79.
- Lipsick, Joseph S. 2004. “synMuv vertebrate—Myb Comes into Focus.” *Genes & Development* 18 (23). Cold Spring Harbor Lab: 2837–44.
- Litovchick, Larisa, Subhashini Sadasivam, Laurence Florens, Xiaopeng Zhu, Selene K. Swanson, Soundarapandian Velmurugan, Runsheng Chen, Michael P. Washburn, X. Shirley Liu, and James A. DeCaprio. 2007. “Evolutionarily Conserved Multisubunit RBL2/p130 and E2F4 Protein Complex Represses Human Cell Cycle-Dependent Genes in Quiescence.” *Molecular Cell* 26 (4). Elsevier: 539–51.
- Liu, B., R. J. Cyr, and B. A. Palevitz. 1996. “A Kinesin-like Protein, KatAp, in the Cells of Arabidopsis and Other Plants.” *The Plant Cell* 8 (1): 119–32.
- Liu, Qili, Xiaozhen Yao, Limin Pi, Hua Wang, Xiaofeng Cui, and Hai Huang. 2009. “The ARGONAUTE10 Gene Modulates Shoot Apical Meristem Maintenance and Establishment of Leaf Polarity by Repressing miR165/166 in Arabidopsis.” *The Plant Journal: For Cell and Molecular Biology* 58 (1): 27–40.
- Liu, Yuanyuan, Shijun You, Mallorie Taylor-Teeples, Wenhua L. Li, Mathias Schuetz, Siobhan M. Brady, and Carl J. Douglas. 2014. “BEL1-LIKE HOMEODOMAIN6 and KNOTTED ARABIDOPSIS THALIANA7 Interact and Regulate Secondary Cell Wall Formation via Repression of REVOLUTA.” *The Plant Cell* 26 (12): 4843–61.
- Liu, Z., M. P. Running, and E. M. Meyerowitz. 1997. “TSO1 Functions in Cell Division during Arabidopsis Flower Development.” *Development* 124 (3): 665–72.

- Li, Wuxing, Changbin Chen, Ullrich Markmann-Mulisch, Ljudmilla Timofejeva, Elmon Schmelzer, Hong Ma, and Bernd Reiss. 2004. "The Arabidopsis AtRAD51 Gene Is Dispensable for Vegetative Development but Required for Meiosis." *Proceedings of the National Academy of Sciences of the United States of America* 101 (29): 10596–601.
- Lloyd, A. M., M. Schena, V. Walbot, and R. W. Davis. 1994. "Epidermal Cell Fate Determination in Arabidopsis: Patterns Defined by a Steroid-Inducible Regulator." *Science* 266 (5184): 436–39.
- Ma, Hong. 2006. "A Molecular Portrait of Arabidopsis Meiosis." *The Arabidopsis Book / American Society of Plant Biologists* 4 (June): e0095.
- Mallory, Allison C., Brenda J. Reinhart, Matthew W. Jones-Rhoades, Guiliang Tang, Phillip D. Zamore, M. Kathryn Barton, and David P. Bartel. 2004. "MicroRNA Control of PHABULOSA in Leaf Development: Importance of Pairing to the microRNA 5' Region." *The EMBO Journal* 23 (16). John Wiley & Sons, Ltd: 3356–64.
- Matsuo, Taira, Hiroyo Kuramoto, Tsutomu Kumazaki, Youji Mitsui, and Tomoko Takahashi. 2012. "LIN54 Harboring a Mutation in CHC Domain Is Localized to the Cytoplasm and Inhibits Cell Cycle Progression." *Cell Cycle* 11 (17). Landes Bioscience: 3227–36.
- Mayer, K. F., H. Schoof, A. Haecker, M. Lenhard, G. Jürgens, and T. Laux. 1998. "Role of WUSCHEL in Regulating Stem Cell Fate in the Arabidopsis Shoot Meristem." *Cell* 95 (6): 805–15.
- McConnell, J. R., and M. K. Barton. 1998. "Leaf Polarity and Meristem Formation in Arabidopsis." *Development* 125 (15): 2935–42.
- McConnell, J. R., J. Emery, Y. Eshed, N. Bao, J. Bowman, and M. K. Barton. 2001. "Role of PHABULOSA and PHAVOLUTA in Determining Radial Patterning in Shoots." *Nature* 411 (June): 709–13.
- Merelo, Paz, Hathi Ram, Monica Pia Caggiano, Carolyn Ohno, Felix Ott, Daniel Straub, Moritz Graeff, et al. 2016. "Regulation of MIR165/166 by Class II and Class III Homeodomain Leucine Zipper Proteins Establishes Leaf Polarity." *Proceedings of the National Academy of Sciences of the United States of America* 113 (42): 11973–78.
- Merelo, Paz, Yakun Xie, Lucas Brand, Felix Ott, Detlef Weigel, John L. Bowman, Marcus G. Heisler, and Stephan Wenkel. 2013. "Genome-Wide Identification of KANADI1 Target Genes." *PloS One* 8 (10): 1–14.
- Mitsui, H., K. Yamaguchi-Shinozaki, K. Shinozaki, K. Nishikawa, and H. Takahashi. 1993. "Identification of a Gene Family (kat) Encoding Kinesin-like Proteins in

- Arabidopsis Thaliana and the Characterization of Secondary Structure of KatA.” *Molecular & General Genetics: MGG* 238 (3): 362–68.
- Moussian, Bernard, Achim Haecker, and Thomas Laux. 2003. “ZWILLE Buffers Meristem Stability in Arabidopsis Thaliana.” *Development Genes and Evolution* 213 (11): 534–40.
- Moussian, B., H. Schoof, A. Haecker, G. Jürgens, and T. Laux. 1998. “Role of the ZWILLE Gene in the Regulation of Central Shoot Meristem Cell Fate during Arabidopsis Embryogenesis.” *The EMBO Journal* 17 (6): 1799–1809.
- Müller, Ralf, Andrea Bleckmann, and Rüdiger Simon. 2008. “The Receptor Kinase CORYNE of Arabidopsis Transmits the Stem Cell–Limiting Signal CLAVATA3 Independently of CLAVATA1.” *The Plant Cell* 20 (4): 934–46.
- Obenchain, Valerie, Michael Lawrence, Vincent Carey, Stephanie Gogarten, Paul Shannon, and Martin Morgan. 2014. “VariantAnnotation: A Bioconductor Package for Exploration and Annotation of Genetic Variants.” *Bioinformatics* 30 (14): 2076–78.
- O’Carroll, D., H. Scherthan, A. H. Peters, S. Opravil, A. R. Haynes, G. Laible, S. Rea, et al. 2000. “Isolation and Characterization of Suv39h2, a Second Histone H3 Methyltransferase Gene That Displays Testis-Specific Expression.” *Molecular and Cellular Biology* 20 (24): 9423–33.
- Ochando, Isabel, Santiago González-Reig, Juan José Ripoll, António Vera, and Antonio Martínez-Laborda. 2008. “Alteration of the Shoot Radial Pattern in Arabidopsis Thaliana by a Gain-of-Function Allele of the Class III HD-Zip Gene INCURVATA4.” *The International Journal of Developmental Biology* 52 (7): 953–61.
- Ohashi-Ito, Kyoko, Yoshihisa Oda, and Hiroo Fukuda. 2010. “Arabidopsis VASCULAR-RELATED NAC-DOMAIN6 Directly Regulates the Genes That Govern Programmed Cell Death and Secondary Wall Formation during Xylem Differentiation.” *The Plant Cell* 22 (10): 3461–73.
- Otero, Sofia, Bénédicte Desvoyes, Ramón Peiró, and Crisanto Gutierrez. 2016. “Histone H3 Dynamics Reveal Domains with Distinct Proliferation Potential in the Arabidopsis Root.” *The Plant Cell* 28 (6): 1361–71.
- Otsuga, D., B. DeGuzman, M. J. Prigge, G. N. Drews, and S. E. Clark. 2001. “REVOLUTA Regulates Meristem Initiation at Lateral Positions.” *The Plant Journal: For Cell and Molecular Biology* 25 (2): 223–36.
- Owen, Heather A., and C. A. Makaroff. 1995. “Ultrastructure of Microsporogenesis and Microgametogenesis in Arabidopsis Thaliana (L.) Heynh. Ecotype Wassilewskija (Brassicaceae).” *Protoplasma* 185 (1-2). Springer-Verlag: 7–21.

- Perou, Charles M., Therese Sørlie, Michael B. Eisen, Matt van de Rijn, Stefanie S. Jeffrey, Christian A. Rees, Jonathan R. Pollack, et al. 2000. "Molecular Portraits of Human Breast Tumours." *Nature* 406 (6797): Nature Publishing Group: 747–52.
- Petersson, Sara V., Annika I. Johansson, Mariusz Kowalczyk, Alexander Makoveychuk, Jean Y. Wang, Thomas Moritz, Markus Grebe, Philip N. Benfey, Göran Sandberg, and Karin Ljung. 2009. "An Auxin Gradient and Maximum in the Arabidopsis Root Apex Shown by High-Resolution Cell-Specific Analysis of IAA Distribution and Synthesis." *The Plant Cell* 21 (6): 1659–68.
- Prigge, Michael J., and Steven E. Clark. 2006. "Evolution of the Class III HD-Zip Gene Family in Land Plants." *Evolution & Development* 8 (4): 350–61.
- Prigge, Michael J., Denichiro Otsuga, José M. Alonso, Joseph R. Ecker, Gary N. Drews, and Steven E. Clark. 2005a. "Class III Homeodomain-Leucine Zipper Gene Family Members Have Overlapping, Antagonistic, and Distinct Roles in Arabidopsis Development." *The Plant Cell* 17 (1): 61–76.
- . 2005b. "Class III Homeodomain-Leucine Zipper Gene Family Members Have Overlapping, Antagonistic, and Distinct Roles in Arabidopsis Development." *The Plant Cell* 17 (1): 61–76.
- Ramsay, Robert G., and Thomas J. Gonda. 2008. "MYB Function in Normal and Cancer Cells." *Nature Reviews. Cancer* 8 (7): 523–34.
- Ravi, Maruthachalam, Fukashi Shibata, Joseph S. Ramahi, Kiyotaka Nagaki, Changbin Chen, Minoru Murata, and Simon W. L. Chan. 2011. "Meiosis-Specific Loading of the Centromere-Specific Histone CENH3 in Arabidopsis Thaliana." *PLoS Genetics* 7 (6): e1002121.
- Rea, S., F. Eisenhaber, D. O'Carroll, B. D. Strahl, Z. W. Sun, M. Schmid, S. Opravil, et al. 2000. "Regulation of Chromatin Structure by Site-Specific Histone H3 Methyltransferases." *Nature* 406 (6796): 593–99.
- Reichert, Nina, Sebastian Wurster, Tanja Ulrich, Kathrin Schmitt, Stefanie Hauser, Leona Probst, Rudolf Götz, et al. 2010. "Lin9, a Subunit of the Mammalian DREAM Complex, Is Essential for Embryonic Development, for Survival of Adult Mice, and for Tumor Suppression." *Molecular and Cellular Biology* 30 (12): 2896–2908.
- Ross, K. J., P. Fransz, S. J. Armstrong, I. Vizir, B. Mulligan, F. C. Franklin, and G. H. Jones. 1997. "Cytological Characterization of Four Meiotic Mutants of Arabidopsis Isolated from T-DNA-Transformed Lines." *Chromosome Research: An International Journal on the Molecular, Supramolecular and Evolutionary Aspects of Chromosome Biology* 5 (8): 551–59.

- Sabatini, S., D. Beis, H. Wolkenfelt, J. Murfett, T. Guilfoyle, J. Malamy, P. Benfey, et al. 1999. "An Auxin-Dependent Distal Organizer of Pattern and Polarity in the Arabidopsis Root." *Cell* 99 (5): 463–72.
- Sadasivam, Subhashini, and James A. DeCaprio. 2013. "The DREAM Complex: Master Coordinator of Cell Cycle-Dependent Gene Expression." *Nature Reviews. Cancer* 13 (8). Nature Publishing Group: 585–95.
- Sadasivam, Subhashini, Shenghua Duan, and James A. DeCaprio. 2012. "The MuvB Complex Sequentially Recruits B-Myb and FoxM1 to Promote Mitotic Gene Expression." *Genes & Development* 26 (5). Cold Spring Harbor Lab: 474–89.
- Saitou, N., and M. Nei. 1987. "The Neighbor-Joining Method: A New Method for Reconstructing Phylogenetic Trees." *Molecular Biology and Evolution* 4 (4): 406–25.
- Sanders, Paul M., Anhthu Q. Bui, Koen Weterings, K. N. McIntire, Yung-Chao Hsu, Pei Yun Lee, Mai Thy Truong, T. P. Beals, and R. B. Goldberg. 1999. "Anther Developmental Defects in Arabidopsis Thaliana Male-Sterile Mutants." *Sexual Plant Reproduction* 11 (6). Springer-Verlag: 297–322.
- Sarkar, Ananda K., Marijn Luijten, Shunsuke Miyashima, Michael Lenhard, Takashi Hashimoto, Keiji Nakajima, Ben Scheres, Renze Heidstra, and Thomas Laux. 2007. "Conserved Factors Regulate Signalling in Arabidopsis Thaliana Shoot and Root Stem Cell Organizers." *Nature* 446 (7137): 811–14.
- Schmid, Markus, Timothy S. Davison, Stefan R. Henz, Utz J. Pape, Monika Demar, Martin Vingron, Bernhard Schölkopf, Detlef Weigel, and Jan U. Lohmann. 2005. "A Gene Expression Map of Arabidopsis Thaliana Development." *Nature Genetics* 37 (5): 501–6.
- Schmit, F., S. Cremer, and S. Gaubatz. 2009. "LIN54 Is an Essential Core Subunit of the DREAM/LINC Complex That Binds to the cdc2 Promoter in a Sequence-Specific Manner." *The FEBS Journal* 276 (19). Wiley Online Library: 5703–16.
- Schoof, H., M. Lenhard, A. Haecker, K. F. Mayer, G. Jürgens, and T. Laux. 2000. "The Stem Cell Population of Arabidopsis Shoot Meristems is Maintained by a Regulatory Loop between the CLAVATA and WUSCHEL Genes." *Cell* 100 (6): 635–44.
- Shapiro, Bruce E., Cory Tobin, Eric Mjolsness, and Elliot M. Meyerowitz. 2015. "Analysis of Cell Division Patterns in the Arabidopsis Shoot Apical Meristem." *Proceedings of the National Academy of Sciences of the United States of America* 112 (15): 2–7.
- Sherr, Charles J., and Frank McCormick. 2002. "The RB and p53 Pathways in Cancer." *Cancer Cell* 2 (2). Elsevier: 103–12.

- Shi, Bihai, Cui Zhang, Caihuan Tian, Jin Wang, Quan Wang, Tengfei Xu, Yan Xu, et al. 2016. "Two-Step Regulation of a Meristematic Cell Population Acting in Shoot Branching in Arabidopsis." *PLoS Genetics* 12 (7): e1006168.
- Siaud, Nicolas, Eloïse Dray, Isabelle Gy, Emmanuelle Gérard, Najat Takvorian, and Marie-Pascale Doutriaux. 2004. "Brca2 Is Involved in Meiosis in Arabidopsis Thaliana as Suggested by Its Interaction with Dmc1." *The EMBO Journal* 23 (6): 1392–1401.
- Sijacic, Paja, Wanpeng Wang, and Zhongchi Liu. 2011. "Recessive Antimorphic Alleles Overcome Functionally Redundant Loci to Reveal TSO1 Function in Arabidopsis Flowers and Meristems." *PLoS Genetics* 7 (11). doi:10.1371/journal.pgen.1002352.
- Sim, Choon Kiat, Sarah Perry, Sana Khalid Tharadra, Joseph S. Lipsick, and Anandasankar Ray. 2012. "Epigenetic Regulation of Olfactory Receptor Gene Expression by the Myb–MuvB/dREAM Complex." *Genes & Development* 26 (22): 2483–98.
- Simon, Alexander L., Eric A. Stone, and Arend Sidow. 2002. "Inference of Functional Regions in Proteins by Quantification of Evolutionary Constraints." *Proceedings of the National Academy of Sciences of the United States of America* 99 (5): 2912–17.
- Slotkin, R. K., M. Vaughn, F. Borges, M. Tanurdzic, J. D. Becker, J. A. Feijó, and R. A. Martienssen. 2009. "Epigenetic Reprogramming and Small RNA Silencing of Transposable Elements in Pollen." *Cell* 136 (3). Elsevier: 461–72.
- Smith, Zachery R., and Jeff A. Long. 2010. "Control of Arabidopsis Apical–basal Embryo Polarity by Antagonistic Transcription Factors." *Nature* 464 (7287). Nature Publishing Group: 423–26.
- Smyth, Gordon K. 2004. "Linear Models and Empirical Bayes Methods for Assessing Differential Expression in Microarray Experiments." *Statistical Applications in Genetics and Molecular Biology* 3 (February): Article3.
- Song, J. Y., T. Leung, L. K. Ehler, C. Wang, and Z. Liu. 2000a. "Regulation of Meristem Organization and Cell Division by TSO1, an Arabidopsis Gene with Cysteine-Rich Repeats." *Development* 127 (10): 2207–17.
- . 2000b. "Regulation of Meristem Organization and Cell Division by TSO1, an \itshape Arabidopsis Gene with Cysteine-Rich Repeats." *Development* 127 (10). The Company of Biologists Limited: 2207–17.
- Stahl, Yvonne, René H. Wink, Gwyneth C. Ingram, and Rüdiger Simon. 2009. "A Signaling Module Controlling the Stem Cell Niche in Arabidopsis Root Meristems." *Current Biology: CB* 19 (11): 909–14.

- Stevens, Rebecca, Mathilde Grelon, Daniel Vezon, Jaesung Oh, Peter Meyer, Claudette Perennes, Severine Domenichini, and Catherine Bergounioux. 2004. "A CDC45 Homolog in Arabidopsis Is Essential for Meiosis, as Shown by RNA Interference–Induced Gene Silencing." *The Plant Cell* 16 (1): 99–113.
- Stracke, R., M. Werber, and B. Weisshaar. 2001. "The R2R3-MYB Gene Family in Arabidopsis Thaliana." *Current Opinion in Plant Biology* 4 (5): 447–56.
- Tachibana, Makoto, Kenji Sugimoto, Tatsunobu Fukushima, and Yoichi Shinkai. 2001. "Set Domain-Containing Protein, G9a, Is a Novel Lysine-Preferring Mammalian Histone Methyltransferase with Hyperactivity and Specific Selectivity to Lysines 9 and 27 of Histone H3." *The Journal of Biological Chemistry* 276 (27): 25309–17.
- Takada, Shinobu, and Gerd Jürgens. 2007. "Transcriptional Regulation of Epidermal Cell Fate in the Arabidopsis Embryo." *Development* 134 (6): 1141–50.
- Takahashi, Naoki, Takehiro Kajihara, Chieko Okamura, Yoonhee Kim, Youhei Katagiri, Yoko Okushima, Sachihito Matsunaga, Ildoo Hwang, and Masaaki Umeda. 2013a. "Cytokinins Control Endocycle Onset by Promoting the Expression of an APC/C Activator in Arabidopsis Roots." *Current Biology: CB* 23 (18): 1812–17.
- . 2013b. "Cytokinins Control Endocycle Onset by Promoting the Expression of an APC/C Activator in Arabidopsis Roots." *Current Biology: CB* 23 (18): 1812–17.
- Takahashi, Y., J. B. Rayman, and B. D. Dynlacht. 2000. "Analysis of Promoter Binding by the E2F and pRB Families in Vivo: Distinct E2F Proteins Mediate Activation and Repression." *Genes & Development* 14 (7): 804–16.
- Talbert, P. B., H. T. Adler, D. W. Parks, and L. Comai. 1995. "The REVOLUTA Gene Is Necessary for Apical Meristem Development and for Limiting Cell Divisions in the Leaves and Stems of Arabidopsis Thaliana." *Development* 121 (9): 2723–35.
- Tamaru, H., and E. U. Selker. 2001. "A Histone H3 Methyltransferase Controls DNA Methylation in Neurospora Crassa." *Nature* 414 (6861): 277–83.
- Tanaka, Y., N. P. Patestos, T. Maekawa, and S. Ishii. 1999. "B-Myb Is Required for Inner Cell Mass Formation at an Early Stage of Development." *The Journal of Biological Chemistry* 274 (40): 28067–70.
- Taylor-Teeple, M., L. Lin, M. de Lucas, G. Turco, T. W. Toal, A. Gaudinier, N. F. Young, et al. 2014. "An Arabidopsis Gene Regulatory Network for Secondary Cell Wall Synthesis." *Nature* 517 (7536): 571–75.

- Thorner, A. R., K. A. Hoadley, J. S. Parker, S. Winkel, R. C. Millikan, and C. M. Perou. 2009. "In Vitro and in Vivo Analysis of B-Myb in Basal-like Breast Cancer." *Oncogene* 28 (5): 742–51.
- Thorstensen, Tage, Paul E. Grini, and Reidunn Birgitta Aalen. 2011. "SET Domain Proteins in Plant Development." *Biochimica et Biophysica Acta* 1809 (8): 407–20.
- Tian, Caihuan, Xiaoni Zhang, Jun He, Haopeng Yu, Ying Wang, Bihai Shi, Yingying Han, et al. 2014. "An Organ Boundary-Enriched Gene Regulatory Network Uncovers Regulatory Hierarchies Underlying Axillary Meristem Initiation." *Molecular Systems Biology* 10 (10). doi:10.15252/msb.20145470.
- Trauth, K., B. Mutschler, N. A. Jenkins, D. J. Gilbert, N. G. Copeland, and K. H. Klempnauer. 1994. "Mouse A-Myb Encodes a Trans-Activator and Is Expressed in Mitotically Active Cells of the Developing Central Nervous System, Adult Testis and B Lymphocytes." *The EMBO Journal* 13 (24): 5994–6005.
- Umezawa, Taishi, Naoyuki Sugiyama, Fuminori Takahashi, Jeffrey C. Anderson, Yasushi Ishihama, Scott C. Peck, and Kazuo Shinozaki. 2013. "Genetics and Phosphoproteomics Reveal a Protein Phosphorylation Network in the Abscisic Acid Signaling Pathway in Arabidopsis Thaliana." *Science Signaling* 6 (270): rs8.
- Waites, R., and A. Hudson. 1995. "Phantastica: A Gene Required for Dorsoventrality of Leaves in *Antirrhinum Majus*." *Development*. dev.biologists.org. <http://dev.biologists.org/content/121/7/2143.short>.
- Wan, Cuihong, Blake Borgeson, Sadhna Phanse, Fan Tu, Kevin Drew, Greg Clark, Xuejian Xiong, et al. 2015. "Panorama of Ancient Metazoan Macromolecular Complexes." *Nature* 525 (7569): 339–44.
- Wang, Xu, Yangyang Bian, Kai Cheng, Li-Fei Gu, Mingliang Ye, Hanfa Zou, Samuel Sai-Ming Sun, and Jun-Xian He. 2013. "A Large-Scale Protein Phosphorylation Analysis Reveals Novel Phosphorylation Motifs and Phosphoregulatory Networks in Arabidopsis." *Journal of Proteomics* 78 (January): 486–98.
- Wang, Ying, Jin Wang, Bihai Shi, Ting Yu, Jiyan Qi, Elliot M. Meyerowitz, and Yuling Jiao. 2014. "The Stem Cell Niche in Leaf Axils Is Established by Auxin and Cytokinin in Arabidopsis." *The Plant Cell* 26 (5): 2055–67.
- Wang, Zhi-Ping, Hui-Li Xing, Li Dong, Hai-Yan Zhang, Chun-Yan Han, Xue-Chen Wang, and Qi-Jun Chen. 2015. "Egg Cell-Specific Promoter-Controlled CRISPR/Cas9 Efficiently Generates Homozygous Mutants for Multiple Target Genes in Arabidopsis in a Single Generation." *Genome Biology* 16 (1): 144.

- Weinberg, R. A. 1995. "The Retinoblastoma Protein and Cell Cycle Control." *Cell* 81 (3): 323–30.
- Wilson, Michael, Tatsuaki Goh, Ute Voß, Anthony Bishopp, Benjamin Péret, and Malcolm Bennett. 2013. "SnapShot: Root Development." *Cell* 155 (5). Elsevier: 1190–1190.e1.
- Wisniewska, Justyna, Jian Xu, Daniela Seifertová, Philip B. Brewer, Kamil Ruzicka, Ikram Blilou, David Rouquié, Eva Benková, Ben Scheres, and Jirí Friml. 2006. "Polar PIN Localization Directs Auxin Flow in Plants." *Science* 312 (5775): 883.
- Yadav, Ram Kishor, Thomas Girke, Sumana Pasala, Mingtang Xie, and G. Venugopala Reddy. 2009. "Gene Expression Map of the Arabidopsis Shoot Apical Meristem Stem Cell Niche." *Proceedings of the National Academy of Sciences of the United States of America* 106 (12): 4941–46.
- Yadav, Ram Kishor, Montreh Tavakkoli, and G. Venugopala Reddy. 2010. "WUSCHEL Mediates Stem Cell Homeostasis by Regulating Stem Cell Number and Patterns of Cell Division and Differentiation of Stem Cell Progenitors." *Development* 3589 (September): 3581–89.
- Yadav, Ram Kishor, Montreh Tavakkoli, Mingtang Xie, Thomas Girke, and G. Venugopala Reddy. 2014. "A High-Resolution Gene Expression Map of the Arabidopsis Shoot Meristem Stem Cell Niche." *Development* 141 (13): 2735–44.
- Yamaguchi, Masatoshi, Nadia Goué, Hisako Igarashi, Misato Ohtani, Yoshimi Nakano, Jennifer C. Mortimer, Nobuyuki Nishikubo, et al. 2010. "VASCULAR-RELATED NAC-DOMAIN6 and VASCULAR-RELATED NAC-DOMAIN7 Effectively Induce Transdifferentiation into Xylem Vessel Elements under Control of an Induction System." *Plant Physiology* 153 (3): 906–14.
- Yang, M., Y. Hu, M. Lodhi, W. R. McCombie, and H. Ma. 1999. "The Arabidopsis SKP1-LIKE1 Gene Is Essential for Male Meiosis and May Control Homologue Separation." *Proceedings of the National Academy of Sciences of the United States of America* 96 (20): 11416–21.
- Yan, Jun, Yiyu Gu, Xiaoyun Jia, Wenjun Kang, Shangjin Pan, Xiaoqing Tang, Xuemei Chen, and Guiliang Tang. 2012. "Effective Small RNA Destruction by the Expression of a Short Tandem Target Mimic in Arabidopsis." *The Plant Cell* 24 (2): 415–27.
- Yee, Adelinda, Xiaoqing Chang, Antonio Pineda-Lucena, Bin Wu, Anthony Semesi, Brian Le, Theresa Ramelot, et al. 2002. "An NMR Approach to Structural Proteomics." *Proceedings of the National Academy of Sciences of the United States of America* 99 (4): 1825–30.

- Yoshida, Saiko, Pierre Barbier de Reuille, Brendan Lane, George W. Bassel, Przemyslaw Prusinkiewicz, Richard S. Smith, and Dolf Weijers. 2014. "Genetic Control of Plant Development by Overriding a Geometric Division Rule." *Developmental Cell* 29 (1): 75–87.
- Zhang, Tian-Qi, Heng Lian, Chuan-Miao Zhou, Lin Xu, Yuling Jiao, and Jia-Wei Wang. 2017. "A Two-Step Model for de Novo Activation of WUSCHEL during Plant Shoot Regeneration." *The Plant Cell*, April. doi:10.1105/tpc.16.00863.
- Zhang, X., H. Tamaru, S. I. Khan, J. R. Horton, L. J. Keefe, E. U. Selker, and X. Cheng. 2002. "Structure of the Vitshape Neurospora SET Domain Protein DIM-5, a Histone H3 Lysine Methyltransferase." *Cell* 111 (1). Elsevier: 117–27.
- Zhan, Ming, Daniel R. Riordon, Bin Yan, Yelena S. Tarasova, Sarah Bruweleit, Kirill V. Tarasov, Ronald A. Li, Robert P. Wersto, and Kenneth R. Boheler. 2012. "The B-MYB Transcriptional Network Guides Cell Cycle Progression and Fate Decisions to Sustain Self-Renewal and the Identity of Pluripotent Stem Cells." *PloS One* 7 (8): e42350.
- Zhao, Xin 'ai, Hirofumi Harashima, Nico Dissmeyer, Stefan Pusch, Annika K. Weimer, Jonathan Bramsiepe, Daniel Bouyer, et al. 2012. "A General G1/S-Phase Cell-Cycle Control Module in the Flowering Plant Arabidopsis Thaliana." *PLoS Genetics* 8 (8): e1002847.
- Zheng, Sanduo, Jia Wang, Yingang Feng, Jinfeng Wang, and Keqiong Ye. 2012. "Solution Structure of MSL2 CXC Domain Reveals an Unusual Zn 3 Cys 9 Cluster and Similarity to Pre-SET Domains of Histone Lysine Methyltransferases." *PloS One* 7 (9). Public Library of Science: e45437.
- Zhong, Ruiqin, and Zheng Hua Ye. 2004a. "Amphivasal Vascular Bundle 1, a Gain-of-Function Mutation of the IFL1/REV Gene, Is Associated with Alterations in the Polarity of Leaves, Stems and Carpels." *Plant & Cell Physiology* 45 (4): 369–85.
- Zhong, Ruiqin, and Zheng-Hua Ye. 2004b. "Amphivasal Vascular Bundle 1, a Gain-of-Function Mutation of the IFL1/REV Gene, Is Associated with Alterations in the Polarity of Leaves, Stems and Carpels." *Plant & Cell Physiology* 45 (4): 369–85.
- Zhong, R., and Z. H. Ye. 1999. "IFL1, a Gene Regulating Interfascicular Fiber Differentiation in Arabidopsis, Encodes a Homeodomain-Leucine Zipper Protein." *The Plant Cell* 11 (11): 2139–52.
- Zhu, Wencheng, Paloma H. Giangrande, and Joseph R. Nevins. 2004. "E2Fs Link the Control of G1/S and G2/M Transcription." *The EMBO Journal* 23 (23): 4615–26.

- Zou, L., and B. Stillman. 1998. "Formation of a Preinitiation Complex by S-Phase Cyclin CDK-Dependent Loading of Cdc45p onto Chromatin." *Science* 280 (5363): 593–96.
- . 2000. "Assembly of a Complex Containing Cdc45p, Replication Protein A, and Mcm2p at Replication Origins Controlled by S-Phase Cyclin-Dependent Kinases and Cdc7p-Dbf4p Kinase." *Molecular and Cellular Biology* 20 (9): 3086–96.
- Zuckerandl, Emile, and Linus Pauling. 1965. "Evolutionary Divergence and Convergence in Proteins." *Evolving Genes and Proteins* 97: 97–166.